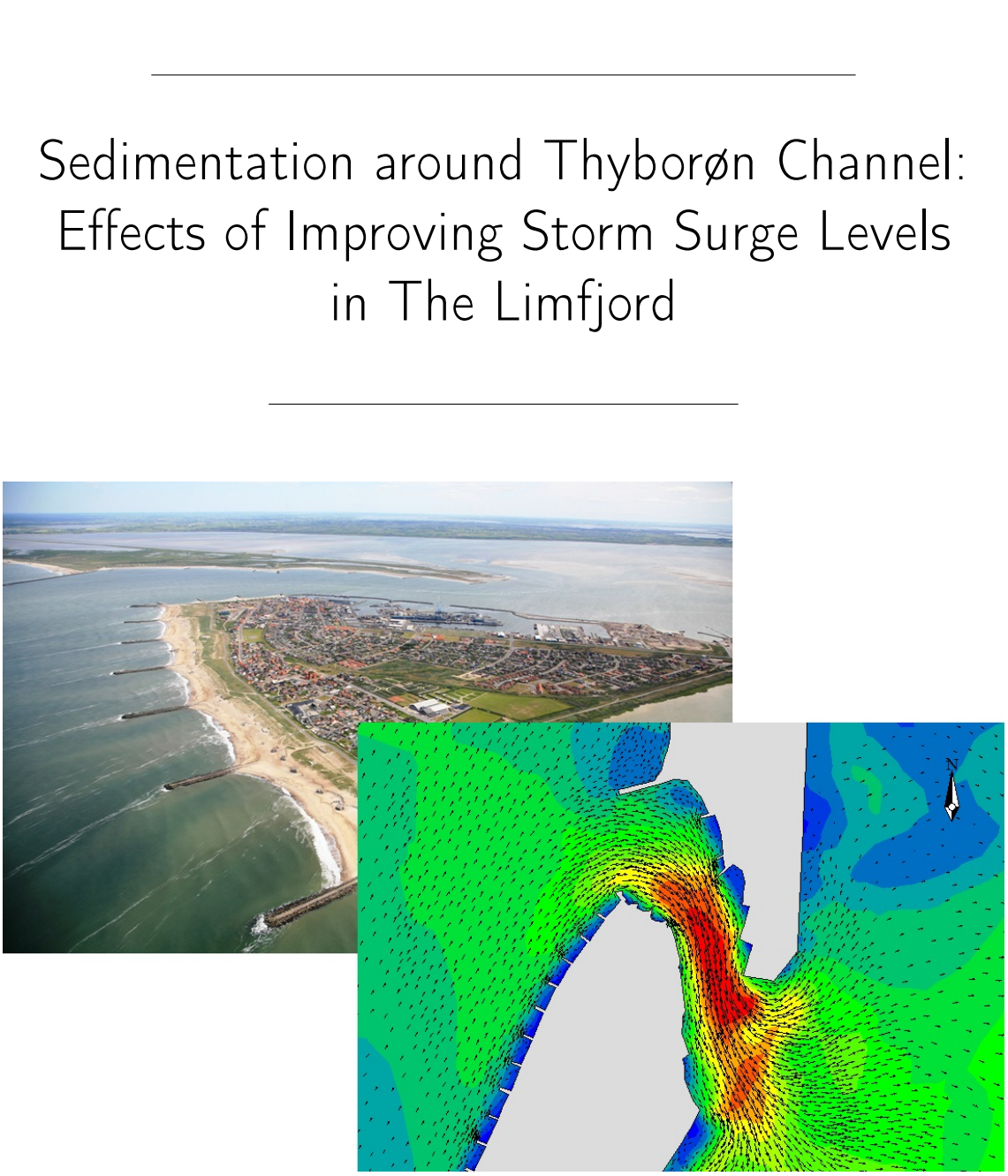

AALBORG UNIVERSITY
STUDENT REPORT

Sedimentation around Thyborøn Channel: Effects of Improving Storm Surge Levels in The Limfjord

Theis Buys Petersen
M.Sc. in Structural and Civil Engineering
Master's thesis
June 8th 2017

AALBORG UNIVERSITY
STUDENT REPORT

The School of Engineering and Science
Study Board of Civil Engineering
Thomas Manns Vej 23, 9220 Aalborg Ø
http://www.ses.aau.dk/

Title

Sedimentation around Thyborøn Channel: Effects of Improving Storm Surge Levels in The Limfjord

Project period

February 2017 - June 2017

Author

Theis Buys Petersen

Supervisors

Torben Larsen
Professor in Hydraulic Engineering (Aalborg University)

Jørgen Q. H. Nørgaard
Associate Professor (Aalborg University)
Senior Coastal Engineer (Ramboll Consulting Engineers)

Main report pages: 58
Appendix pages: 42
Completed on June 8th 2017

Synopsis:

The Danish Limfjord experiences increased storm surge levels due to an increasing cross section in Thyborøn Channel which connects the Limfjord to the North Sea. Several suggestions to a solution to the problem have been made, among them building a dam with a sluice to be closed during storms. This project assesses the sediment related consequences of implementing the proposed solutions. The assessment is made through simulations of sediment transport in the area caused by both severe and relatively mild storms chosen through analyses on meteorological and oceanographic data. The simulations are made in the software suit MIKE 21 which couples simulations of wave, flow, and sediment transport fields to model realistic processes accurately and efficiently. It is found that the construction of a dam and extension of a groyne would significantly improve sediment conditions in the area compared to only extending the groyne. Adding the dam, while expensive, is further found to improve manoeuvrability of ships in the entrance to Thyborøn Harbour and has been proved in other work to improve oxygen levels in the Limfjord.

Danish abstract

I Limfjorden opleves øgede vandstande forårsaget af storme fra vest, der presser vand ind gennem Thyborøn Kanal. Klimaændringer øger stormenes styrke, men en anden vigtig faktor er, at Thyborøn Kanal udvider sig, hvilket tillader mere vand at strømme gennem den under storm. Kystdirektoratet (KDI) har med hjælp fra Dansk Hydraulisk Institut (DHI) konkluderet, at en indsnævring af Thyborøn Kanal er den bedste løsning på problemet. Forlængelse af høfder og konstruktion af en dæmning med sluser til vand og skibsfart præsenteres som løsningsforslag til indsnævring af kanalen. Udvidelse af høfden til at indsnævre indløbet vurderes af KDI som det mest fordelagtige valg baseret på prisen, og at den begrænser stormvandstandsudviklingen.

Dette projekt undersøger de forventede forandringer i Thyborønområdets sedimentation forårsaget af to løsningsforslag: (1) forlængelse af høfde (2) konstruktion af en dæmning samt forlængelse af høfde. Begge forslag sammenholdes med en referencemodel modelleret ud fra de nuværende forhold i området. Målet er at vurdere på de sedimentmæssige konsekvenser af at implementere løsningsforslagene samt give en anbefaling til løsningen af problematikken baseret herpå.

Vurderingen af de sedimentmæssige konsekvenser af udvidelserne er baseret på simuleringer lavet i DHIs softwarepakke MIKE 21, der estimerer sedimenttransport baseret på løbende opdatering af kombinerede bølge-, strøm- og dybdeforhold. To storme er valgt til simuleringer: en kraftig fra januar 2005 og en mildere fra december 2005. På den måde kan både spidssituationers og relativt almindelige vejrforholds indflydelse på områdets bathymetri vurderes. Stormene er valgt på baggrund af sedimenttransporttendenser estimeret ud fra 17 års bølgedata sluttende i 2012.

Simuleringerne viser tendenser for stor erosion i indløbet til kanalen ved udvidelse af høfden grundet acceleration af strømmen. Sedimentet fra erosion aflejres både i og ud for kanalen. Ved tilføjelse af dæmningen ses stor aflejring af sediment i indløbet, men kanalen selv er fri for erosion og bypasset forøges, hvilket betyder mindre kysterosion og dermed mindre behov for kystfodring.

Det konkluderes, at erosionen i høfdeudvidelsesmodellens indløb kan få store økonomiske konsekvenser pga. nødvendigheden af oprensning rundt i området. De økonomiske konsekvenser forværres af, at erosionen ses både i den kraftige og milde stormsimulering, hvilket tyder på, at problemet ikke begrænser sig til hårdt vejr. Konstruktionsomkostnignerne for dæmningsforslaget er noget højere, men sedimentationsmæssigt betragtes forslaget overlegent. Forsøg på at bringe omkostninger til dæmningen ned besværliggøres af Thyborøn Havns planer om udvidelse sydover.

Det anbefales at implementere sedimentbegrænsede modeller for høfteudvidelsesforslaget for at undersøge omfanget af erosionen i indløbet. Herudover anbefales det, at simulere længere, roligere perioder for at få indblik i, om den akkumulerede transport bliver for stor.

Preface

This master's thesis is written as part of the Master's programme in Structural and Civil Engineering at Aalborg University. It sheds light on the challenges regarding sedimentation in the Thyborøn area given the solutions proposed by KDI [2012] to the increasing storm surge levels in the Limfjord caused by an expanse of Thyborøn Channels cross section.

Great gratitude is addressed to Per Sørensen, Head of Coastal Research at the Danish Coastal Authorities, for help procuring coastal data for the project. Credit for the aerial photo shown on the front page goes to The Danish Coastal Authorities.

Reading guide

References to sources are made using the Harvard method, and a complete source list is found in the bibliography. Source references are made with either "[Surname/organisation, Year]" or "Surname/organisation [Year]".

The report contains figures and tables, which are enumerated according to the respective chapter. For example, the first figure in Chapter 5 is 5.1, the second 5.2 and so on. If a north arrow is not shown in a figure, north is towards the top of the page.

Table of contents

Introduction 1

Thyborøn Channel is the only waterway connecting the North Sea and the Kattegat through Jutland making it an important trade route for agricultural exports and fishing. Figure 1.1 shows the location of Thyborøn Channel and the surrounding area. When the channel was opened, large erosion was seen in the area. This erosion led to the construction of groynes in the channel and on the surrounding tongues. The groynes are numbered as seen in Figure A.1.

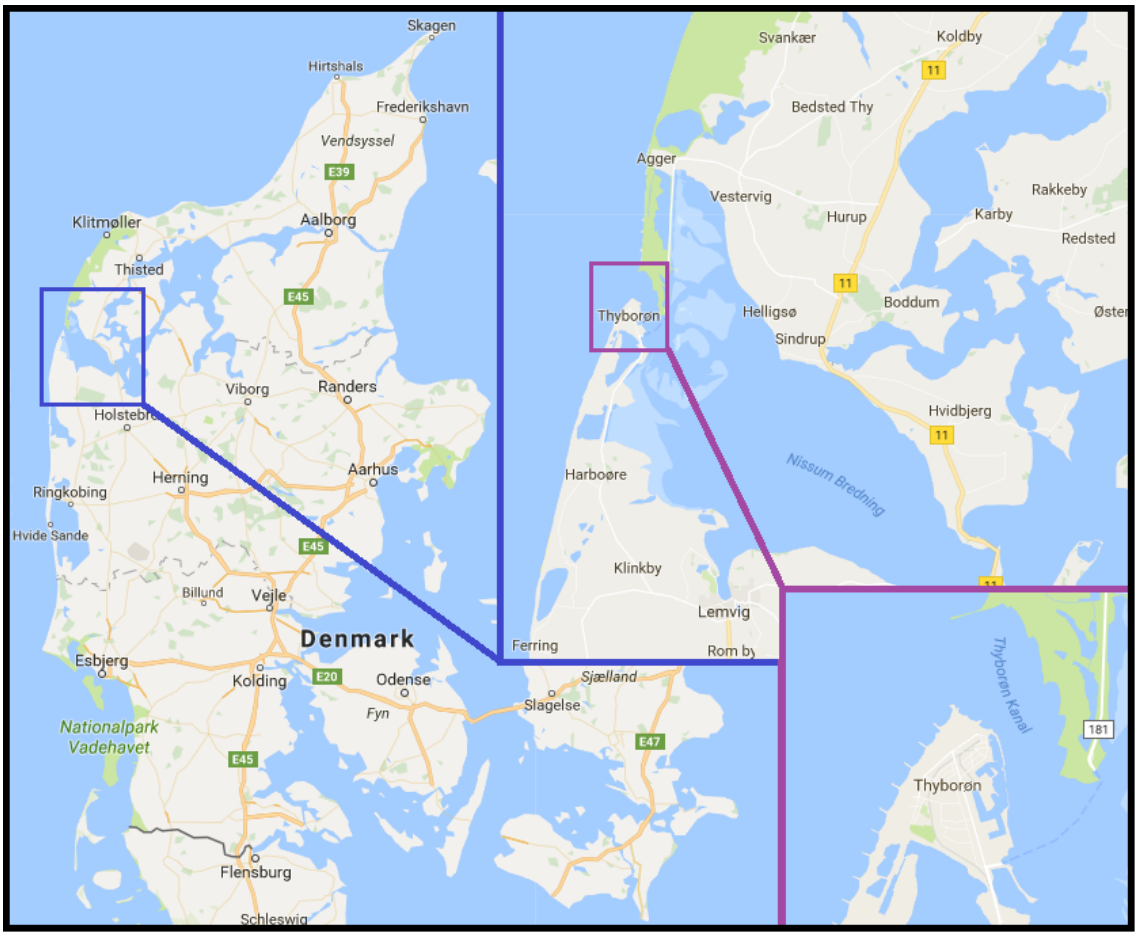

Figure 1.1 Location of Thyborøn Channel on the west coast of Denmark [Google, 2017].

The channel has been in constant change since it was first opened and is one of the oldest coastal issues in Denmark. As such it has been the focus of attention several times, and now, once more, it is being discussed by coastal engineers as plans are being formulated to increase coastal protection in the area.

1.1 Historical development of the Thyborøn area

Between 1100 and 1825 the Limfjord and North Sea were separated by a small isthmus. A storm in 1825 broke through the isthmus and created a channel at Agger north of Thyborøn. By 1834 the Agger Channel had increased to a sailable size, but by 1860 sedimentation had once again closed it off, for traffic. In 1862 another storm surge broke the isthmus further south and created Thyborøn Channel. In 1874 it was decided to build groynes to keep the new channel from closing as had happened to the previous breakthrough at Agger. In 1905-08 construction of Thyborøn Harbour was started in the channel as the coastal protection was deemed sufficient to stop the coastal erosion in the channel and on the tongues [KDI, 2011] [KDI, 1999].

The groynes shown in Figure A.1 were constructed between 1875 and 1968. They are the result of efforts to stabilise the channel and tongues. When it was created, the channel was almost E-W oriented, but because the dominant sediment transport was southbound it soon changed to WNW-ESE. Large erosion on the tongues bordering the channel prompted authorities to construct groynes 54, 56, 57, and 59 on the southern tongue in the period 1875-1883. The reduction in northbound sediment transport from the southern tongue led to the southern transport being more prominent causing the orientation of the channel to shift towards NW-SE. Between 1885 and 1897 groynes 33-53, 55, 58, and 60-63 were build to stabilise the southern tongue and the southern part of the channel. In 1905-1914 groynes 72-96, 68, 69, and 71 were build, while groyne 72 was extended. The construction of groynes 68 and 69 and the extension of 72 led to a dramatic change in flow through the channel. The changed flow created a tongue south of groyne 68 that was protected by groynes 65-67 build in 1963-1968 [KDI, 1999]. Sketches of the channel from different years between 1874 and 1991 can be seen in Figure A.2.

The groynes built to keep the channel open worked. However, the channel started growing in cross section resulting in increased water level in the Limfjord during western storms. In 1946 it was decreed by law to close the channel off. A dam including two sluices, one for shipping and one for water to flow through, was to be built. In the fifties, however, a doctoral thesis by Bruun [1954] sparked a new debate as to the necessity of closing the channel. This debate led to the removal of the law in 1970 under the condition that the coastal authorities monitored the development at Thyborøn. The problem of increasing cross section persists, leading to worries regarding Thyborøn Channels stability [KDI, 2012].

Recently, plans to extend Thyborøn Harbour southward have been formulated in order to continue business growth by accommodating larger ships. The area along the coastline south of the harbour is relatively shallow allowing for construction of new docks and hinterland. An overview of the planned extension is shown in Figure A.3 [Rambøll, 2014].

1.2 Challenges inside the Limfjord

The increased cross section causes a larger flow into the channel and therefore a larger transport of sediment. As of 2007 the sedimentation has necessitated extraordinary dredging, which, coupled with the cost of protecting the shores inside the Limfjord from increased water levels, has prompted new debate on what can be done to quell the issue [KDI, 2012]. The dredged areas are marked in Figure 1.2.

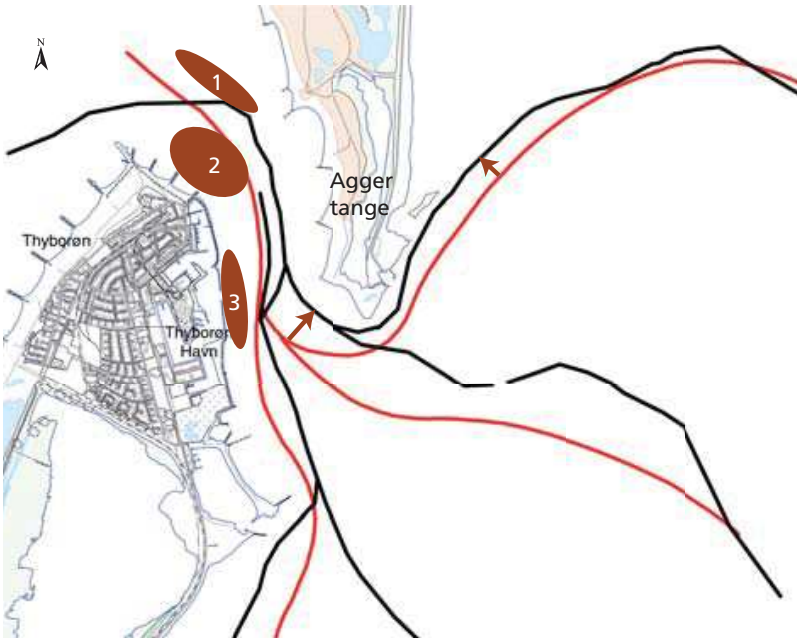

Figure 1.2 Main shipping lanes (red = 1937, black = 2005) and primary dredging areas in Thyborøn Channel.

In addition to the effect on sedimentation on the west coast of Jutland (from here on simply called the west coast), Thyborøn Channel has opened up the Limfjord to effects of change in water level on the west coast. This has led to large water levels during storm surges which is only made worse by the increase of the cross section in the channel caused by erosion.

Additionally, the Limfjord experiences deoxygenation during the summer months due to a lack of water flow. The net flow is east, but the water exchange is not sufficient to ensure acceptable water quality [Nørgaard et al., 2014].

Thyborøn Harbour, which was constructed in the channel after it was deemed safe from erosion, has reported difficult manoeuvring conditions outside the harbour and would like the solution to improve this [KDI, 2012]. The difficult manoeuvring conditions are caused by increased wave disturbance which, according to Knudsen and Sørensen [2011], has three causes. Firstly, larger cross section in the entrance to Thyborøn Channel causes more wave energy to enter the channel. Secondly, the so-called “sand pillow” in area 2 of Figure 1.2 refracts the waves towards the harbour. Finally, a decrease in depth outside the harbour has led to larger shoaling in the area.

Finally, climate changes are causing water levels to rise and storms to grow larger. This can not be solved locally at Thyborøn, but it should be kept in mind when designing coastal structures.

1.3 Report composition

The report is composed of certain steps to ease readability. The steps are explained in more detail below.

- Introduction to the area and the problems in the region.
- State of the art shortly summarising relevant external investigations into the issues in the Thyborøn area, their conclusions, and whether it can be of use in the present project. Furthermore, it is described what this report seeks to add to the collective knowledge on the problem.
- An introduction to the physics involved in sediment transport at Thyborøn and a description of the sediment transport system found in the Thyborøn area.
- Choice of modelling framework used in the project, the extent of the domain modelled, and the interaction between the models is described.
- Presentation and assessment of available data and what it is used for in the report.
- Estimating the sediment transport on the tongues surrounding the channel in order to select a period to be modelled in further analyses.
- Modelling the flow of water in the Limfjord which is utilised in the sediment model that covers a large part of the west coast and Thyborøn Channel.
- Modelling of the sediment transport in and around Thyborøn Channel using said data from the model covering the Limfjord. Presentation and discussion of sedimentation results.
- Final discussion, conclusion, and recommendations for further work.

The area and its problems have been described. Next some of the work conducted on the subject by others is listed, and their conclusions summarised to gather knowledge on the problem at hand. Following this, an introduction to the physics of the problem and a description of the local sediment transport system is made. With the problem described, a modelling framework for the sediment transport in the area is chosen and scenarios are introduced. The data used in the different models is presented and its quality and extent is discussed. Then the exact simulation periods are chosen by use of an estimate on the potential sediment transport rates in the area. Finally sediment transport simulations are modelled to better estimate the actual sediment transport in the area and results are presented followed by a conclusion on the project and recommendations for further work.

State of the art 2

This chapter outlines what has previously been investigated in relation to the problems at Thyborøn Channel, which solutions have been proposed, their pros and cons, and what this study aims to contribute with. Additionally, a description of the present and historical sediment transport situation at Thyborøn is presented.

2.1 Previous studies

Regarding the erosion of the coastline, The Danish Coastal Authorities (KDI) are obligated to perform a thorough inspection every 25 years [KDI, 1999]. The latest was conducted in 1999. It focuses on the tongues surrounding the channel, documenting wind- and wave-conditions, water levels, and developments in the sedimentation in the channel and on the tongues. It is found that the coastline in the area is kept constant through groynes and substantial beach nourishment, but that it is highly sensitive to human interventions such as dredging. It also documents statistics for highest water levels expected in the area. The report is used in the present project for increased understanding of the sediment related issues in the area, its history, and the coastal processes in the area.

KDI also conducted an investigation between 2009 and 2012 that concerns the storm surge water levels and assesses the different solutions proposed for the problems [KDI, 2012]. Regarding water level statistics the investigation found that the storm surge levels predicted by previous reports are too low. The report suggests two strategies; one where nothing is done at the channel, but the coastal protection of the affected areas is increased regularly, and one where the storm surge levels are kept in check by keeping the cross section of Thyborøn Channel artificially constant. According to KDI, the most promising solution is an extension of groyne 59 as shown in Figure 2.1. This strategy is expected to have a positive effect on all parameters investigated. The report is used for background knowledge on the area and its reported issues.

A paper titled “Influence of Closing Storm Surge Barrier on Extreme Water Levels and Water Exchange; the Limfjord, Denmark” investigates the effects of implementing a storm surge barrier in the channel on water levels during storms [Nørgaard et al., 2014]. It is concluded that a barrier would decrease the storm surge water levels significantly and that the water quality in the Limfjord could be increased by controlling the flow of water. Some of the discoveries made during the modelling made in the paper is used in the present project to speed up the process. Furthermore, the description of the problems regarding storm surge water levels and deoxygenation are relevant for the present project.

The Danish Hydraulic Institute (DHI) has also contributed to the investigations performed on the subject with their report "The Morphological Evolution Around Thyborøn - an Inlet at the North Sea" [Knudsen et al., 1995]. It investigates the sediment transport in and around Thyborøn Channel and concludes that the channel widens as a result of storms from SW. The modelling includes the effect of clayey subsoils on the sediment transport. This makes the investigation valuable for the current project as a tool to discuss the influence of the clay layer.

DHI further investigated the morphological changes in the channel through a study on the change in storm surge water levels in the Limfjord caused by different depths of the channel. It was found that a 25 % increased maximum depth in the channel leads to a 12 cm increase in water depth at Thyborøn, 10 cm at Lemvig, but only 1 cm at Løgstør [Knudsen et al., 1995]. The parameter variation in the study is useful for understanding the impact of Thyborøn Channel on the Limfjord.

A technical note by Knudsen and Sørensen [2011] investigates wave disturbance experienced at Thyborøn Harbour. It is concluded that increased cross section in the channel entrance, lower depth outside the harbour, and the creation of the so called "sand pillow" north of the harbour is causing the wave disturbance.

On the subject of sedimentation in tidal inlets in general, Hayes [1980] describes the evolution of an inlet under different conditions. He also illustrates the morphology in tidal inlets such as Thyborøn Channel. The findings for tidal inlets in Hayes [1980] paper are used as a comparison to Thyborøn Channel.

Gao and Collins [1994] wrote a paper on the influence of factors other than tidal prisms on tidal inlet equilibriums. They found that the main factors affecting tidal inlet equilibriums are: tidal prisms, flood and ebb durations, freshwater discharge, and sediment transport through the entrance. Reference is made to the O'Brien method suggested by O'Brien and Dean [1972] which predicts the stability of a tidal inlet based on hydraulics of the inlet, equilibrium between cross sectional area and tidal prism, and stability of an inlet against closing.

2.2 Solutions proposed by KDI

As previously mentioned, KDI has analysed different proposals for solutions to the issues at Thyborøn including extending different groynes in the channel and even adding a dam with a sluice. The two solutions investigated in this report are shown in Figures 2.1 and 2.2. The first solution, extending groyne 59, aims to maintain a constant cross section in Thyborøn Channel through the different construction phases I-III in order to keep the storm surge levels constant. The other, extending groyne 59 and adding a dam, aims to decrease the water level during storms while still allowing entry for ships and water through different sluices [KDI, 2012]. These two proposals are further investigated in the present report.

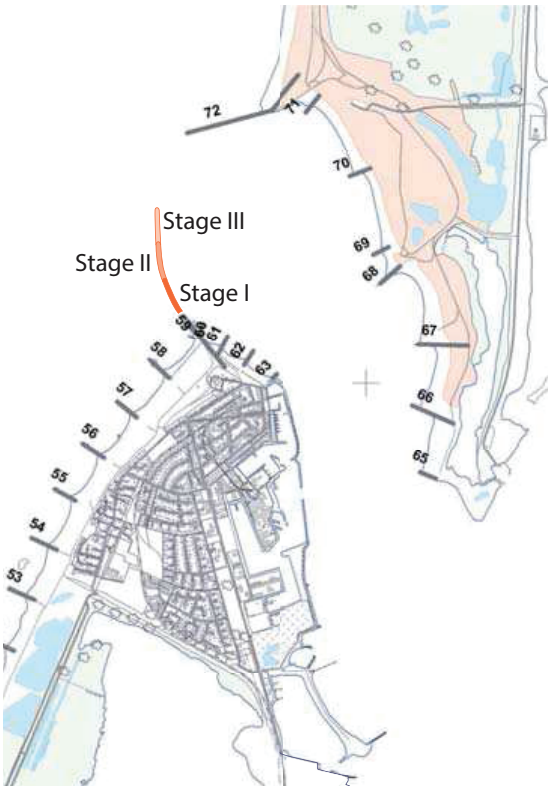

Figure 2.1 Solution proposed by KDI [2012, p. 13]. Extension of groyne number 59.

Figure 2.2 Solution proposed by KDI [2012, p. 17]. Construction of dam with sluice and extension of groyne 59.

2.2.1 Requirements of a solution

It may be unrealistic to expect a solution to solve all the problems stated while still being economically feasible, but an ideal solution to the problem should include the following:

- Reversal or stop of the increase in water level during storms from western directions.
- Decrease in sedimentation in an around the channel and an increase in sediment bypass.
- The possibility of Thyborøn Harbour being used as an emergency harbour for ships during storms.
- Improvement of navigational conditions for ships entering the harbour.
- A decrease in the experienced deoxygenation during the summer in the Limfjord.

2.2.2 Pros and cons of the solutions

The two solutions both address the problem of increased storm surge levels in the Limfjord, but to different extend and with different side effects. Pros and cons associated with extending groyne 59 as shown in Figure 2.1 are [KDI, 2012]:

- Pros of the groyne 59 extension solution:
  - Status quo until 2050 regarding water levels during storms
  - Decreased sedimentation in the channel
  - Possibility of Thyborøn harbour as emergency harbour
  - Improved navigational capabilities in the channel
- Cons of the groyne 59 extension solution:
  - No difference in expected flow through the Limfjord meaning the oxygen levels will likely remain the same
  - No decrease in the expected water level in the Limfjord compared to current conditions

For the second solution, extending groyne 59 and adding a dam as show in Figure 2.2, the pros and cons are [KDI, 2012]:

- Pros of extending groyne 59 and adding a dam:
  - Drastic decrease in the water level inside the Limfjord during storms
  - Decreased sedimentation in the channel
  - Use of Thyborøn Harbour as an emergency harbour
  - Ability to control the flow through the Limfjord leading to a healthier straight
  - Improved navigational capabilities in the channel
  - Abrogation of the ferry connecting Thyborøn and Agger in favour of a permanent connection
- Cons of extending groyne 59 and adding a dam:
  - The dam makes it a significantly more expensive alternative
  - Necessity of protecting Thyborøn against increased water levels during storms caused by the inability for the water to progress into the Limfjord

2.3 Present study

This project seeks to assess the changes in sediment transport in and around Thyborøn Channel caused by implementing different solutions proposed for the Thyborøn issues. This is done by modelling a large part of the west coast and Limfjord in the numerical software suit MIKE 21 which is a 2D, depth averaged, numerical approach that can be applied to problems of the kind described. Specifically the two different solutions described in Chapter 2.2 are examined. Expected scenarios of both large and moderate sediment transport are simulated to investigate the two solutions during different conditions in order to better evaluate them. Finally, the sediment transport properties evaluated from the simulations, and other aspects of the solutions, are discussed in order to present an overall favourable suggestion.

2.4 System description

In order to better understand the problem at hand, the physics of sediment transport at Thyborøn and their effects are described.

The principles behind sediment transport are described in Appendix B. In short, cross-shore currents transport sediment away from shore during storms where the longshore current carries it down the coastline. When the groynes were built in the 1960s it was believed that the waves only contributed to the longshore current in the breaking zone. Thus it was believed that extending groynes past this zone would completely stop the longshore sediment transport [KDI, 1999].

The effects of undertow, circular flow, and so-called rip currents were however not included in those considerations. The longshore current generated by the waves outside the breaking zone generates a circular flow between each set of groynes that carries sediment from the shore to outside the reach of the groynes. A rip current is created when waves hit the groyne protected beach at an angle creating a set-up at the farthest groyne [KDI, 1999]. The processes are illustrated in Figure 2.3. Undertow, illustrated in Figure 2.4, is a flow of water at the seabed close to shore which balances the increased mean water level from wave set-up. With the knowledge of these phenomena it is concluded that the groynes do not completely remove, but only limit the longshore transport. This is supported by the observation of 100 meters of coastal retreat at the groynes in this century [KDI, 1999].

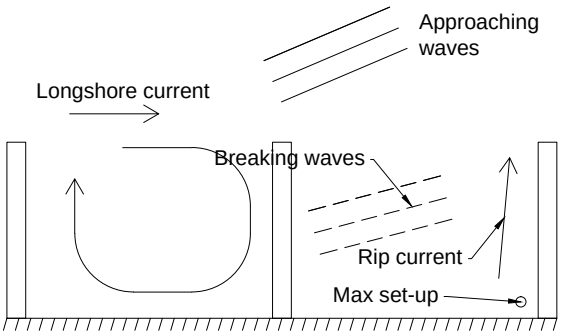

Figure 2.3 Illustration of circular flow from longshore current (left) and rip current from set-up (right). Inspired by KDI [1999].

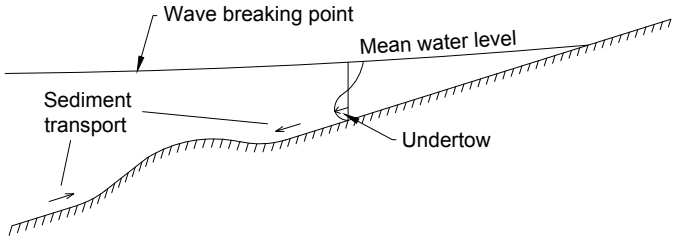

Figure 2.4 Illustration of undertow caused by wave set-up. Inspired by KDI [1999].

2.4.1 Sediment transport in the Thyborøn area

The coastline in the Thyborøn area is kept relatively constant through coastal protection such as groynes. The protection prevents natural equilibrium of sediment transport which necessitates beach nourishment. Figure 2.5 shows a sediment budget for the west coast created by KDI [2001].

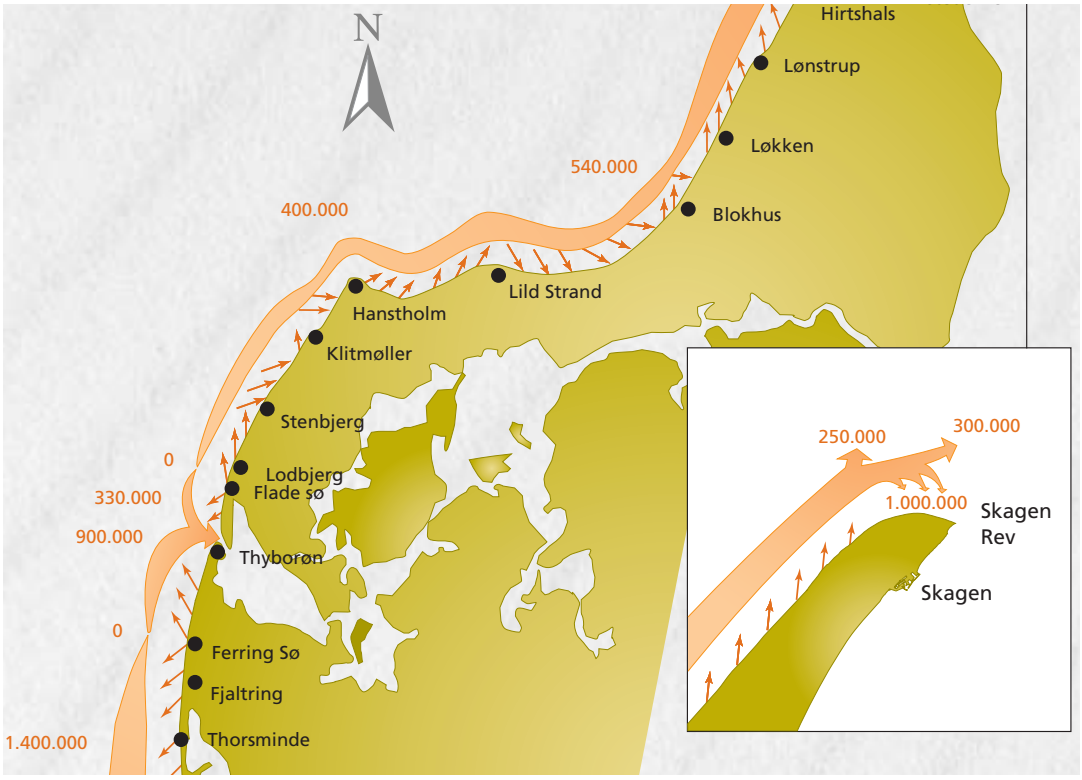

Figure 2.5 Sediment budget for the west coast of Jutland as of 2001 [KDI, 2001].

When Thyborøn Channel opened, the sediment that had previously shifted north and south depending on the currents was now sucked into the channel creating a massive erosion of both the northern and southern coastlines. If nothing had been done, the channel would most likely have closed itself off, like Agger Channel before it. However, the erosion prompted the coastal authorities to start dredging the channel and constructing groynes on the tongues north and south of it to keep it open for traffic [KDI, 2012]. Keeping the channel open has the adverse effect that during storms where a large wind set-up is present on the west coast all sediment is carried with the flow into the Limfjord where the water level is lower.

When considering sediment transport a commonly used term is a “null-point”. It denotes a point on a coastline where the average net transport over 20-30 years is zero. Two null-points can be seen in Figure 2.5. The transport from such a point is directed away in both directions [Larsen and Beck, 2015].

It is believed that, before Agger Channel opened in 1825, the primary null-point for sediment transport was located at Lodbjerg as seen in Figure 2.6. After the breakthrough, however, another

null-point was created south of the channel at Ferring Sø by Bovbjerg, illustrated in Figure 2.6. The second null point was created because the channel now sucked in the sediment travelling south from the null-point at Lodbjerg. It is estimated that 700 000 m^3/year of sediment deposits on the sand banks past the channel, shown in Figure 2.7. Because of the new null-point the net transport at Ferring Sø is now zero compared to 400 000 m^3/year before, leading to an increase in erosion south of Ferring Sø [Larsen and Beck, 2015].

Hayes [1980] describes the sand banks as a *flood-tidal delta* as they are found on the landward side of the inlet. This means that the primary sediment accumulation happens on the landward side of the inlet stemming from the seaward side. Thus, the problem of suction of sediment into Thyborøn Channel is further proven. The large wave energy from the North Sea means that there is close to no *ebb-tidal delta* which is formed as sediment from the landward side settles in the seaward entrance to the channel.

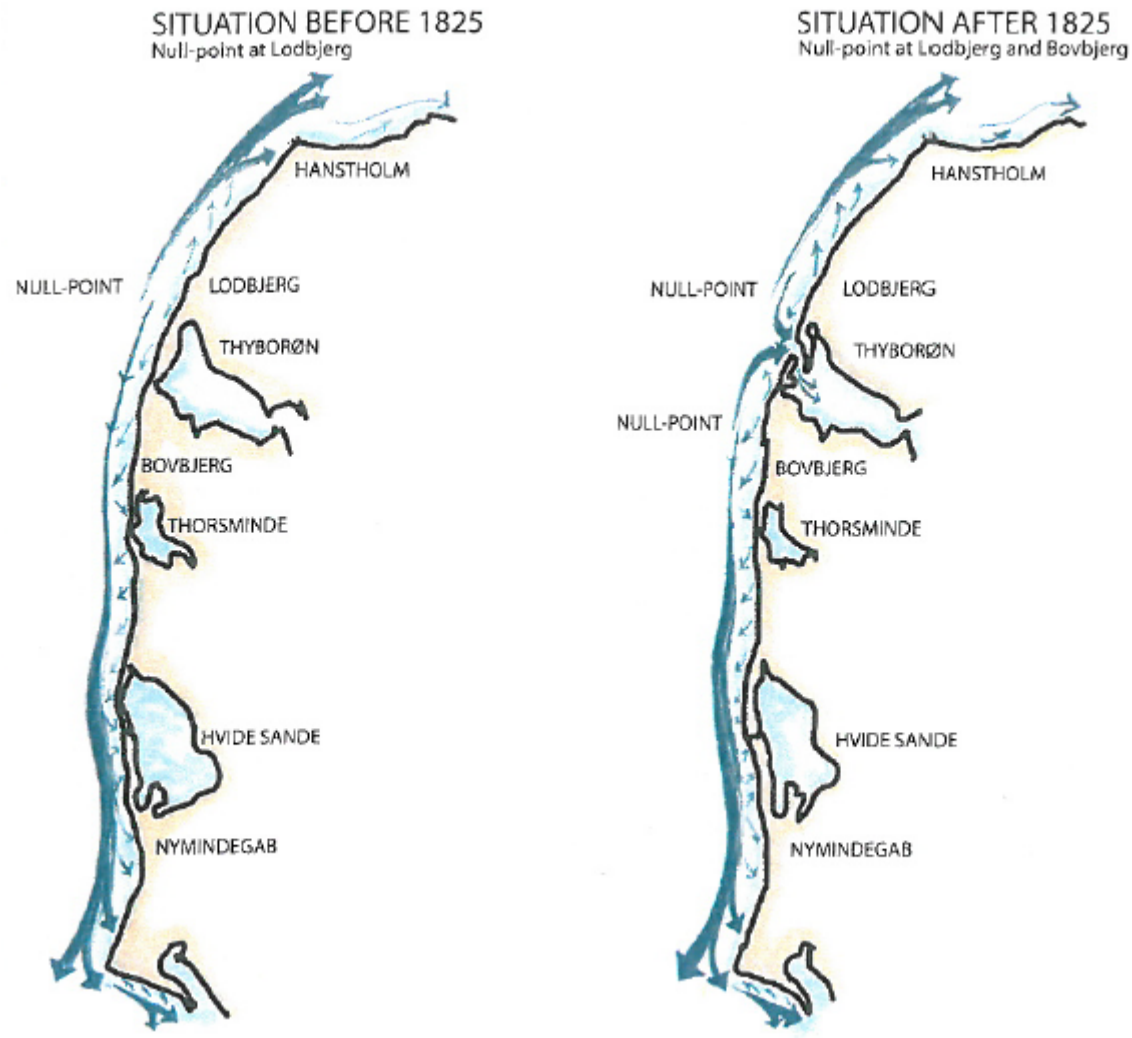

Figure 2.6 Change in sediment transport on the Danish west coast caused by the break through at Thyborøn [Larsen and Beck, 2015].

Figure 2.7 Sand banks created by sedimentation from the west coast through Thyborøn Channel [Google, 2017].

Choice of modelling tool and extent of domain 3

This chapter outlines the models applied to the problem at hand. The components of the models are described and their core assumptions discussed. Considerations regarding choice of modelling periods are made. Finally, the modelling structure employed in the analyses, i.e. what models are constructed and why, is described.

Before choosing a model framework certain parameters are discussed. Firstly, as the sedimentation on a coastline cannot be simplified to a local area, a large part of the west coast will have to be modelled. As such, a 2D model is chosen instead of 3D in order to bring down the computational time which enables more simulations and thereby a more flexible approach. Furthermore, as sediment transport primarily depends on horizontal flow, the 2D approach is further accepted compared to 3D which would better model the vertical flow properties.

3.1 Periods for modelling

Sediment transport is a near continuous process going on at every sandy coast over long periods of time, so ideally an equally long period of about 20-30 years should be modelled. This is, however, unrealistic with the available computational power. Instead shorter periods are chosen based on tendencies for longer periods.

A simple model for predicting sediment transport tendencies is the formula proposed by Kamphuis [2010] based on experimental data. It predicts potential sediment transport rates assuming an infinite straight beach with infinite amounts of sand and a constant beach profile which extends far into the sea. As such the formula cannot be used in the channel, but it is often used to get an estimate of the potential sediment transport rates in a beach area for further analysis. It is expected to overestimate the transport compared to actual rates due to the assumptions mentioned, but it is sufficient for tendency modelling.

3.2 Choice of model framework

The problems with sediment accumulation in the Thyborøn area (described previously in this chapter and in Chapter 2.4) necessitate a framework capable of adequately modelling; firstly, the flow through the Limfjord and secondly, the sediment transport conditions in the Thyborøn

area, both in 2D. It should utilize wind, wave, and water level data as forcings and boundary conditions. Furthermore, it should be efficient enough to simulate a duration of about 7 days within a reasonable amount of time.

Based on these conditions Mike 21 Coupled Model FM provided by DHI is chosen for modelling. The framework is composed of different modules that model different aspects of the problem as described below.

3.2.1 Employed MIKE 21 Coupled Model FM modules

The **Spectral Wave** (SW) module simulates the wave field in an area using bathymetry, wind, flow, and current conditions. A directionally decoupled formulation of the wave action equation in horizontal Cartesian coordinates is used, meaning that the wave field, bathymetry, and current field are assumed constant. This assumption should not affect the results much as the fields and bathymetry are still updated for each time step in the simulation. The approximation of 2D means that breaking waves do not stir up sediment for the current to carry down the shore leading to conservative results [DHI, 2015c].

The **Hydrodynamics** (HD) module simulates the flow in an area using the wave field created in the SW module. For 2D application the module solves the incompressible Reynolds averaged Navier-Stokes equations under the assumptions of hydrostatic pressure and Boussinesq's eddy viscosity for momentum transfer from turbulent eddies. Another assumption is that the velocity is depth averaged, meaning that undertow, mixing, and a boundary proposed by Fredsoe [1984] are averaged out [DHI, 2015b]. Not taking undertow into account fully might influence sediment transport rates. This is because, realistically, the seaward flow on the bottom close to shore would carry sediment to deeper waters where the longshore current would carry it down the shore [DHI, 2015a].

The **Sand Tranport** (ST) module takes waves and currents into account when calculating the sediment transport field for the domain in a sediment transport table created using the MIKE 21 toolbox utility "Generation of Q3D Sediment Table". The tool uses a quasi three dimensional hydrodynamics model to solve the force balance across the water column. Then it uses the force balance to interpolate values for sediment transport rates given different combinations of water level, current speed, directions, etc. The ST module assumes infinite amounts of sand in the ground. This poses a problem as the actual conditions in the area are clayey below 0.5-1.0 m. Thus, the results are checked for violations of this condition in Chapter 6.4. Another assumption made in the ST module is: The current velocity is set to the depth averaged velocity calculated in the HD module. This is conservative as, theoretically, the velocity goes toward zero when approaching the sea bed. However, as depth decreases, flow becomes more constant over depth and more sediment transport happens, so the assumption is not too conservative [DHI, 2015b].

3.3 Modelling structure

Two different 2D models are created as outlined in Table 3.1. The main model is the so-called Thyborøn model. Its purpose is to assess sedimentation in and around Thyborøn Channel. It includes the modules SW, HD, and ST which are coupled in one model to more correctly model the connection between sediment transport, wave field, and current conditions. If the modules had been separated, a decrease in e.g. water depth from the ST module would not affect the waves and flow leading to model errors in subsequent time steps. The coupling ensures that the flow increases as a result of the shallower water leading to an increased sediment flux.

Table 3.1 Overview of models created in MIKE 21.

Model name	Implemented modules	Use of model
Thyborøn	Coupled HD, ST & SW	Assessing sediment transport in and around Thyborøn Channel
Limfjord	HD	Generating boundary conditions for the Thyborøn model

Because large models with dense meshes increase computational time dramatically, a second model is made using only the HD module. This model, called the Limfjord model, provides the flow at the entrance to the Limfjord as a boundary condition (BC) to the Thyborøn model. The principle is illustrated in Figure 3.1. During western storms water from the North Sea flows through Thyborøn Channel into the Limfjord carrying sediment with it to the sand banks in Nissum Bredning. Because the place of interest is the channel, however, Nissum Bredning and the rest of the Limfjord can be excluded from the sediment calculations. For this reason only informations regarding the flow in the boundary between Nissum Bredning and Thyborøn Channel is needed. Using this method, the larger Limfjord model can be run once for each storm, and its results used in multiple analyses of the sedimentation around Thyborøn using the Thyborøn model.

As the Limfjord can be seen as a straight with openings in each end, and mixing and local flows are not of interest, a 2D description is sufficient to model the flow through the Limfjord. Furthermore, the computational time increases dramatically when switching to 3D. For these reason a 2D model is employed in the Thyborøn area as well. The models each employ a mesh comprised of triangular elements connected by nodes. The governing equations are solved for the center of each element and interpolated using the surrounding elements.

3.3.1 Connection between the models

As illustrated in Figure 3.1 there is an overlap of the two models. This overlap allows for flow data to be extracted from the Limfjord model on a common boundary with the Thyborøn model where it can be used as boundary condition. Figure 3.2 shows a close up of the boundary in question.

The boundary conditions of the Limfjord and Thyborøn models are further described in Chapters 5.4.1 and 6.1, respectively.

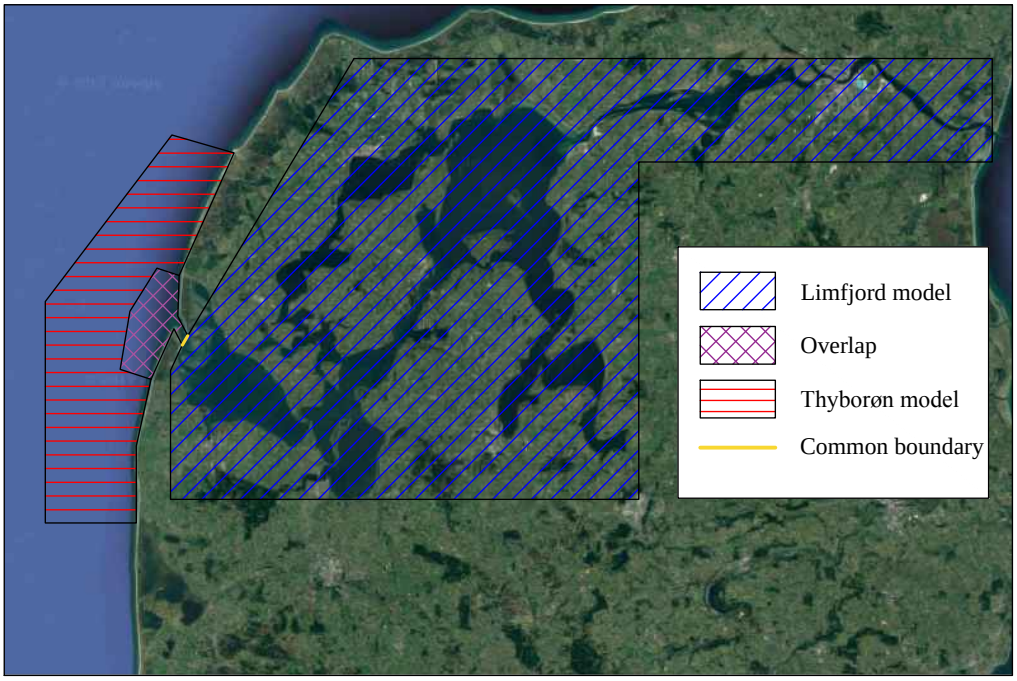

Figure 3.1 Principle of shared boundary between the Limfjord and Thyborøn models. Background image from Google [2017].

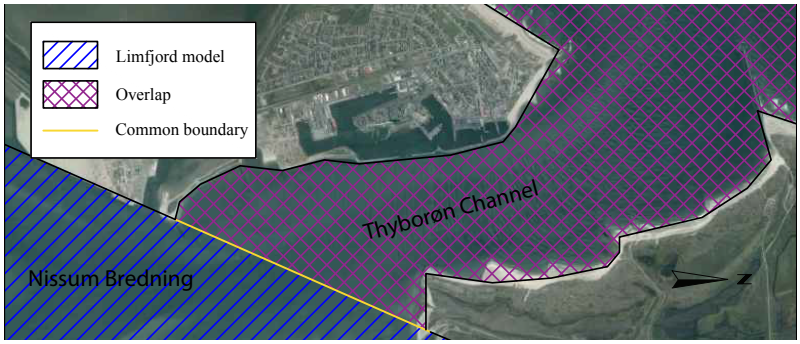

Figure 3.2 Close up of the boundary between Thyborøn Channel and Nissum Bredning. Background image from Google [2017].

Data presentation and assessment 4

This chapter presents and assesses the available data used throughout the report. Discussions are made on whether the quality and extent of the data are sufficient.

4.1 Wind data

For use as forcings in the MIKE models a windspeed series measured at Thyborøn Harbour is obtained. The wind speed and direction is 10 min averaged and was measured at 10 m height throughout 2005. A wind rose of the data is shown in Figure 4.1. Figure 4.2 shows the location of the wind gauge. As expected, the strongest winds blow from the North Sea. There are some periods lacking data as the device was off-line. They are however not prevalent in the periods chosen for further analysis in Chapter 5.3. If data for more years had been available, the amount simulateable storms would increase, but the storms present in the data are found to be sufficient for the intended purpose.

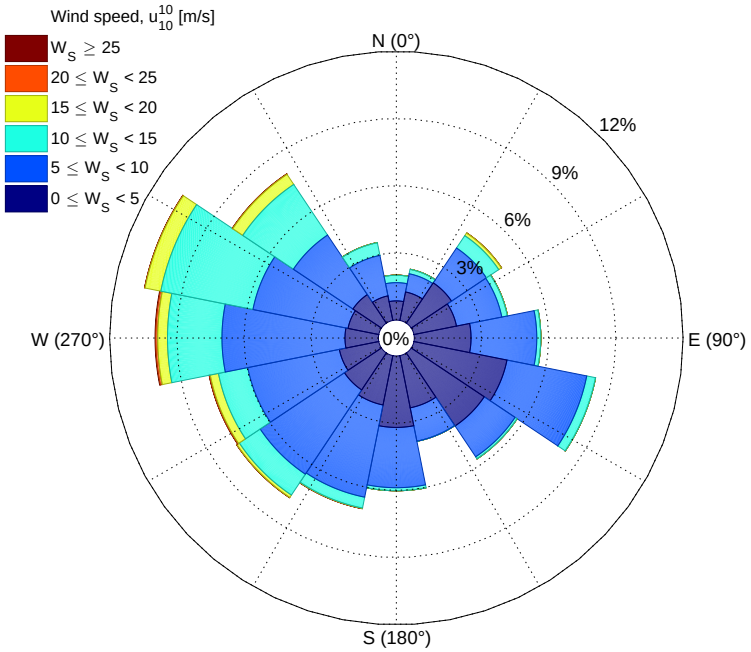

Figure 4.1 Rose of wind data used in simulations.

Figure 4.2 Position of wind gauge that measured the wind series used in the report [Google, 2017].

4.2 Surface elevation data

Surface elevation time series for Hals, Thyborøn, Løgstør, and Skive throughout 2005 are available. Figure 4.3 shows the locations where surface elevations have been measured. The specific points are: 24011 (Thyborøn), 21191 (Skive Harbour), 20423 (Løgstør Harbour), and 06044 (Hals).

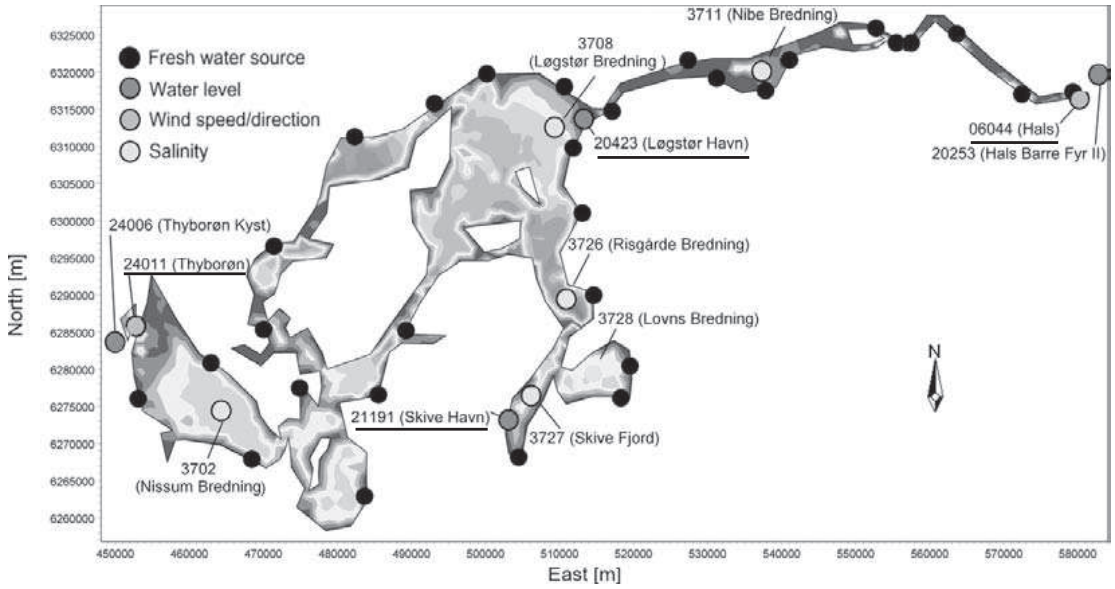

Figure 4.3 Map of the measuring points for the different surface elevation time series used throughout the report [Nørgaard et al., 2014]. Data is available from the underlined locations.

The data from Hals and Thyborøn are used as boundary conditions when modelling the Limfjord. The data from Løgstør and Skive is used to calibrate said model. The surface elevation for Thyborøn and Skive were measured inside their respective harbours. This surface elevation may be slightly different from outside the harbour, but the expected difference is assumed small enough

to be ignored. All four data sets are ten minute averages. The amount of surface elevation data available fits the purpose quite well as these data cover the same time period as the wind data.

4.3 Wave data

Hindcasted wave data is available from the location shown in the lower left corner of Figure 4.4. The data represent hourly averages of spectral wave height, H_{m0}, peak wave period, T_p, and mean wave direction, α_0, in the period 1994-2011.

The wave data is used when estimating the sediment flux tendencies at Thyborøn and as boundary conditions when modelling the wave field in the area around Thyborøn. There are gaps in the data from where the buoy has been off-line. The gaps are discussed when encountered throughout the report.

Figure 4.5 shows a wave rose of the data obtained from the hindcasting. The vast majority of the data is concentrated in the WNW direction. The correlation plot in Figure 4.6 presents the correlation between significant wave height and peak wave period. Good correlation is seen for wave heights above 2 m while there is some uncertainty for heights below. Correlation plots for directions S through N are shown in Appendix C. The larger sea states from western directions show good correlation.

17 years of data collection seems like a long time, but for processes with large return periods, like storms, it is a bit too short. Therefore, data from a longer period would mean less uncertainty on the simulations of the large storm.

Figure 4.4 Wave hindcasting point outside Fjaltring [Google, 2017].

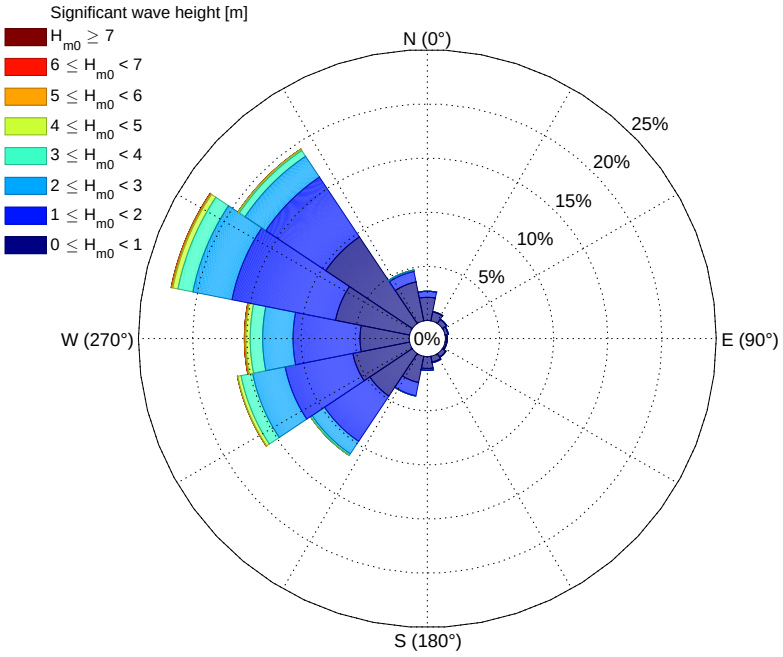

Figure 4.5 Rose of wave data from hindcasting at Fjaltring.

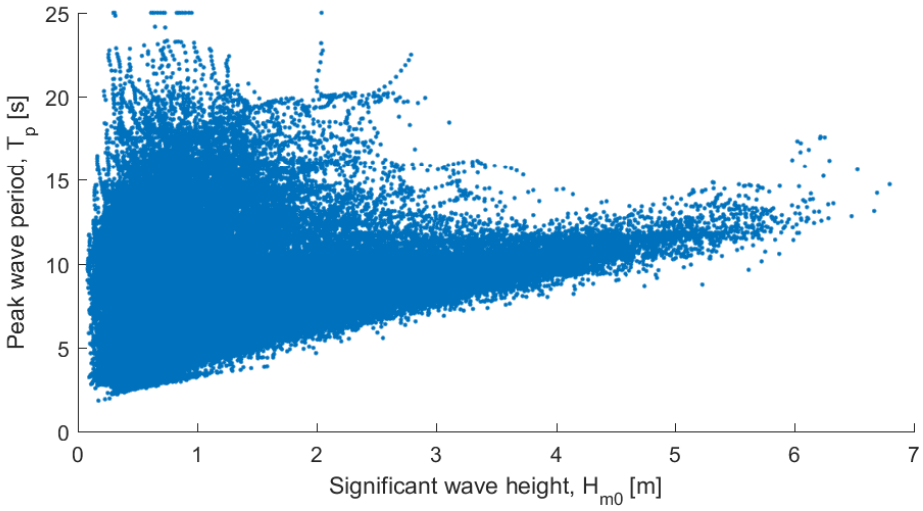

Figure 4.6 Correlation between significant wave hight and peak wave period for all wave data hindcasted outside Fjaltring. Plots for individual directions are shown in Appendix C.

4.4 Soundings

Bathymetries are required for use in MIKEs different modules. For this purpose, soundings of part of the North Sea and the Limfjord are interpolated. The soundings east of Løgstør in the Limfjord make up a grid of 50 m. Data west of Løgstør and off the west coast are in a grid of 100 m. Additionally, a bathymetry file for the Limfjord is a available from previous simulations

[Nørgaard et al., 2014]. All soundings and the bathymetry bathymetry are shown in Figures 4.7 and 4.8, respectively. A denser grid of soundings would be desirable as 100x100 is considered quite coarse for sediment transport modelling purposes, but as this is not available, the data is used.

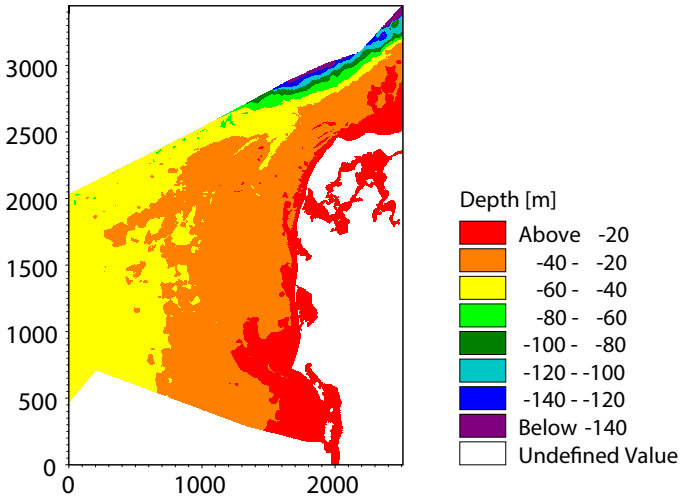

Figure 4.7 Soundings from the North Sea.

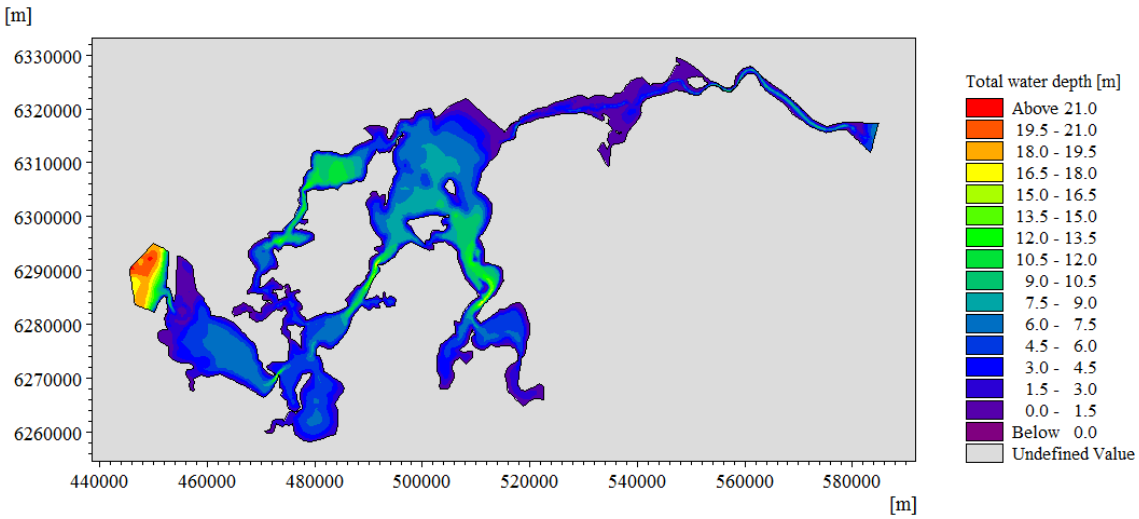

Figure 4.8 Bathymetry from previous simulations modelled by Nørgaard et al. [2014].

Extensive beach profile measuring is carried out on the west coast by KDI. Beach profiles for the coastline north and south of the channel are available from the years 1985, 1990, 2000, 2005, and 2010. Measurements are available for every two meters from shore on the numbered lines marked in Figure 4.9. The beach profile data is used when assessing sediment transport tendencies on the tongues north and south of Thyborøn Channel. Large amounts of data are available, but the quality is hampered by the ongoing beach nourishment which makes it difficult to draw conclusions on the sediment transport changes in the area.

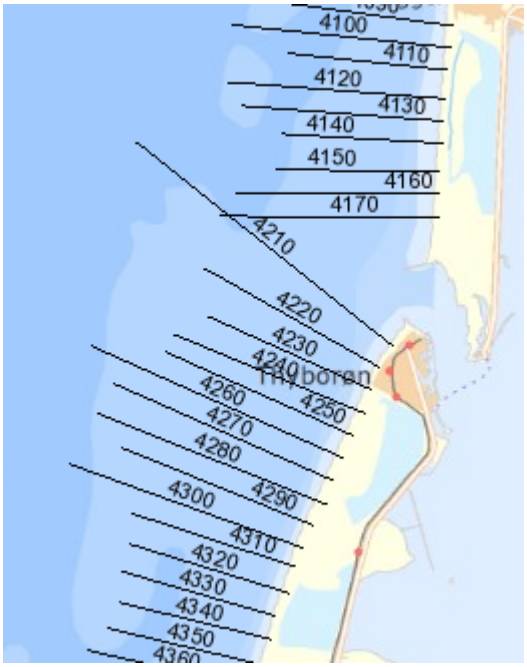

Figure 4.9 Numbered measuring lines used by KDI for mapping the beach profile [KDI, 2017].

Choice of storms and modelling of BC 5

Using the formula described by Kamphuis [2010], this chapter analyses the potential sediment flux at the coastlines north and south of Thyborøn Channel. This is done to help choose a period for simulation of sediment transport in MIKE 21. Subsequently the Limfjord model is documented and calibrated in order to generate boundary conditions for the Thyborøn model.

5.1 Sediment transport using Kamphuis' formula

Kamphuis's formula is an empirical formula experimentally developed to predict the potential sediment flux across a straight beach with a constant profile [Kamphuis, 2010]. It is implemented as an estimate of the potential sediment flux across the Harboøre and Agger Tongues, shown in Figure 5.1, in order to assess the tendencies in the area.

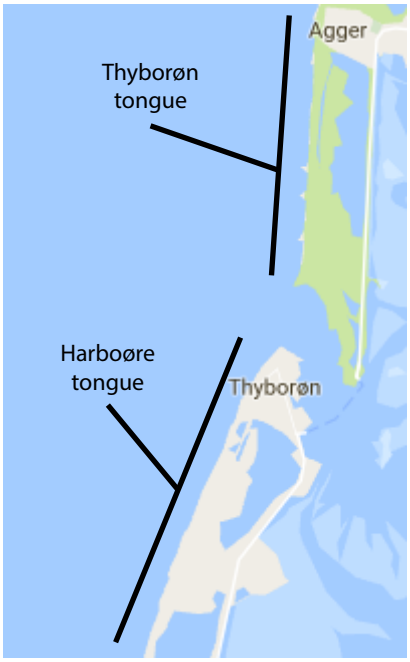

Figure 5.1 Location of the Harboøre and Agger tongues [Google, 2017]. Background image from Google [2017].

When using the formula, wave data for the area is needed. For this purpose, data from a wave buoy near Fjaltring, described in Chapter 4.3 is used. The position of the buoy is shown in Figure 4.4. It is assumed that the data can be directly applied to the Thyborøn area without any transformation. This is a rather crude estimation, as the beach profile varies, however it is deemed sufficient for an

early estimate as it is only used to determine the period more thoroughly modelled using numerical software. Thus, the assumption should not affect the sediment conditions modelled later.

The formula itself is shown in Equation 5.1. The results give the sediment transport pr. hour assuming a straight infinitely long sandy beach profile that extends far off-shore with infinite amounts of sand available [Kamphuis, 2010]. Geotechnical borings in the area provided by Geus [2017] show a tendency for the sea bed to be about 0.5-1.0 m sand overlaying clay and silt. This poses a problem for the infinite material assumption as clay erodes slower than sand, resulting in a smaller flux. Furthermore the tongues in question violate the assumption of infinitely long stretches and the groynes in the area reduce the flux drastically. The assumption of a sandy profile to far off shore seems to hold up in the area. As a result of the assumptions the actual sediment transport is expected to be less than the on predicted by Kamphuis's formula. However for the purpose of showing tendencies between weather conditions and sediment transport rates it holds up.

$$Q_k = 7.3 H_{m0b}^2 T_{0p}^{1.5} m_b^{0.75} D_{50}^{-0.25} \sin^{0.6}(2\alpha_b) \tag{5.1}$$

where

Q_k	Sediment transport [m^3/h]
H_{m0b}	Significant breaking wave height [m]
T_{0p}	Deep water period [s]
m_b	Breaking bottom slope
D_{50}	Median grain diameter [m]
α_b	Angle of breaking wave with shore [°]

The slopes used in the calculations are extracted from the 2010 beach profile data described in Chapter 4.4. The mean grain diameter is used as a calibration factor to match the sediment transport on the stretches to the one documented by KDI [2001].

The breaking wave parameters, H_{m0b}, m_b, and α_b used in the formula are described in Appendix D. The formula is validated in Appendix E by predicting the sediment transport at Fjaltring using the hindcasted wave data and comparing to the sediment budget devised by KDI [2001].

5.2 Sedimentation tendency results and discussion

Figures 5.2 and 5.3 show potential sediment transport rates at the Agger and Harboøre tongues predicted by Kamphuis formula. Positive values denote northbound sediment transport. The majority of the transport happens during the winter storms easily spotted in the results.

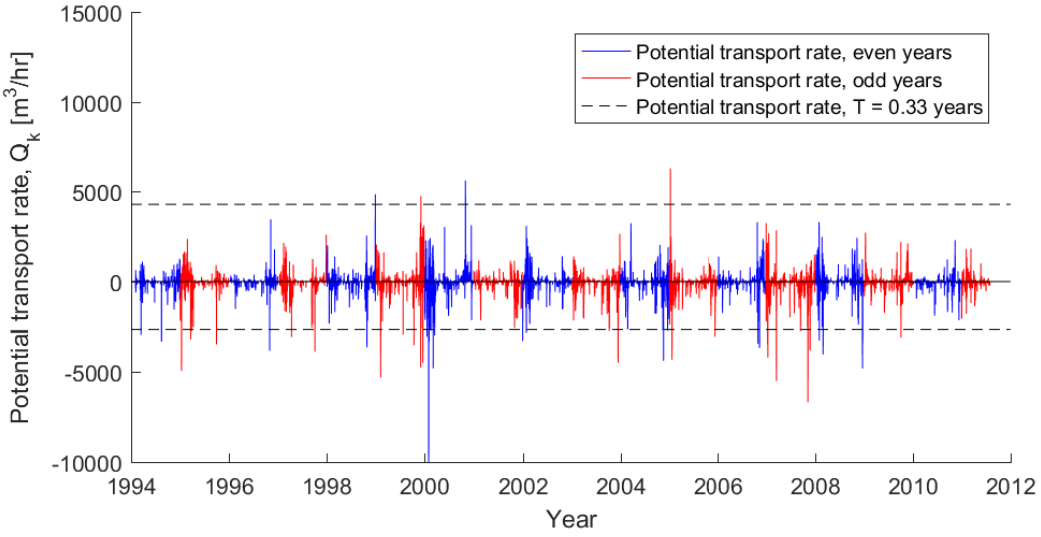

Figure 5.2 Sediment transport at the Agger tongue. Positive values denote northbound transport.

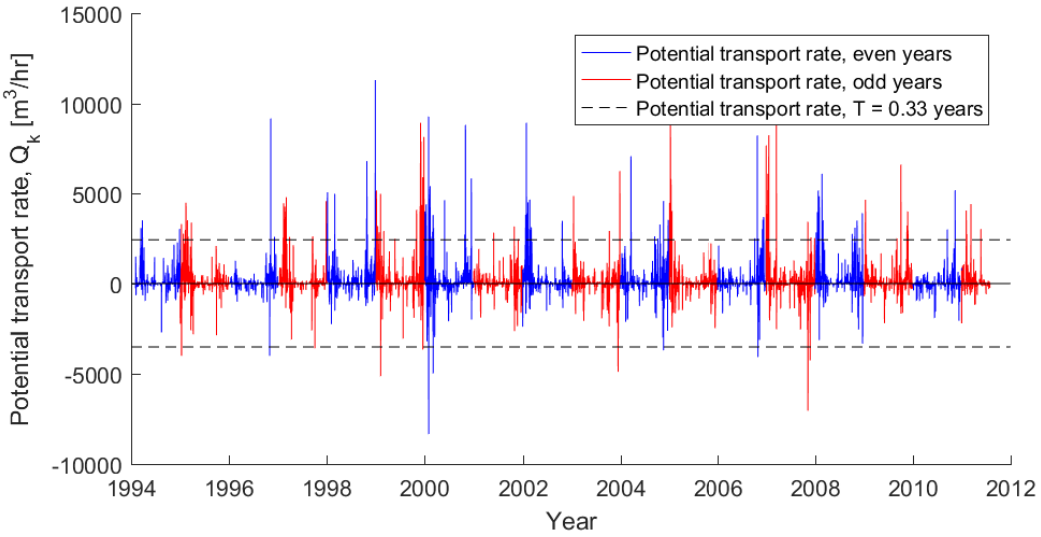

Figure 5.3 Sediment transport at the Harboøre tongue. Positive values denote northbound transport.

The transport rates shown in Figures 5.2 and 5.3 vary due to the difference in the waves' angle of attack relative to the coastline. Similarly, a storm from WNW may cause a negative transport on the Agger tongue, but a positive one on the Harboøre tongue as the tongues curve inward towards Thyborøn Channel like a funnel. Figures 5.4 and 5.5 show sediment transport roses of the tongues. As expected from Figure 2.5, it is evident that the net transport from both tongues is towards Thyborøn Channel.

Figures 5.2 and 5.3, however, do not show the influence of wave direction, height, and period. Therefore wave scatter diagrams similar to Table 5.1 have been created for each direction. They can be seen in Appendix F. As an example, the number corresponding to $T_p = 12\,\text{s}$ and $H_{m0} = 2.5\,\text{m}$ is the percentage of waves coming from W with $T_p \in (11, 12]$ and $H_{m0} \in (2, 2.5]$, relative to the

total amount of waves in the data.

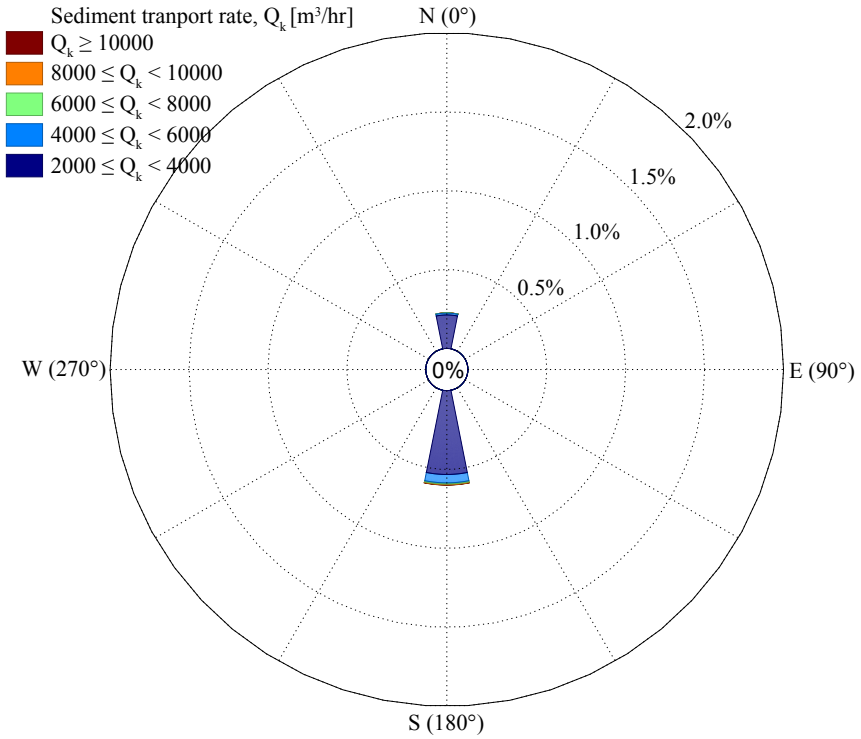

Figure 5.4 Rose of potential sediment transport rates at the Agger tongue.

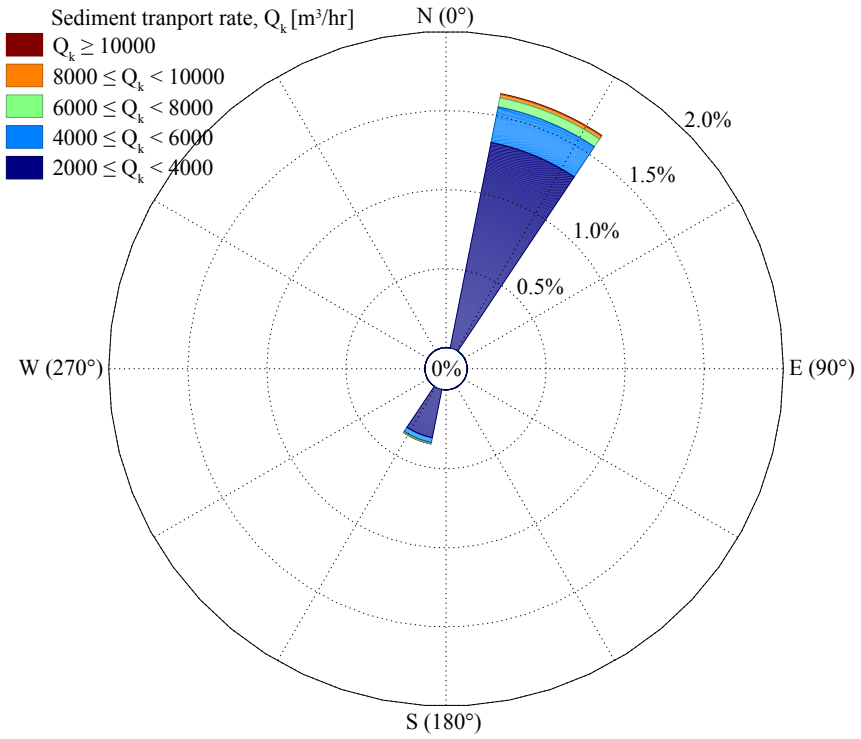

Figure 5.5 Rose of potential sediment transport rates at the Harboøre tongue.

Table 5.1 Scatter matrix of waves from W.

W	Peak period, T_p [s]																								
Significant wave height, H_{m0} [m]	1	2	3	4	5	6	7	8	9	10	11	12	13	14	15	16	17	18	19	20	21	22	23	24	25
0.5	-	0.00	0.01	0.05	0.38	0.09	0.04	0.06	0.11	0.06	0.08	0.06	0.03	0.02	0.02	0.00	0.00	0.00	0.00	-	-	0.00	-	-	-
1.0	-	-	0.00	0.12	0.65	1.07	0.56	0.18	0.10	0.10	0.16	0.16	0.15	0.11	0.06	0.05	0.02	0.02	0.01	0.01	-	0.00	0.00	-	-
1.5	-	-	-	0.00	0.14	0.69	0.99	0.75	0.19	0.08	0.07	0.07	0.09	0.10	0.16	0.08	0.05	0.03	0.01	0.01	0.00	0.00	-	-	-
2.0	-	-	-	-	0.00	0.13	0.68	0.88	0.59	0.13	0.04	0.04	0.03	0.03	0.04	0.03	0.02	0.02	0.00	0.01	-	-	-	-	-
2.5	-	-	-	-	-	0.00	0.18	0.49	0.62	0.26	0.06	0.02	0.02	0.01	0.00	0.01	0.01	0.00	0.01	0.01	0.01	-	-	-	-
3.0	-	-	-	-	-	-	0.01	0.18	0.42	0.36	0.08	0.01	0.00	0.01	0.00	0.00	0.00	-	0.00	0.01	0.00	-	-	-	-
3.5	-	-	-	-	-	-	-	0.02	0.18	0.38	0.10	0.02	0.01	-	-	-	-	-	0.00	-	-	-	-	-	-
4.0	-	-	-	-	-	-	-	0.00	0.03	0.21	0.16	0.03	0.01	-	0.00	-	-	-	-	-	-	-	-	-	-
4.5	-	-	-	-	-	-	-	-	0.00	0.06	0.15	0.05	0.00	0.00	-	-	-	-	-	-	-	-	-	-	-
5.0	-	-	-	-	-	-	-	-	0.00	0.01	0.07	0.07	0.01	0.00	-	-	-	-	-	-	-	-	-	-	-
5.5	-	-	-	-	-	-	-	-	-	0.00	0.01	0.04	0.01	0.00	0.00	-	-	-	-	-	-	-	-	-	-
6.0	-	-	-	-	-	-	-	-	-	-	0.00	0.01	0.02	0.01	0.00	-	-	-	-	-	-	-	-	-	-
6.5	-	-	-	-	-	-	-	-	-	-	-	0.00	0.01	0.00	0.00	-	-	-	-	-	-	-	-	-	-
7.0	-	-	-	-	-	-	-	-	-	-	-	-	-	-	0.00	-	-	-	-	-	-	-	-	-	-

Tables 5.2 and 5.3 are created by multiplying each entry of the scatter matrix by the sediment transport rate expected from the given combination of T_p and H_{m0}. Thus, they show a weighted expected sediment transport which is a measure of what sea states are expected to contribute most to the average transport in the area. In the case shown for the Agger tongue in Table 5.2, most sediment is expected for sea states with $H_{m0} \in (3.0, 3.5]$ and $T_p \in (9, 10]$. Appendix F shows the scatter matrices and weighted potential sediment transport matrices for different compass directions.

Table 5.2 Weighted potential sediment transport matrix of waves from W at the Agger tongue. All transport values are in 10^5 m^3/hour. Positive values denote northbound transport.

W	Peak period, T_p [s]																								
Significant wave height, H_{m0} [m]	1	2	3	4	5	6	7	8	9	10	11	12	13	14	15	16	17	18	19	20	21	22	23	24	25
0.5	-	0.0	0.0	0.0	0.0	0.0	0.0	0.0	0.0	0.0	0.0	0.0	0.0	0.0	0.0	0.0	0.0	0.0	0.0	-	-	0.0	-	-	-
1.0	-	-	0.0	0.1	0.6	1.3	0.8	0.3	0.2	0.2	0.4	0.4	0.5	0.4	0.2	0.2	0.1	0.1	0.0	0.1	-	0.0	0.0	-	-
1.5	-	-	-	0.0	0.4	2.4	4.0	3.5	1.0	0.5	0.5	0.6	0.8	0.9	1.7	1.0	0.7	0.4	0.1	0.2	0.0	0.0	-	-	-
2.0	-	-	-	-	0.0	0.9	5.4	8.0	6.1	1.6	0.5	0.6	0.6	0.6	0.9	0.7	0.5	0.5	0.1	0.5	-	-	-	-	-
2.5	-	-	-	-	-	0.1	2.4	7.3	10.7	5.1	1.3	0.4	0.5	0.2	0.1	0.2	0.3	0.1	0.5	0.9	0.6	-	-	-	-
3.0	-	-	-	-	-	-	0.2	4.0	10.9	10.5	2.7	0.6	0.2	0.4	0.1	0.1	0.1	-	0.1	0.9	0.3	-	-	-	-
3.5	-	-	-	-	-	-	-	0.8	6.6	15.4	4.7	1.0	0.4	-	-	-	-	-	0.1	-	-	-	-	-	-
4.0	-	-	-	-	-	-	-	0.1	1.4	11.2	10.1	2.0	0.5	-	0.1	-	-	-	-	-	-	-	-	-	-
4.5	-	-	-	-	-	-	-	-	0.1	4.0	11.9	4.1	0.2	0.1	-	-	-	-	-	-	-	-	-	-	-
5.0	-	-	-	-	-	-	-	-	0.1	0.7	6.5	7.6	0.8	0.2	-	-	-	-	-	-	-	-	-	-	-
5.5	-	-	-	-	-	-	-	-	-	0.1	1.3	5.4	2.0	0.6	0.1	-	-	-	-	-	-	-	-	-	-
6.0	-	-	-	-	-	-	-	-	-	-	0.5	2.0	4.0	1.6	0.8	-	-	-	-	-	-	-	-	-	-
6.5	-	-	-	-	-	-	-	-	-	-	-	0.3	1.3	0.8	0.2	-	-	-	-	-	-	-	-	-	-
7.0	-	-	-	-	-	-	-	-	-	-	-	-	-	-	0.2	-	-	-	-	-	-	-	-	-	-

Tables 5.1, 5.2, and 5.3 show the common tendency that, on average, the majority of sediment transport occurs during rough seas, but not the largest storms as they are less frequent. However, large storms may cause destabilization of dunes dramatically increasing sediment transport.

Table 5.3 Weighted potential sediment transport matrix of waves from W at the Harboøre tongue. All transport values are in 10^5 m^3/hour. Positive values denote northbound transport.

W	Peak period, T_p [s]																								
Significant wave height, H_{m0} [m]	1	2	3	4	5	6	7	8	9	10	11	12	13	14	15	16	17	18	19	20	21	22	23	24	25
0.5	-	0.0	0.0	0.0	0.1	0.0	0.0	0.0	0.1	0.0	0.1	0.1	0.0	0.0	0.0	0.0	0.0	0.0	0.0	-	-	0.0	-	-	-
1.0	-	-	0.0	0.3	2.0	4.2	2.6	1.0	0.6	0.7	1.2	1.4	1.5	1.2	0.7	0.7	0.4	0.3	0.1	0.2	-	0.0	0.0	-	-
1.5	-	-	-	0.0	1.2	7.6	12.8	11.1	3.1	1.4	1.6	1.8	2.6	2.9	5.3	3.2	2.1	1.2	0.4	0.5	0.1	0.0	-	-	-
2.0	-	-	-	-	0.1	2.8	17.2	25.3	19.3	4.9	1.6	2.0	1.8	1.7	2.8	2.3	1.5	1.5	0.4	1.4	-	-	-	-	-
2.5	-	-	-	-	-	0.2	7.5	23.2	33.8	16.1	4.2	1.2	1.5	0.8	0.3	0.6	0.9	0.4	1.5	2.7	1.8	-	-	-	-
3.0	-	-	-	-	-	-	0.7	12.6	34.4	33.1	8.5	1.8	0.6	1.2	0.3	0.2	0.3	-	0.2	2.6	1.0	-	-	-	-
3.5	-	-	-	-	-	-	-	2.5	20.9	48.5	14.6	3.0	1.3	-	-	-	-	-	0.2	-	-	-	-	-	-
4.0	-	-	-	-	-	-	-	0.3	4.3	35.3	31.5	6.1	1.6	-	0.2	-	-	-	-	-	-	-	-	-	-
4.5	-	-	-	-	-	-	-	-	0.4	12.6	37.4	13.0	0.6	0.2	-	-	-	-	-	-	-	-	-	-	-
5.0	-	-	-	-	-	-	-	-	0.3	2.1	20.2	23.7	2.6	0.6	-	-	-	-	-	-	-	-	-	-	-
5.5	-	-	-	-	-	-	-	-	-	0.2	4.2	17.0	6.3	1.8	0.4	-	-	-	-	-	-	-	-	-	-
6.0	-	-	-	-	-	-	-	-	-	-	1.5	6.4	12.4	5.1	2.4	-	-	-	-	-	-	-	-	-	-
6.5	-	-	-	-	-	-	-	-	-	-	-	0.8	4.0	2.5	0.6	-	-	-	-	-	-	-	-	-	-
7.0	-	-	-	-	-	-	-	-	-	-	-	-	-	-	0.6	-	-	-	-	-	-	-	-	-	-

5.3 Choice of storms for further modelling

Ideally when assessing sedimentation at a site, both long and short periods should be investigated as short term sediment transport rates differ drastically from long term ones. However due to time limitations only short periods can be modelled in this project, therefore storms are considered.

From the tendencies investigated with the Kamphuis formula it is seen that storms account for the largest sediment transport rates. As such a 20 year rough weather period is modelled to assess the sediment transport in the area. As it is also important to analyse what happens in the area during less extreme events a second storm with a return period of a three per year is chosen.

When choosing storms for further simulations, certain considerations have to be made. Firstly, as wind data is only available for 2005 the number of available storms is reduced considerably. Secondly, the storm should generate transport, which interesting conclusions about the area can be drawn from. In this case two storms are chosen, one expected to cause common sediment transport and one which stresses the limits of the area. On this basis the periods highlighted in Figures 5.6, 5.7, and Table 5.4 are chosen. The return periods are based on the 17 years of wave data presented in Chapter 4.3, which introduces some uncertainty on the 20 year storm. The milder storm is chosen, partially based on its flow direction being opposite the large storm's, and partially because the average significant wave height and peak period resemble the ones shown by the weighted sediment transport matrices to cause the largest transport over time.

Table 5.4 Chosen simulation periods.

Predicted sediment transport	Simulated period	Return period of storm
Large	07/01-05 20:00 - 10/01-05 20:00	20 years
Medium	12/12-05 12:00 - 16/12-05 12:00	0.33 years

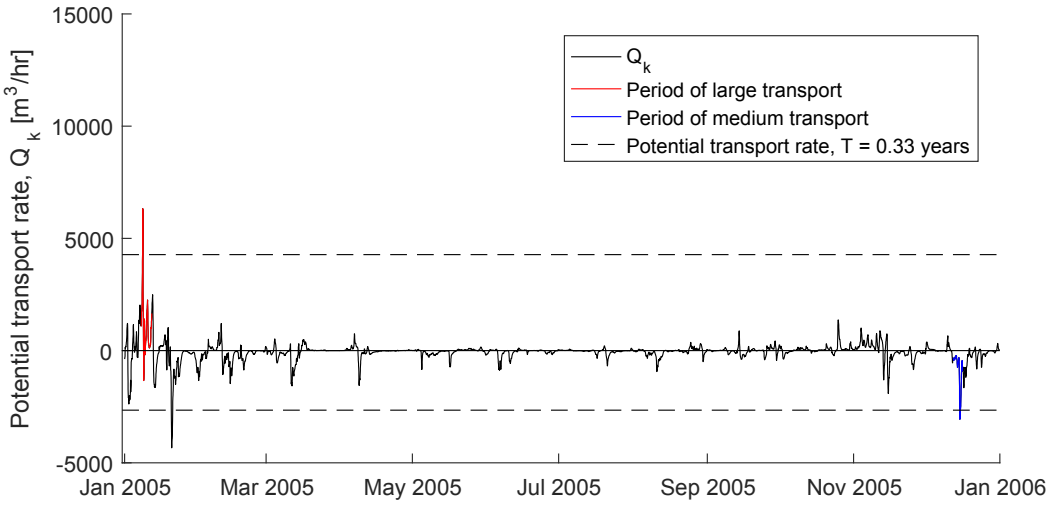

Figure 5.6 Predicted transport during periods chosen for further modelling. Agger tongue.

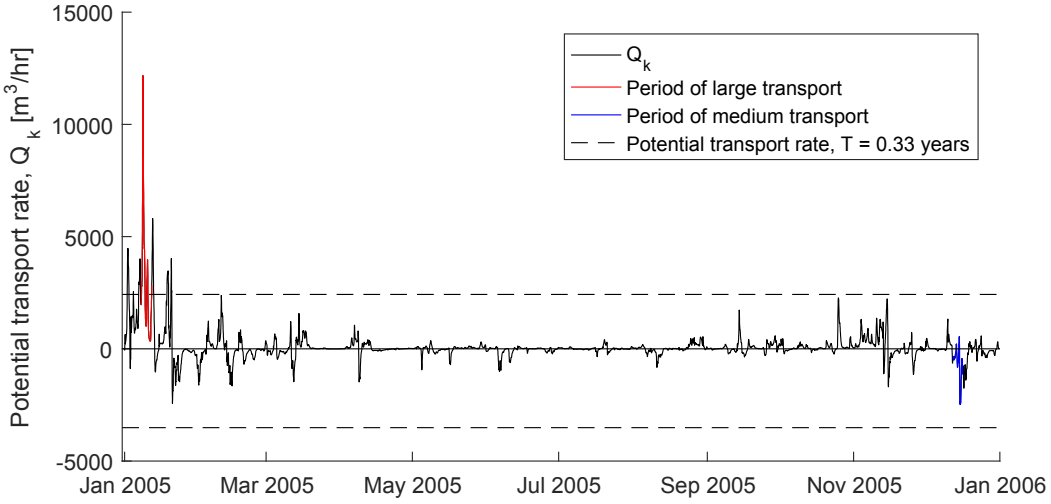

Figure 5.7 Predicted transport during periods chosen for further modelling. Harboøre tongue.

The storms chosen are named after the month of their occurrence. Thus, the large storm is called the January storm and the milder one is called the December storm. Figures 5.8 and 5.9 show the wind series of the January and December storms, respectively. The exact start and ending times are chosen to ensure relatively calm weather in the beginnings and ends of the simulation periods.

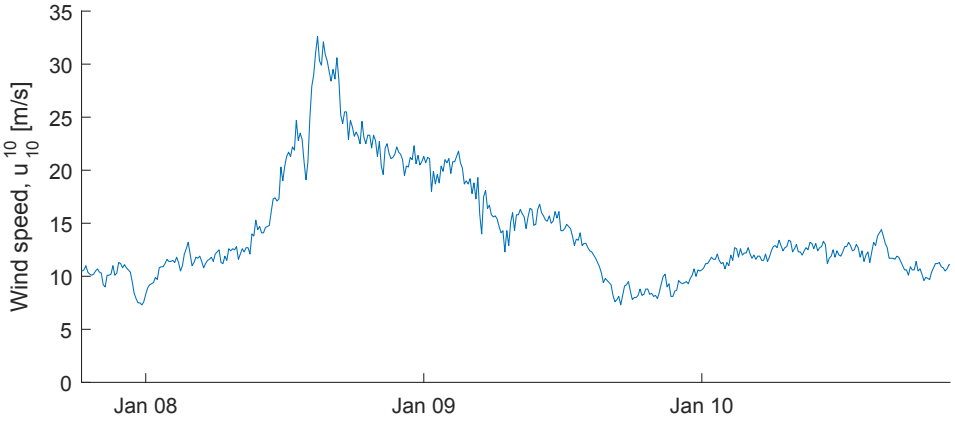

Figure 5.8 Wind series of the severe January storm.

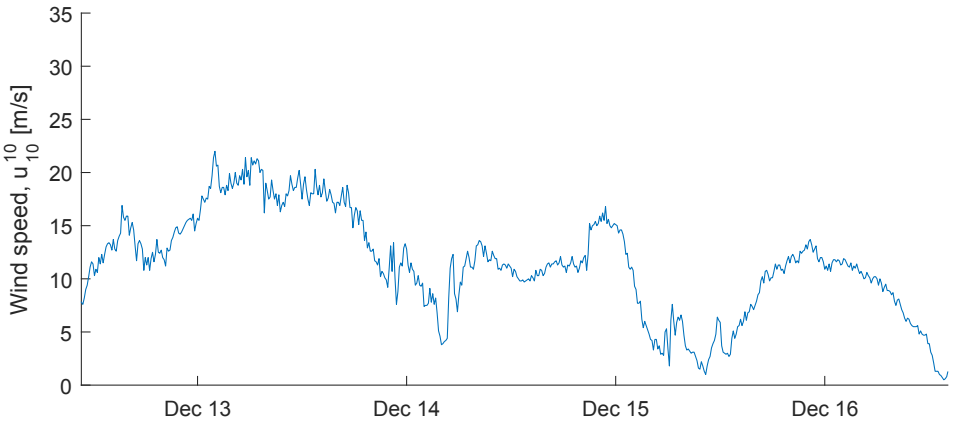

Figure 5.9 Wind series of the relatively mild December storm.

5.4 Generation of BC for the Thyborøn model

To avoid modelling the inside of the Limfjord repeatedly, a separate model is developed for the fjord using only the HD module. From this model flow velocities are extracted corresponding to the boundary that separates the main model from the Limfjord. The principle is explained in Chapter 3.3.

5.4.1 Limfjord model set-up

As flow dominates the problem, high order time integration and space discretion schemes are used in the HD module [DHI, 2017]. The time step in both the transport and shallow water equations is chosen automatically by the model from an interval of 0.01-30 s to satisfy the imposed CFL-condition of CFL < 0.8. Barotropic density is employed in order to save computational time. A Smagorinsky formulation is used for turbulence modelling.

Flooding and drying is implemented meaning that as the water level becomes shallower, the problem is reformulated and finally the cell is removed from the calculation. The reformulation sets the momentum fluxes to zero only taking into account mass fluxes. As the water depth increases the problem is reformulated to the original equations. Since the ST module is not activated in the Limfjord model, no bed change occurs. Thus, only changes in surface elevation can trigger the flood and dry mechanics.

Domain

Soundings are interpolated from a grid of 50 m east of Løgstør and 100 m west of Løgstør and off the west coast. Figure 5.10 shows the interpolated bathymetry. There is no depth cut-off as flood and dry is enabled. Thyborøn Harbour is not included in the modelling which could affect the flow in the channel but the impact is considered small enough to not interfere considerably with the results.

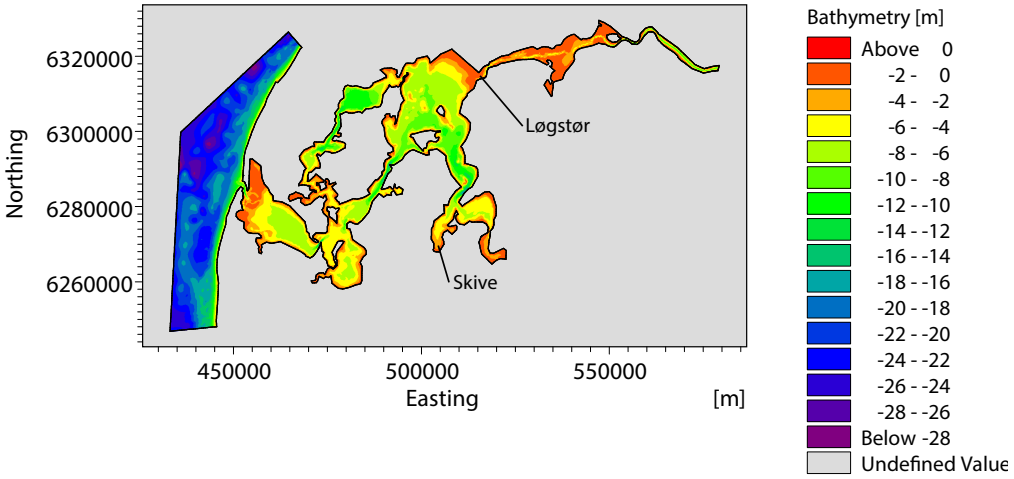

Figure 5.10 Bathymetry used for simulations of flow velocities in the Limfjord. Various models include less of the west coast.

The bottom stress, $\vec{\tau_b}$, caused by the roughness of the sea bed is implemented using a quadratic friction law shown in Equation(5.2). The Nikuradse roughness height is used as a calibration factor that accounts for bed roughness and is thus not necessarily physically realistic.

$$\begin{aligned} \frac{\vec{\tau_b}}{\rho_0} &= c_f \vec{u}_b |\vec{u}_b| \\ c_f &= \frac{g}{(Mh^{1/6})^2} \\ M &= \frac{25.4}{k_s^{1/6}} \end{aligned} \tag{5.2}$$

where

$\overrightarrow{\tau_b}$	Seabed stress
ρ_w	Density of water
c_f	Drag coefficient between seabed and water
$\overrightarrow{u}_b$	Flow velocity at the seabed
M	Manning number
g	Gravitational acceleration
h	Water depth
k_s	Nikuradse roughness height

Boundary conditions and forcings

Figure 5.11 illustrates the use of surface elevation time series from Thyborøn and Hals Harbour as boundary conditions on their respective ends of the Limfjord. The boundary condition at Thyborøn is asserted a bit into the North Sea to avoid shock waves in the channel.

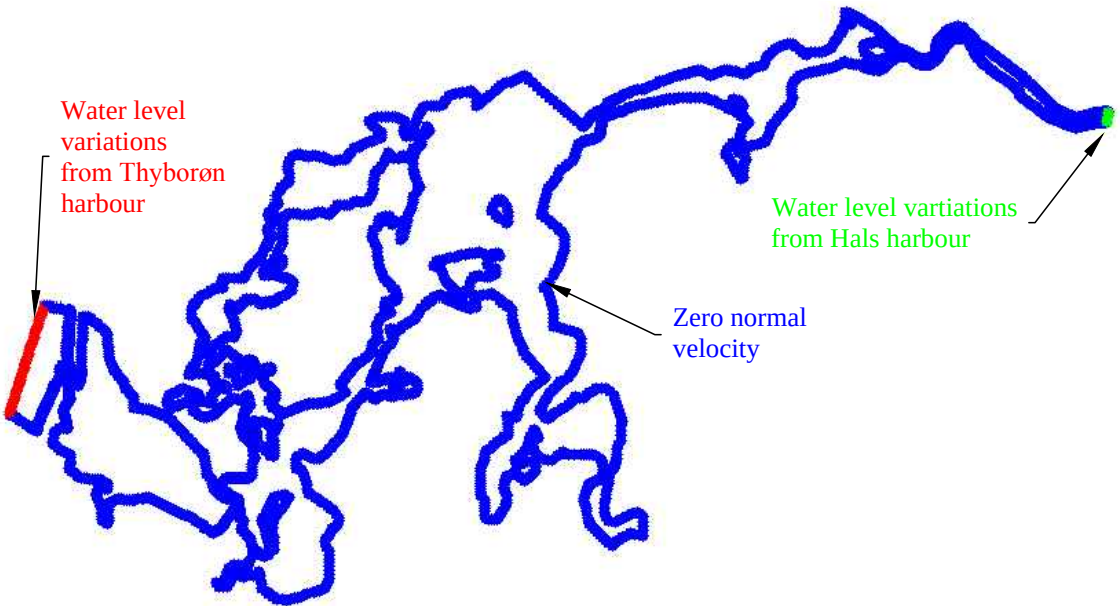

Figure 5.11 Illustration of the boundary conditions applied in the Limfjord model.

The Limfjord model is forced using a wind series measured at Thyborøn described in Chapter 4.1. The wind speed and direction is assumed constant throughout the Limfjord at each time step which introduces some model uncertainty, but during storms large low pressure areas lead to similar wind directions and speeds over large areas which supports the assumption [Ahrens, 2012].

Concerning friction between air and water, Nørgaard et al. [2014] suggests that a drag coefficient, c_d, linearly varying with wind speed best models the area. Drag coefficients of 0.002 and 0.005

are implemented at 7 and 25 m/s, respectively. The stress exerted by wind on the surface, $\overline{\tau_s}$ is modelled through the empirical relation [DHI, 2017]:

$$\overline{\tau_s} = \rho_a c_d |u_w| \overline{u_w} \tag{5.3}$$

where

$\overline{\tau_s}$	Surface stress
ρ_a	Density of air
c_d	Empirical drag coefficient of air
$\overline{u_w}$	$= (u_v, v_v)$, wind speed 10 m above surface

Coriolis and tidal forces are taken into account, however infiltration, wave radiation, and precipitation/evaporation are all assumed zero for the problem at hand as they are not expected to influence the flow significantly.

5.4.2 Calibration

To better assure accuracy of the model during peak velocities the storm of January 2005 is used for calibration. Time series of surface elevation variations for Løgstør and Skive are used for reference in the calibration. Figure 5.10 shows the locations the model is calibrated to. Even though flow velocities are the sought output from the model, it is calibrated to surface elevations. This is done as only surface elevation data, described in Chapter 4.2, is available for the Limfjord. The reasoning behind this choice is described in Chapter 3.3. In short, if the Limfjord is seen as a straight, differences in water level governs the flow.

When calibrating the model different factors including mesh density, mesh shape, bed resistance, and boundary conditions are varied. Table 5.5 shows a selection of the different combinations of input modelled. Lim27 features a larger roughness in the narrow Aggersund near Løgstør to simulate the effect of the narrows on water flow.

Table 5.5 Combinations of input used during calibration of the Limfjord model. The different meshes can be seen in Appendix G.

Model name	Mesh version	Roughness height, k_s [m]
Lim24	V5	0.9
Lim27	V6	0.9 & 6.8
Lim30	V6	0.9
Lim32	V7	0.9
Lim33	V8	0.9

Meshes and boundary conditions modelled

As show in Table 5.5 different meshes are modelled for calibration. The meshes can be seen in Appendix G. The differences between the meshes and their boundary conditions are:

V5: A large part of the west coast was included to investigate the effect on the water flow into Thyborøn Channel. It was found to be excessive and therefore reduced in later iterations. The water level variations at Thyborøn were applied at the entrance to the channel and zero water level change was imposed on the North Sea boundary. The other boundary condition are as specified in Figure 5.11.

V6: Significantly less of the west coast is modelled and much coarser. Boundary conditions are applied as illustrated in Figure 5.11.

V7: Larger density was employed in narrow parts like Thyborøn Channel, Aggersund at Løgstør, and Oddesund east of Nissum Bredning. Boundary conditions are applied as illustrated in Figure 5.11.

V8: An even denser mesh in order to check convergence. Boundary conditions are applied as illustrated in Figure 5.11.

Calibration results and discussion

Figures 5.12 and 5.13 show the results of the models compared with the calibration basis.

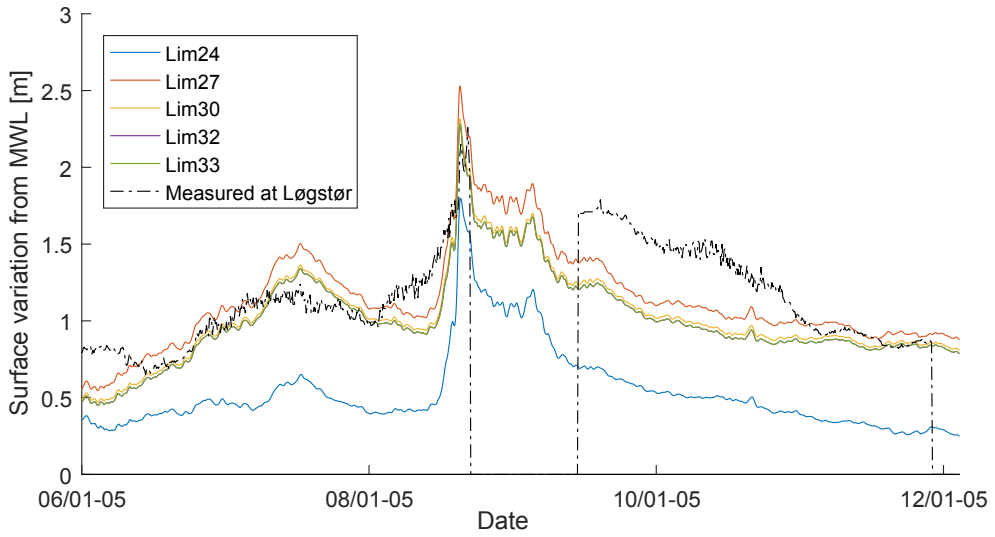

Figure 5.12 Surface elevation variation of the calibration simulations compared to measurements at Løgstør. Lim32 and Lim33 coincide.

Figure 5.12 shows good correlation between the measured surface elevation variations and the ones from model Lim33 at the peak of the storm. Furthermore, Lim30, Lim32, and Lim33 yield very similar results suggesting mesh density independence is obtained. The gap in the

measurements at Løgstør is unfortunate, but the model seem to predict the water level fairly well before and after the fall-out suggesting that it is also applicable to the period of missing data. Lim27 features a rougher sea bed east of Løgstør. This difference yields larger water levels at Løgstør as the water is slowed down in the narrows to the east.

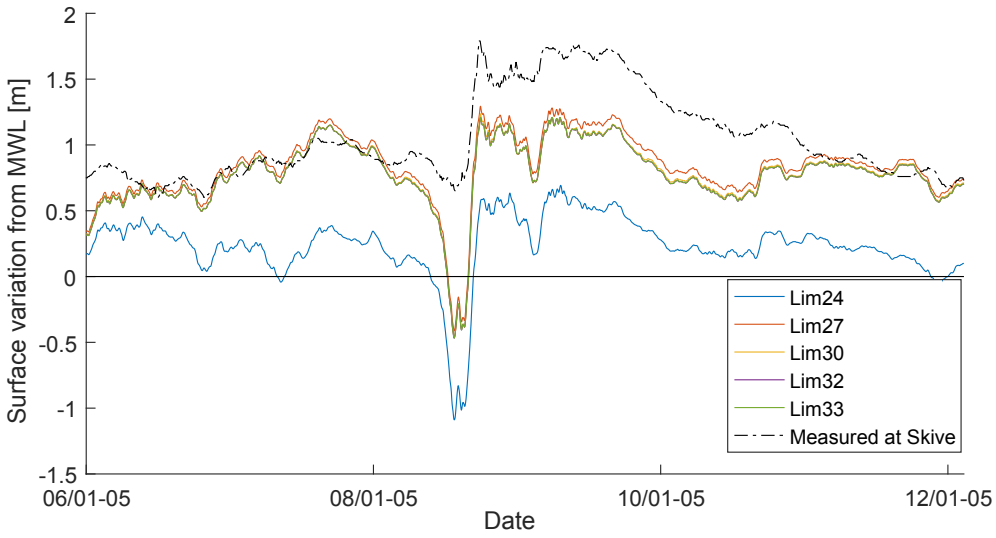

Figure 5.13 Surface elevation variation of the calibration simulations compared to measurements at Skive. Lim32 and Lim33 coincide.

Figure 5.13 shows a large difference between the model and calibration data just before the storm. As the discrepancy is not present at Løgstør it is likely caused by an uncertainty in the wind direction creating a wind set-down at Skive. Due to the discrepancy in wind direction, an analysis using only tidal variations is presented in Appendix H. The results are inconclusive due to difficulties isolating only the tides from the signal leading to an offset in phase, but the amplitudes are modelled acceptably.

Amplitudes are expected to affect the magnitude of velocities, whereas the phase influences *when* the flow rates occur. The discontinuities in the phase may be caused by the retraction of the boundary condition from Thyborøn Channel towards the sea. As amplitudes are modelled satisfactorily, model Lim32 is accepted for further use in the Thyborøn model for simulation of sedimentation on the west coast and in Thyborøn Channel.

Figure 5.14 is a comparison of the largest velocities found in the cross section between Nissum Bredning and Thyborøn Channel at each time step. Figure 5.15 compares the flow velocity across the same cross section at the peak of the storm. With the exception of model Lim24 there si little difference in the velocities from model to model, however Lim32 and Lim33 predict slightly larger flow than the rest. This further supports the choice of Lim32 as the best compromise between computational time and accuracy.

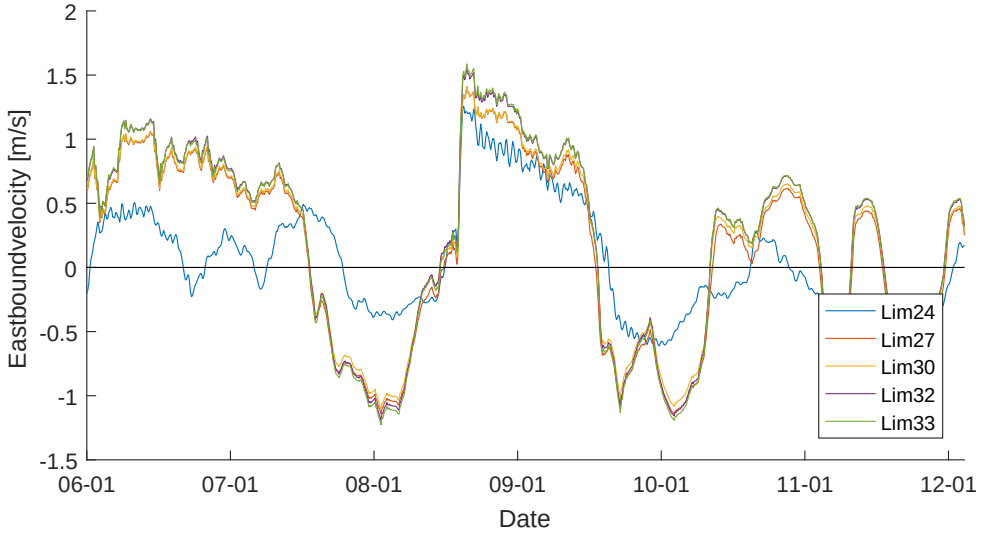

Figure 5.14 Comparison over time of velocities in the cross section between Thyborøn Channel and Nissum Bredning obtained from the different models.

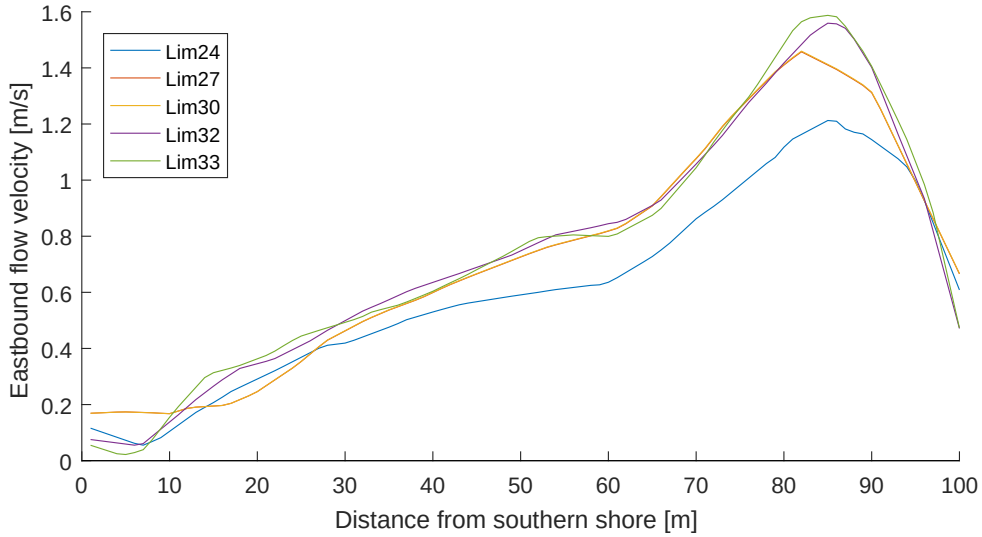

Figure 5.15 Comparison of velocities throughout the cross section between Thyborøn Channel and Nissum Bredning at the time of peak velocity. Lim27 and Lim30 coincide.

Comparing Figures 5.14 and 5.15 it is apparent that the change in bed resistance between Lim27 and Lim30 has a negligible impact on the flow at Thyborøn Channel. The change of mesh density between Lim32 and Lim33 does not change the flow velocities significantly, suggesting that the model is converged at Lim32.

Sediment modelling in the Thyborøn area 6

In this chapter the sediment flux in and around Thyborøn Channel is simulated using MIKE 21 coupling the HD, ST, and SW modules together. Firstly, the domain, boundary conditions, and key aspects of the model set-up are presented. Then results are presented and discussed based on comparison of sediment transport plots and tables.

6.1 Thyborøn model set-up

The model consists of the three modules HD, SW, and ST described in Chapter 3.2.1. They operate over the same domain and time constraints. The domain is described below and the simulated scenarios modelled are described in Chapter 5.3. The assumptions made in the different modules are described and discussed in Chapter 3.2.1.

Regarding time and spacial steps, they are related by the Courant-Friedrich-Lévy (CFL) number which is used in the stability criteria for the simulations. Thus, a spacial discretisation can be made and then the time step is determined from the condition of CFL < 0.8 given water depth and current velocity. Although computationally unrealistic, modelling each grain of sand individually could provide very precise results. Instead, a maximum element area is determined in order to balance precision and computational time. For the modelling in this project 2000 m^2 is set as the largest element area in the finer parts of the mesh. In practice though, many of the elements are smaller because automatic meshing of areas close to land with complicated geometry necessitate more nodes.

6.1.1 Domain and mesh

The bathymetry and mesh used in the Thyborøn reference model are shown in Figures 6.1 and 6.2, respectively. The bathymetries and meshes for the groyne extension and dam models are similar except for the extension of groyne 59. Thyborøn Harbour is not included in any of the models. The absence of the Harbour affects the flow and therefore the sediment transport in the channel. However, the impact on the difference between the models, which is what is compared in the results, should be small. Had the harbour been implemented, the resulting disturbance of the flow around the harbour would likely result in more sedimentation outside the port inlet. It proved necessary to increase the depth in the area just off the boundary at Nissum Bredning to avoid an

error in the model causing simulation halts. The dam is modelled as a straight line correlating with the boundary of the model.

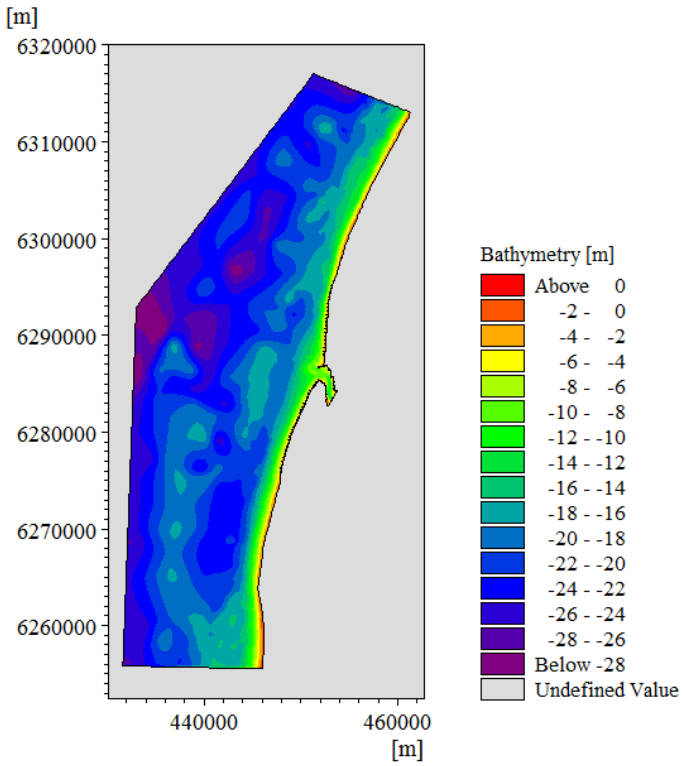

Figure 6.1 Bathymetry used in the reference Thyborøn model. The groyne extension model is the same bathymetry but with an added groyne corresponding to Figure 2.1.

The bathymetry shows some irregularities likely created by the interpolation of depths. These are averaged out during simulation as the ST module updates the bathymetry. The bathymetry has been "warmed up" by running a simulation of the January storm to simulate winter conditions and then extracting the final bathymetry for further simulations.

The mesh shown in Figure 6.2 is a cut-out of the whole mesh. This is done to better visualize the details of the channel. The dense mesh covers the beach to the end of the coastal protected zone. The mesh is denser at the place of interest and progressively coarser farther away. There are three different mesh densities, they increase fivefold for each step outwards. A mesh density analysis is documented in appendix I.

6.1.2 Spectral Wave module

To minimise computational time, only relevant wave directions are considered. These are identified from the wave series used as boundary condition as SSW through NNW for both storms. Bottom friction, white capping, wave breaking, and diffraction are all taken into account through default values. The wave data from Fjaltring is used as the seaward boundary condition. The

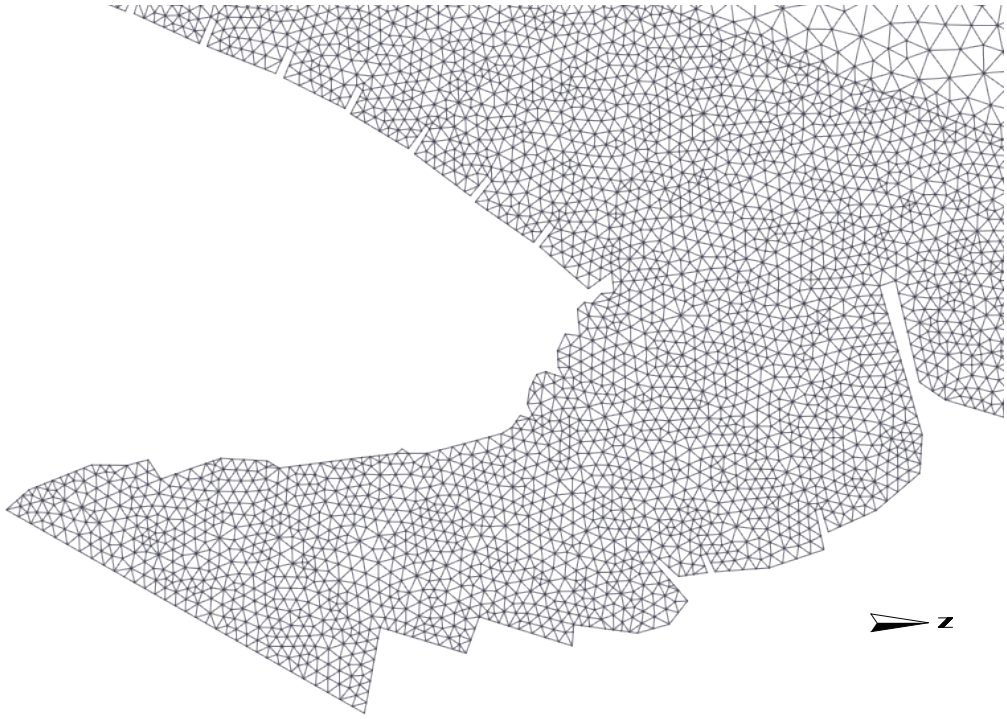

Figure 6.2 Cut-out of mesh used in the Thyborøn reference model.

channel and land boundaries are fully absorbing as shown in Figure 6.3. A soft start routine that linearly increases wave parameters from zero to the specified value over one hour, is employed to avoid shock waves.

6.1.3 Hydrodynamic module

Barotropic density, Smagorinsky formulation for eddy viscosity with a constant of 0.28, and a Nikuradse roughness height of 0.9 for bed resistance is all assumed. Coriolis and tidal forces are included in the model. As the simulated domain is relatively small, wind is assumed constant throughout the domain using the wind data from Thyborøn. This assumption is supported by the relatively constant wind speeds and directions caused by large low pressure areas during storms [Ahrens, 2012]. Friction coefficients between wind and sea are defined as in the Limfjord model; linearly varying from 0.002 at 7 m/s to 0.005 at 25 m/s. Figure 6.4 shows the boundary conditions imposed in the HD module for the different scenarios. The Nissum Bredning boundary condition is velocities and surface elevation variations from the Limfjord model for the reference and groyne extension model. For the dam model the boundary is considered shoreline as the sluice is closed during storms. Similarly to the SW module a soft start routine for the wind speed is employed to avoid shock waves.

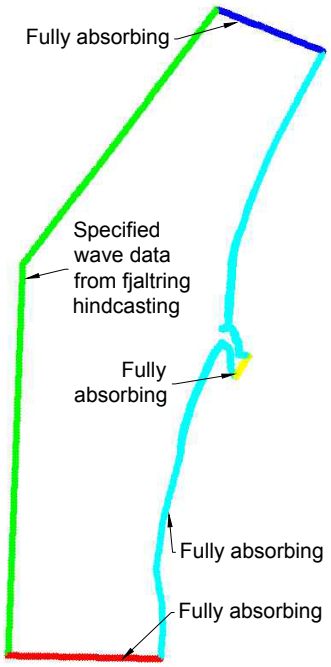

Figure 6.3 Boundary conditions used in the SW module of the Thyborøn model.

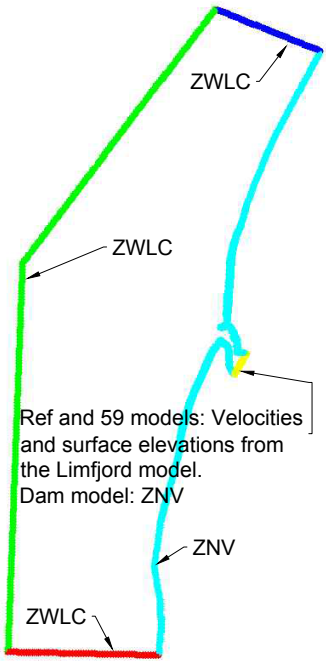

Figure 6.4 Boundary conditions in the HD module of the Thyborøn model. ZNV stands for "zero normal velocity", ZWLC is "zero water level change", and ZSFG is "zero sediment flux gradient".

6.1.4 Sand Transport module

The grain diameter is set to 0.15 mm with a grading coefficient of 1.1 and a porosity of 0.4. The grain diameter is assumed based on calibration of the Kamphuis formula to transport rates specified in Figure 2.5. The grading coefficient and porosity are default values. The sediment properties are assumed constant throughout the domain. Based on borings from Geus [2017], this assumption is rather crude. The borings suggest top soils ranging from clay to medium sand, but assuming only sand should lead to conservative results. Further, the database suggests that the sand layer is about 0.5-1 m in thickness. If more sediment transport is predicted by the model, the results are conservative. Figure 6.5 shows the boundary conditions for the different scenarios.

Figure 6.5 Boundary conditions used in the ST module of the Thyborøn model. ZSDG is "Zero sediment flux gradient".

6.1.5 Scenarios simulated in the Thyborøn model

The scenarios simulated in the Thyborøn model correspond to the January and December storms chosen (see Chapter 5.3) coupled with a reference bathymetry, a groyne 59 extension bathymetry, and a bathymetry for groyne 59 extension and addition of a dam. The results of the simulations are compared relative to the reference model in order to evaluate differences in sediment transport. This eliminates some of the modelling errors.

In order to investigate whether the simulation periods are long enough to ensure that the majority of the sediment transport has occurred, an additional simulation named JanRefLong is made. This simulation is based on the JanRef model, but the period is about eight days compared to three. The exact period is 05/01-05 03 am to 13/01-05 00 am. Thus, a total of seven simulations are made in the Thyborøn model (excluding convergence analysis).

Table 6.1 Scenarios simulated in the Thyborøn model.

Storm	Bathymetry	Duration	Scenario name
January	Reference	3 days	JanRef
	Groyne 59 extension	3 days	Jan59
	Groyne 59 extension & adding a dam	3 days	JanDam
December	Reference	3 days	DecRef
	Groyne 59 extension	3 days	Dec59
	Groyne 59 extension & adding a dam	3 days	DecDam
January	Reference	8 days	JanRefLong

6.2 Sediment results from short storm period simulations

The results generated by the simulated scenarios described in Chapter 6.1.5 are extracted in different forms. To get and overview of the area, results such as flow patterns and changes in bed level are extracted as color coded plots. To better assess the net transport locally, sediment transports are extracted along so-called *flux lines*. These lines are placed strategically to obtain knowledge on how much sediment enters the shipping lane outside the channel and where it goes from there. The rates are then summed through time and space during post processing in order to evaluate the sediment transport during storms. Further explanation of the flux lines is given in Chapter 6.2.3 where their results are presented and discussed.

The results section for the sediment modelling at Thyborøn consists of the following parts; Firstly,

bed level changes to the bathymetries caused by the storms are analysed. Then, local transport is assessed by comparing the transport across the flux lines in the different simulations. Hereafter, a simulation of a longer period of the January storm is assessed to gauge the necessity of longer simulation periods. Finally, comments are made on the availability of erodible sediment in the area.

6.2.1 Bed level changes after the January storm

The large storm of January 2005 chosen in Chapter 5.3 has been simulated on the three bathymetries. Figures 6.6-6.8 show the accumulated total bed level changes caused by the January storm on the bathymetries. Figures J.1-J.5 show the flow fields for the January storm at the peak of the in- and outflows.

Figure 6.6 shows signs of inflow in the JanRef model rushing past the southern groynes eroding area I. Then, as the flow is led into the channel past groyne 59, it bends and slows down leading to sedimentation off groyne 59. Next, the flow erodes area II and carries the sediment with it to the sand banks in Nissum Bredning. During the rush back into sea (Figure J.2) after a set-up in the Limfjord, water is pushed past the harbour, eroding the entrance in area IV and depositing just north of it. Further north, the flow erodes the coast around area III before it reaches deep water west and north of it and deposits the sediment. These flows lead to erosion in the northern part of the inlet and accretion in the southern part. The sand pillow mentioned in Chapter 1.2 is enlarged in the simulation.

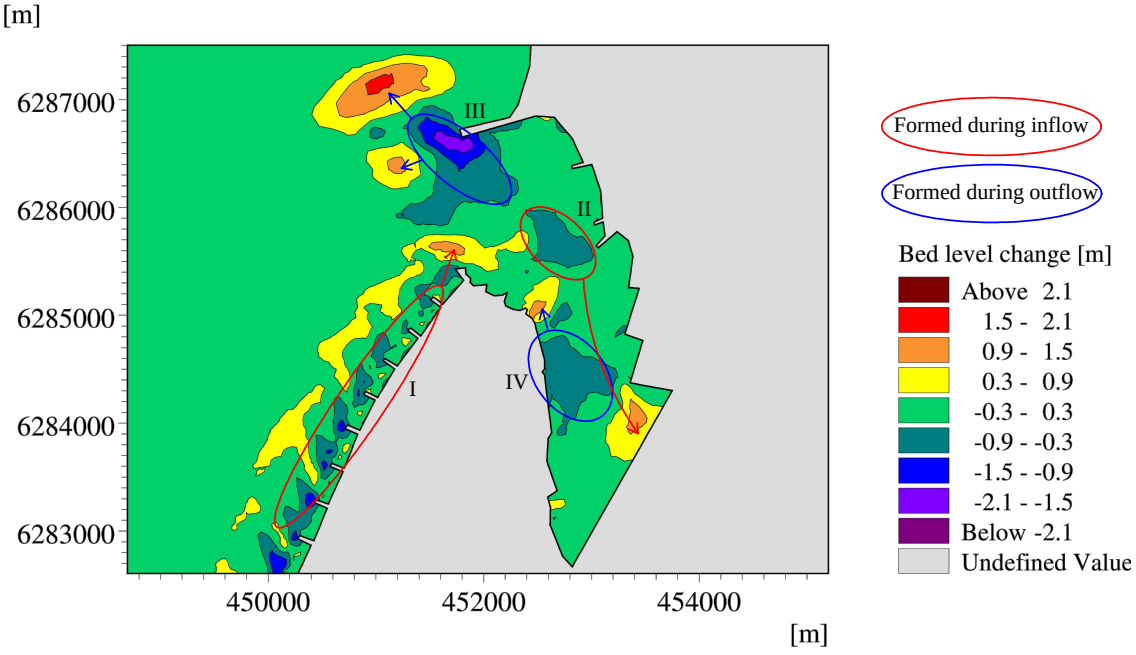

Figure 6.6 Accumulated bed level change of the reference bathymetry after the January storm.

Unlike in the reference model, the smaller opening in the groyne extension model shown in Figure 6.7 means that both in- and outflow lead to extensive erosion in area IV, the inlet. The reason is the increased current speed in the entrance seen in Figures J.3 and J.4. During inflow, sediment from area I and II settles outside the entrance while area IV deposits in the shipping lane inside the channel. During outflow, the sand pillow is enlarged from area III, while the sediment from area IV is led north. The sedimentation in the shipping lane could prove problematic for ships with large drafts.

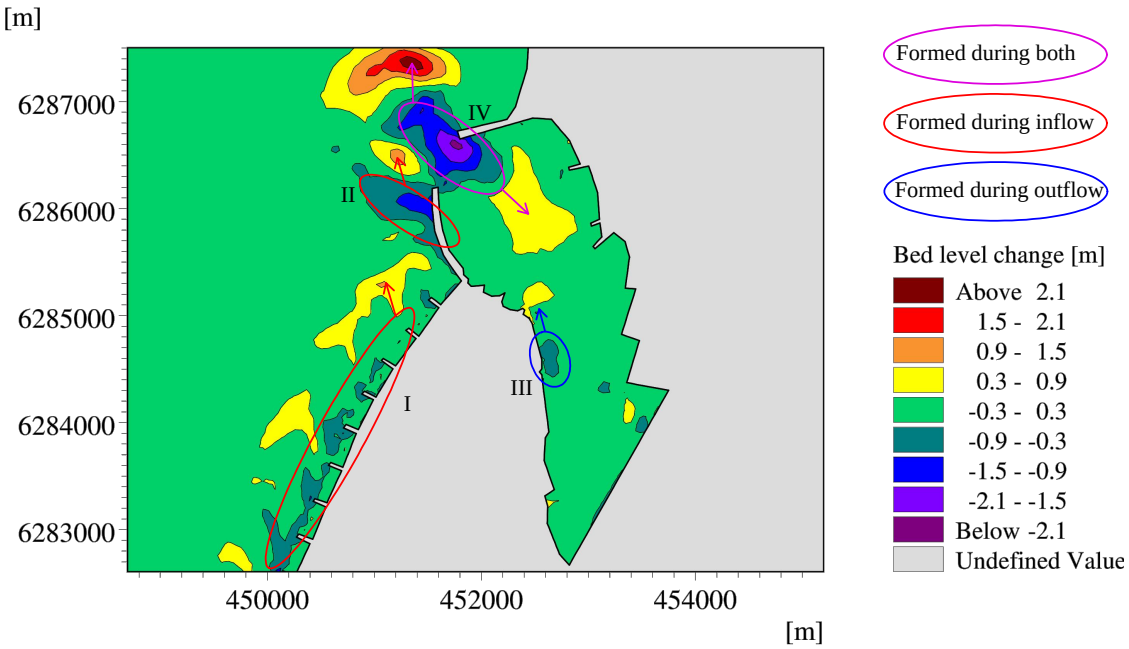

Figure 6.7 Accumulated bed level change of the groyne extension bathymetry after the January storm.

As opposed to the JanRef and Jan59 models, JanDam in Figure 6.8 shows no sedimentation in the channel. This is caused by the lack of flow through the channel as the sluice is closed during storms. JanDam does however show large sedimentation in the shipping lane from area II caused by the relatively low depth averaged current speed which could prove problematic for the maintenance of the channel depth.

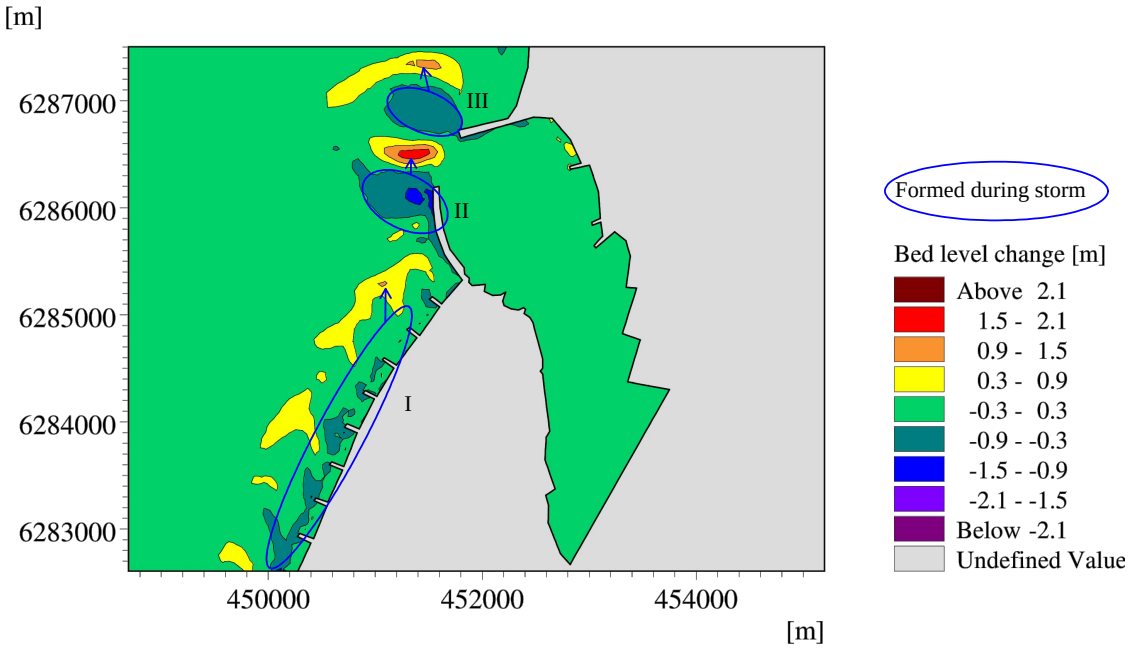

Figure 6.8 Accumulated bed level change of the dam bathymetry after the January storm.

6.2.2 Bed level changes after the December storm

The relatively mild storm of December 2005 chosen (see Chapter 5.3) has been simulated on the three bathymetries. The December storm causes the accumulated bed level changes seen in Figures 6.9-6.11 and the flow fields for in- and outflow shown in Figures J.6-J.10.

The flow close to shore in the DecRef model is accelerated around the northern groyne 72 picking up sediment in area III of Figure 6.9. After the groyne, the flow slows down depositing sediment just off the groyne. Then the flow accelerates again eroding area II as it is sucked into the channel. Apart from close to the Nissum Bredning boundary, where the depth was artificially increased as described in Chapter 6.1, the sedimentation from the December storm does not interfere with the main shipping lanes in the channel shown in Figure 1.2.

The accumulated bed level change in the Dec59 model in Figure 6.10, shows the same tendencies as the Jan59 model, only less prevalent due to the lower current speeds seen, when comparing Figures J.8 and J.3. Very little sediment transport is predicted further inside the channel and on the sand banks. This means less dredging is expected to be necessary in areas 2 (sand pillow) and 3 in Figure 1.2.

Figure 6.11 shows the accumulated change of bed level in the DecDam model. As expected, very little sediment transport is present inside the channel. As opposed to the January storm, however, the December storm does not cause sedimentation in the shipping lane outside the inlet. This is caused by the much lower current speeds seen, when comparing Figures J.10 and J.5. Large

sedimentation is seen at the tip of groyne 72 from area I, suggesting that prolonged exposure to the conditions of the December storm might lead to deposition of sediment in the inlet.

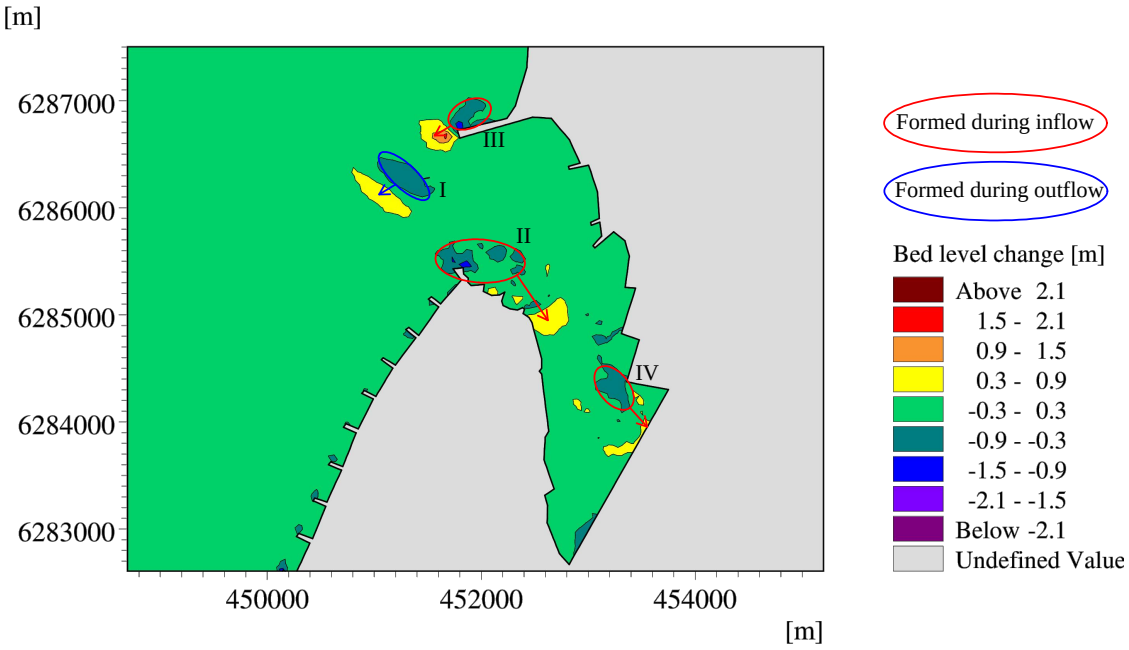

Figure 6.9 Accumulated bed level change of the reference bathymetry after the December storm.

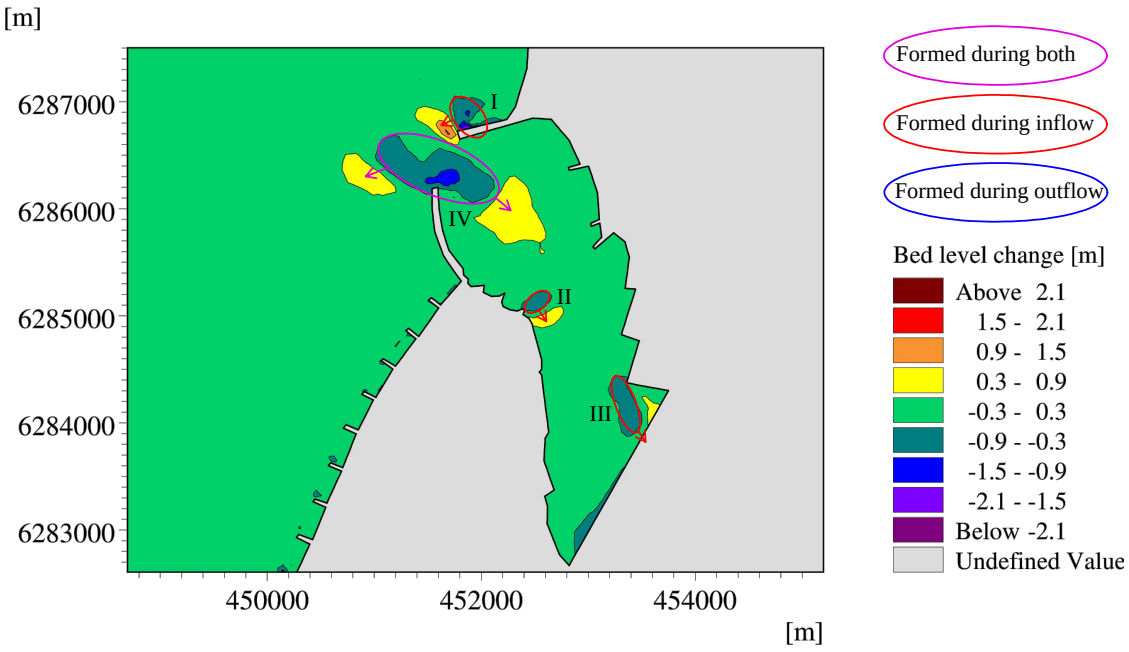

Figure 6.10 Accumulated bed level change of the groyne extension bathymetry after the December storm.

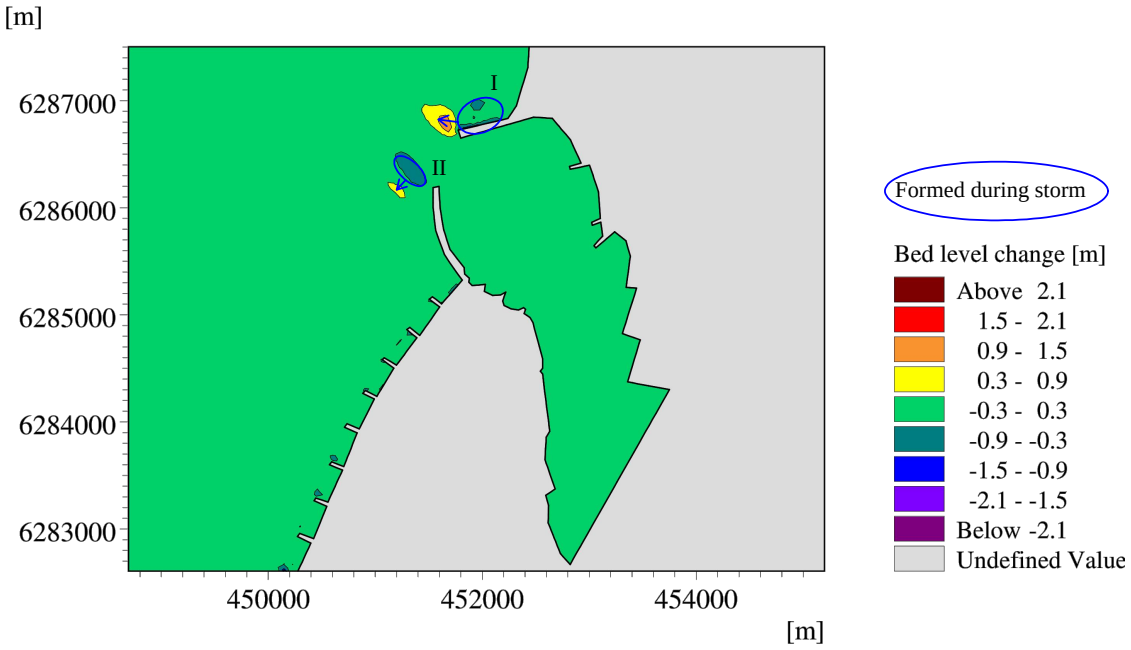

Figure 6.11 Accumulated bed level change of the dam bathymetry after the December storm.

6.2.3 Sediment transport across flux lines

Figures 6.12-6.15 show the accumulated net sediment transport across the described flux lines during the different storms on the different bathymetries. The net sediment transports recorded in the simulations are compared in Tables 6.2-6.7. The relative values are calculated based on reference values from one of the flux lines or simulations in each table. For example, the transport through the channel is relative to the sediment entering the channel through flux line 1a or 1b depending on the model. The reference is marked in each table.

The flux lines are placed as seen in Figures 6.12-6.15 to assess three main aspects of sediment transport in the area. (1) Flux lines 1a, 1b, 5a, 5b, and 6 are placed as shown to assess bypass past the shipping lane. (2) Flux lines 1a and 1b are placed in order to assess how much enters the channel. Flux line 2 is chosen in order to assess if potential sedimentation happens close to the inlet or further in. Flux line 3 is placed in order to investigate how much sedimentation is expected on the sand dunes in Nissum Bredning. (3) The last two flux lines, 4 and 7, are placed to assess the effect of the changed bathymetry on the sediment budget of the west coast.

The flux lines that are not limited in both ends, i.e. the ones on the west coast, are extended to a depth of ~20 m in order to include the near shore transport. Transport may also occur on deeper waters, but the majority travels along the shallows as described in Appendix B.

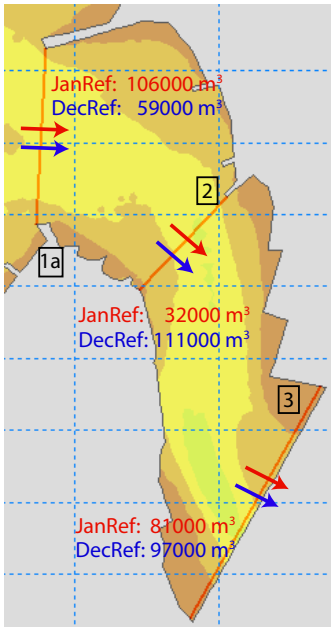

Figure 6.12 Accumulated net transport across flux lines in the channel of the reference model for both storms.

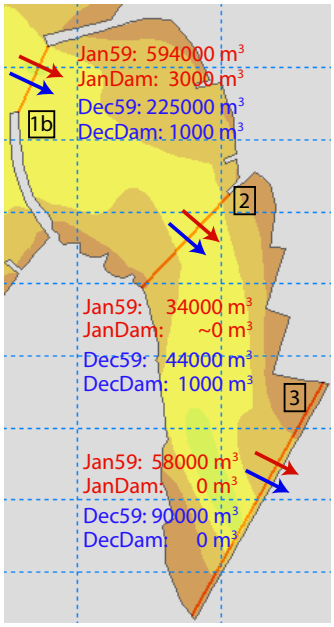

Figure 6.13 Accumulated net transport across flux lines in the channel of the groyne extension and dam models for both storms.

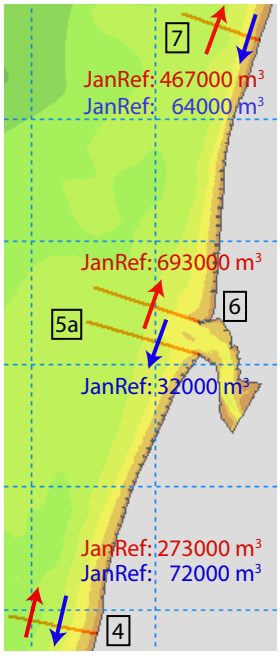

Figure 6.14 Accumulated net transport across flux lines on the west coast of the reference model for both storms.

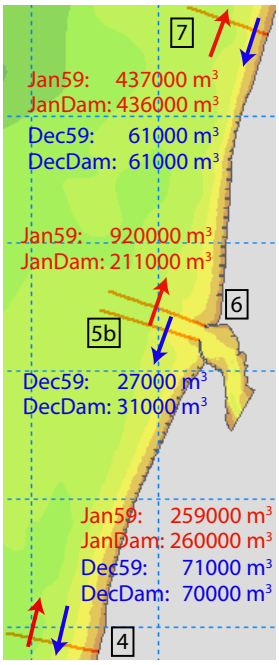

Figure 6.15 Accumulated net transport across flux lines on the west coast of the groyne extension and dam models for both storms.

Table 6.2 shows what happens to the sediment after it enters the shipping lane through flux line 5a/5b during the January storm. More sediment leaves than enters the shipping lane for both the JanRef and Jan59 models suggesting erosion in the lane during outflow (see Figures J.2 and J.4). Thus, what appears to be large bypasses in the JanRef and Jan59 models are not considered realistic, while the one in the JanDam model is. This conclusion supports what was found from the bed level change in Figures 6.6 and 6.7. The large transport into the channel in Jan59 compared to JanRef is likely caused by the increased flow velocity documented in Figures J.1 and J.3.

Table 6.2 Net sediment transport to and from the shipping lane and how much enters the channel during the January storm. See Figures 6.12-6.15 for flux line placements and transport directions.

Flux lines	Simulated acc. net transport [m^3]		
	JanRef	Jan59	JanDam
5a & 5b (Reference)	358000 (100 %)	880000 (100 %)	327000 (100 %)
1a & 1b	106000 (30 %)	594000 (67 %)	3000 (1 %)
6	693000 (190 %)	920000 (105 %)	211000 (64 %)

Table 6.3 shows the sediment transport across the flux lines in the channel shown in Figures 6.12 and 6.13. The results suggest that more sediment reaches the sand banks past flux line 3 than what passes the center at flux line 2. This is an inconsistency likely caused by a lack of available sediment transport from the Nissum Bredning boundary during outflow. An interesting tendency is seen in the Jan59 model; more sediment enters the channel due to the increased flow velocity in the inlet seen in Figure J.3 than in the reference model, but the amounts crossing flux line 2 are the same. This suggests that the extra transport settles just behind the entrance. The same tendency is seen in the bed level change of model Jan59 shown in Figure 6.7.

Table 6.3 Net sediment transport through Thyborøn Channel during the January storm. See Figures 6.12 and 6.13 for flux line placements and positive directions.

Flux lines	Simulated acc. net transport [m^3]		
	JanRef	Jan59	JanDam
1a & 1b (Reference)	106000 (100 %)	594000 (100 %)	3000 (100 %)
2	32000 (30 %)	34000 (6 %)	~0 (7 %)
3	81000 (76 %)	58000 (10 %)	0 (0 %)

Table 6.4 shows that similar amounts of sediment enters and exits the domain through flux lines 4 and 7 for the different models. This is likely because the effects of the transport changes at the channel do not reach flux line 7 during the short storm period. The similar transports across flux lines 4 and 7 also suggests that the channel has no effect on the current speeds far from the channel. The larger “bypasses” across flux line 6 of the JanRef and Jan59 models are caused by erosion of the inlet and channel during outflow leading to the conclusion that the actual bypasses of these models are much lower.

Table 6.4 Net sediment entering and leaving the domain during the January storm. See Figures 6.14 and 6.15 for flux line placements and transport directions.

Flux lines	Simulated acc. net transport [m^3]		
	JanRef (Reference)	Jan59	JanDam
4	273000 (100 %)	259000 (95 %)	260000 (95 %)
6	693000 (100 %)	920000 (132 %)	211000 (30 %)
7	467000 (100 %)	437000 (102 %)	436000 (102 %)

Table 6.5 shows the sediment transport across flux lines 1a, 1b, 5a, 5b and 6, during the milder December storm. The previously discussed tendency of the groyne extension model to erode the inlet and carry the sediment into the channel is present for the December storm as well. However, the outflow shown in Figure J.9 is not strong enough to initiate transport which leads to large net transport past flux line 1b into the channel. The remaining aspects of the table are more consistent with the expectations. The DecRef simulation shows some bypass, but mainly transport into the channel. The DecDam model, on the other hand, excels at bypassing sediment even though there is still some sedimentation in the shipping lane. As shown in Figure J.10 the flow velocities in the DecDam simulation are much lower than the others. This leads to less transport into the shipping lane, and as the transport out of it is comparable to the other models, the relative bypass is larger.

Table 6.5 Net sediment transport to and from the shipping lane and how much enters the channel during the December storm. See Figures 6.12-6.15 for flux line placements and transport directions.

Flux lines	Simulated acc. net transport [m^3]		
	DecRef	Dec59	DecDam
6 (Reference)	104000 (100 %)	104000 (100 %)	47000 (100 %)
1a & 1b	59000 (57 %)	225000 (215 %)	1000 (2 %)
5a & 5b	32000 (30 %)	26000 (25 %)	31000 (65 %)

Table 6.6 shows the sediment transport in the channel generated by the December storm. The Dec59 model shows large accretion in the area between flux lines 1b and 2 as expected from the accumulated bed level change seen in Figure 6.10. The lack of sediment transport into the domain through the eastern boundary is seen in the amount that passes flux line 3. Had the model received enough sediment from the boundary, the net transport would likely be lower. Regarding the DecDam model, very little sediment enters the channel, but the amount that does, is carried past flux line 2. In the DecRef model, the erosion of area II in Figure 6.9 is reflected in the increased transport past flux line 2 compared to 1a.

Table 6.6 Net sediment transport through Thyborøn Channel during the December storm. See Figures 6.12 and 6.13 for flux line placements and transport directions.

Flux lines	Simulated acc. net transport [m^3]		
	DecRef	Dec59	DecDam
1a & 1b (Reference)	59000 (100 %)	225000 (100 %)	1000 (100 %)
2	111000 (186 %)	44000 (20 %)	1000 (70 %)
3	97000 (162 %)	90000 (40 %)	0 (0 %)

Table 6.7 shows how much sediment enters and exits the domain during the December storm. As for the January storm, comparable amounts of sediment enters and leaves the domain. This is likely due to the effects of the sedimentation changes at the channel not reaching the area in the short period of the storm. The large bypass of the DecDam model is reflected in the results, especially considering the effects of the outflow on the transport downstream in the DecRef and Dec59 models discussed previously.

Table 6.7 Net sediment entering and leaving the domain during the December storm. See Figures 6.14 and 6.15 for flux line placements and transport directions.

Flux lines	Simulated acc. net transport [m^3]		
	DecRef (Reference)	Dec59	DecDam
7	64000 (100 %)	61000 (95 %)	61000 (95 %)
5a & 5b	32000 (100 %)	27000 (83 %)	31000 (96 %)
4	72000 (100 %)	71000 (99 %)	70000 (98 %)

6.3 Sediment results from long storm period simulation

As explained in Chapter 5.3, a simulation featuring an extended period on the reference bathymetry was made in order to investigate whether the relatively short simulation periods in the original analyses are sufficient. The simulation period is extended from three to eight days between 05/01-05 and 13/01-05. From the results, bed level changes for each day are extracted and plotted in Figures 6.16-6.23.

In the first two days, very little transport is seen because the storm has not yet begun. There are hints of transport caused by outflow due to wind set-up in the Limfjord. This set-up results in a slight increase in water level as the storm hits, lower current speed for inflow, and larger speed for outflow. During days three and four, large transport caused by the peak of the storm is seen in the areas explained in Chapter 6.2. Days five and six show signs of the water in the Limfjord receding to the North Sea, carrying sediment with it. This trend continues into days seven and eight suggesting that water is still receding. The increase in intensity from days six to seven is explained by a change in wind direction to no longer oppose the outflow.

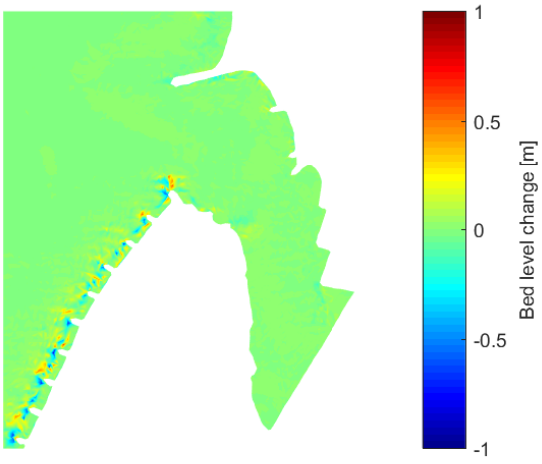

Figure 6.16 Bed level change during the first day of the JanRefLong model.

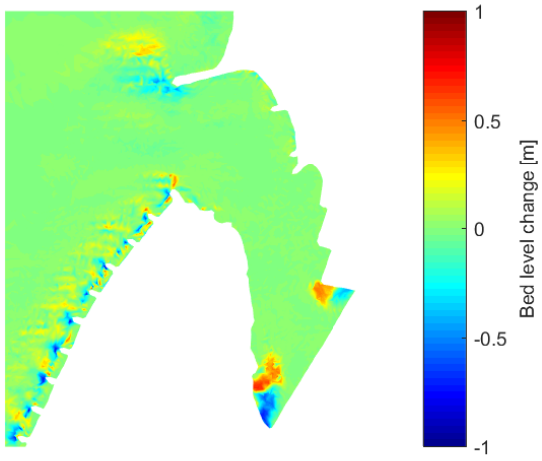

Figure 6.17 Bed level change during the second day of the JanRefLong model.

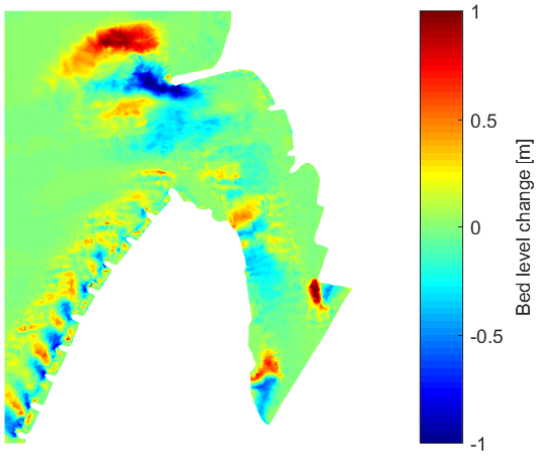

Figure 6.18 Bed level change during the third day of the JanRefLong model.

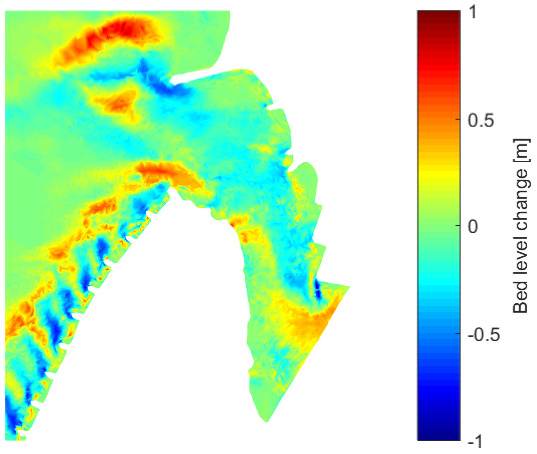

Figure 6.19 Bed level change during the fourth day of the JanRefLong model.

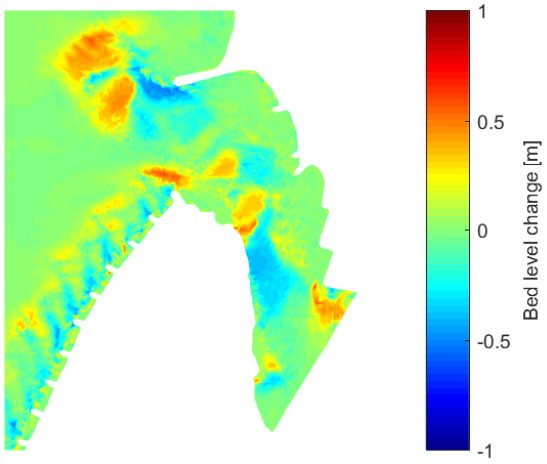

Figure 6.20 Bed level change during the fifth day of the JanRefLong model.

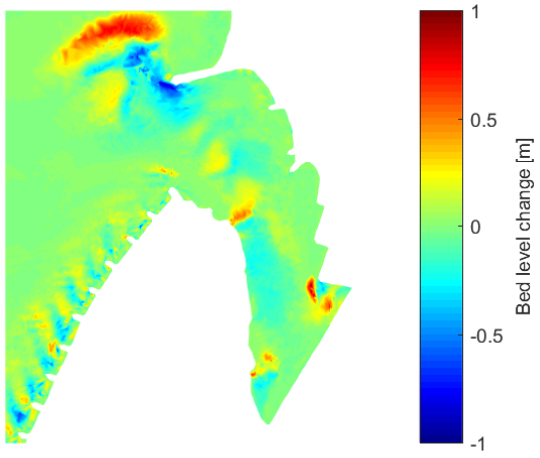

Figure 6.21 Bed level change during the sixth day of the JanRefLong model.

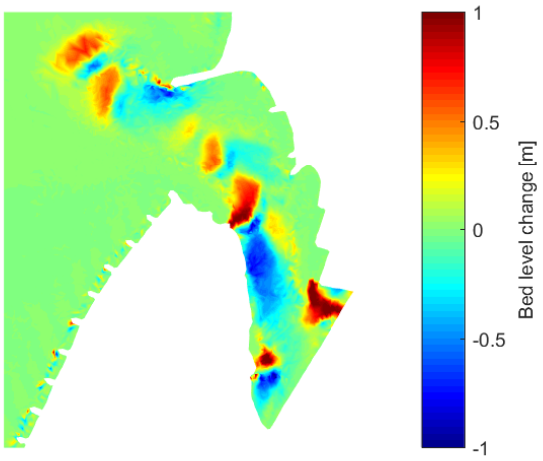

Figure 6.22 Bed level change during the seventh day of the JanRefLong model.

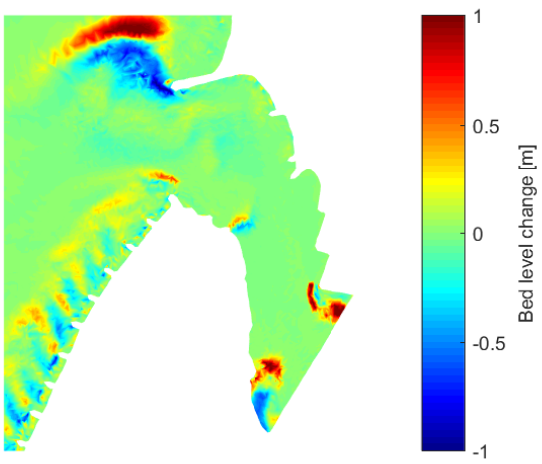

Figure 6.23 Bed level change during the eighth day of the JanRefLong model.

The analysis employing a longer simulation period suggests that the primary sedimentation happens during days 3-6 of the period modelled, i.e. during the peak of the storm and 2-3 days after. Ergo, the simulated periods of three days are a bit short leading to less reversal of the transport and therefore a larger net transport into the channel.

6.4 Issues with availability of sediment

As mentioned in Chapter 3.2.1, the ST module assumes infinite amounts of sand on the sea bed. This is a rather crude assumption at Thyborøn as borings suggest that no more than 0.5-1.0 m of sand is available in the area outside the channel [Geus, 2017]. As such, the large erosion in the inlet seen in the groyne extension models Jan59 and Dec59 might not be as prevalent in actuality. However, if the depth does not increase, the flow velocities will remain large in the area, sustaining the large suction causing a drastic decrease in the bypass of sediment. Simulations including the clayey sublayer performed by Knudsen et al. [1995, Fig. 9] suggest that a large amount of the erosion off the inlet is stopped by the clayey layer.

In the JanRef model, large erosion is seen in the inlet at the end of groyne 72. This erosion is likely overestimated due to the assumption of an infinite sand layer meaning that the sediment transport into the channel could be drastically lower than predicted.

Another issue with availability of sediment is that not enough sediment seems to enter the domain through the boundary between Nissum Bredning and Thyborøn Channel. Extending the modelled domain to include part of Nissum Bredning might solve this issue. This is not done in the present report due to time limitations.

Discussion, conclusion, and further studies

7

This chapter reiterates the important conclusions and discussions made throughout the report in order to suggest a design based on the knowledge obtained from the performed simulations. The report is then rounded off by suggesting analyses that could further clarify the issues associated with the different solutions to the problems in the Limfjord.

Two solution proposals on how to stabilise or reverse the increased storm surge water levels experienced in the Limfjord due to increasing cross section of Thyborøn Channel have been assessed. One solution suggests extending the groyne in the southern part of the entrance to stop the increased water levels. The other solution suggests extending the same groyne, but adding a dam in Nissum Bredning with sluices for traffic and water in order to completely reverse the water level increase. The solutions were compared with each other and the present site conditions. Increased need for dredging in the channel has been reported. Therefore, limiting deposition of sediment within the channel was an important factor when choosing between the solutions.

The analyses performed in the present study consisted of simulations of two different storms, one from January and one from December 2005, on three different bathymetries. The bathymetries were: one for a reference model of the area, one for the solution of extending the groyne, and one for the model both addition a dam and extending the groyne.

The **reference** simulations showed the tendency the in- and outflow affect the inlet differently leading to erosion in the north and accretion in the south. Further, large accretion was seen on a sand dune located north of the harbour. Due to refraction, this dune causes wave disturbance in Thyborøn Harbour. It was decided not to model Thyborøn Harbour which likely lead to larger erosion in the area where the harbour inlet would have disturbed the flow, slowing it down.

The **groyne extension** simulations showed large acceleration of the current in the narrower inlet. This acceleration leads to erosion which deposits in multiple areas in- and outside the channel complicating dredging operations. The same tendency was seen during severe and mild storms, suggesting that the problem may not be limited to storm situations. Furthermore, extending the groyne did not halt the creation of the sand dune causing wave disturbance in Thyborøn Harbour. However, the smaller entrance into the Limfjord caused by extending the southern entrance groyne lead to less wave energy entering the domain.

The wind set-up simulated in Thyborøn Channel when adding a **dam** seemed lower than expected suggesting that not enough fetch was modelled. This may have lowered the sediment transport

as larger waves might reach the shore with a larger set-up. Having said that, the dam almost completely stopped sedimentation in the channel when closed. Further, the lower current speeds caused by a lack of suction into the channel lead to less overall erosion. Because of the dam, sedimentation was only seen in the shipping lane outside the inlet. Thus, when adding the dam, dredging is necessary in only one location - compared to multiple locations without the dam. Summarily regarding sedimentation, the proposal including a dam is considered superior to only extending the groyne.

Regarding oxygen depletion in the Limfjord during the summer, a dam could be used to improve the water environment. Another important aspect to consider is that the ferry connecting the Harboøre and Agger tongues could be replaced by a road on the dam.

A fundamental difference between the proposal of only extending the groyne and the proposal of extending the groyne *and* adding a dam is that the latter blocks all flow into the fjord, completely reversing the problematic storm surge water levels whilst the first only limits the amount of water entering the fjord. By that logic, and with the improved sedimentation in mind, the dam model seems like the natural choice. However, as the coast inside the Limfjord already has a measure of protection against raised water levels, a complete reversal may not be necessary. Furthermore, the addition of the dam is estimated by KDI [2012] to cost DKK 1580 million more than only extending the groyne. Relative to the groyne extension solution this is an additional 95 %. However, the many advantages of being able to close the channel off, could tip the decision in favour of a dam in spite of the large construction costs. Thus, the results of the simulations in this report are used to propose alternative dam designs.

Building the dam as a straight line sketched by the blue proposal in Figure 7.1 would cut down construction costs. Alternatively, the location shown by the red line in the figure could be considered. Constructed along the read line, the dam would protect Thyborøn from increased water levels and the harbour from wave disturbance. Unfortunately, both alternatives interfere with the plans of extending the harbour to the south necessitating the wide path of the dam proposed by KDI [2012]. If expectations for the extension are lowered, the blue proposal in Figure 7.1 might work if the entrance to the southern harbour basin was moved further north as shown.

Figure 7.1 Sketch of alternative dam placements proposed based on results from project [Google, 2017].

7.1 Further studies

Further studies on the subject could include simulation of longer periods in order to estimate the sediment transport in the Thyborøn area during relatively calm weather. Such a study would shed light on the day to day transport at the channel which, given a long enough period, could amount to large changes in bathymetry.

Another interesting study is to extend the model domain to include part of the sand banks in Nissum Bredning. This might solve the experienced problem with lack of sediment entering the model from the eastern boundary at Nissum Bredning causing unrealistically high net transport towards the sand banks.

Moreover, a model including Thyborøn Harbour and more of the North Sea could be implemented in order to ascertain a more realistic set-up at the dam during the storm. This would be necessary in order to secure Thyborøn Harbour against the increased water level that would inevitably follow construction of the dam.

Finally, implementing models with limited amounts of sediment on the seabed could clarify how much a clayey sublayer would limit the erosion seen in the inlet region of the groyne extension simulations. Such a model might also change the net transport towards the sand banks in Nissum Bredning. The reasoning behind this is that the sand banks constitute a near inexhaustible supply of sediment for seaward transport. On the contrary, transport towards the sand banks seem to hinge on large areas of thin sand layers which may deplete.

Bibliography

Ahrens, **2012**. C. Donald Ahrens. *Meteorology Today: An Introduction to Wather, Climate, and the Environment*. ISBN-13: 978-0-8400-5499-9. Cengage Learning, tenth edition edition, 2012.

Bruun, **1954**. Per Bruun. *Coast Stability*, 1954.

DHI, **2017**. DHI. *MIKE 21/3 Coupled Model FM Hydrodynamic Module User Guide*, 2017.

DHI, **2015a**. DHI. *MIKE 21 & MIKE 3 Flow Model FM Hydrodynamic and Transport module Scientific Documentation*, 2015. Scientific documentation. Release 2016.

DHI, **2015b**. DHI. *MIKE 21 & MIKE 3 Flow Model FM Sand Transport Module Scientific Documentation*, 2015. Scientific documentation. Release 2016.

DHI, **2015c**. DHI. *MIKE 21 & MIKE 3 Flow Model FM Spectral Wave module Scientific Documentation*, 2015. Scientific documentation. Release 2016.

DMI, **2017**. DMI. *Dansk Meterologisk Institut - Vandstand*. URL: https://www.dmi.dk/hav/maalinger/vandstand/, 2017.

Fredsoe, **1984**. J. Fredsoe. *Turbulent Boundary Layer in Wave-Current Motion*. Journal of Hydraulic Engineering, 1984.

Gao and Collins, **1994**. S. Gao and M. Collins. *Tidal Inlet Equilibrium, in Relation to Cross-sectional Area and Sediment Transport Patterns*. Esturaine, Coastal and Shelf Science, 1994.

Geus, **2017**. Geus. *De Nationale Geologiske Undersøgelser for Danmark og Grønland*, 2017.

Google, **2017**. Google. *Google Maps*. URL: https://www.google.dk/maps, 2017.

Hayes, **1980**. M. O. Hayes. *General Morhpology and Sediment Patterns in Tidal Inlets*. Sedimentary Geology, 1980.

Kamphuis, **2010**. J. William Kamphuis. *Itroduction to coastal engineering and management*. ISBN: 978-981-283-484-3, Advanced Series on Ocean Engineering - Vol 30. World Scientific, 2010.

KDI, **2017**. KDI. *Kystdirektoratets Kystatlas*. URL: www.kystatlas.dk, 2017. Downloaded: 21/03-17.

KDI, **2001**. KDI. *Sediment budget Vestkysten*, 2001.

KDI, **2012**. KDI. *Thyborøn Kanal og Vestlige Limfjord - Teknisk resumé*, 2012.

KDI, **1999**. KDI. *Thyborøn 25 års eftersyn*, 1999.

KDI, **2011**. KDI. *Thyborøn Kanal 2009*, 2011.

Knudsen and Sørensen, **2011**. S.B. Knudsen and C. Sørensen. *Bølgeuro i Thyborøn Havn - Tekniskknotat. Kystdirektoratet.*, 2011.

Knudsen et al., **1995**. Soeren B. Knudsen, Signe M. Ingvardsen, Holger T. Madsen, Carlo Soerensen and Bo B. Christensen. *The Morphological Evolution around Thyborøn - An Inlet at the North Sea*, 1995.

Kystinspektoratet, **1995**. Kystinspektoratet. *Thyborøn kanal, 1995*, 1995.

Larsen and Beck, **2015**. Torben Larsen and Jørgen Bülow Beck. *Thyborøns Kanals Betydning for Kysterosion på den Jyske Vestkysts Sydlige Del*. Vand & Jord, 22, 2015.

Liu, **2001**. Zhou Liu. *Sediment Transport*. 3rd edition. Aalborg University, 2001.

Liu and Frigaard, **2001**. Zhou Liu and Peter Frigaard. *Generation and analysis of random waves*. 3rd edition. Laboratoriet for Hydraulik og Havnebygning, Aalborg University, 2001.

Nørgaard et al., **2014**. Jørgen Q. H. Nørgaard, Thomas R. Bentzen, Torben Larsen, Thomas L. Andersen and Steffen Kvejborg. *Influence of Closing Storm Surge Barrier on Extreme Water Levels and Water Exchange; the Limfjord, Denmark*. Coastal Engineering Journal, 56, 2014.

O'Brien and Dean, **1972**. M. P. O'Brien and R. G. Dean. *Hydraulics and sedimentary stability of coastal inlets*. Coastal Engineering Proceedings, 1972.

Rambøll, **2014**. Rambøll. *Thyborøn Havn - VVM for udvidelse, 1995*, 2014.

AALBORG UNIVERSITY
STUDENT REPORT

Sedimentation around Thyborøn Channel: Effects of Improving Storm Surge Levels in The Limfjord - Appendices

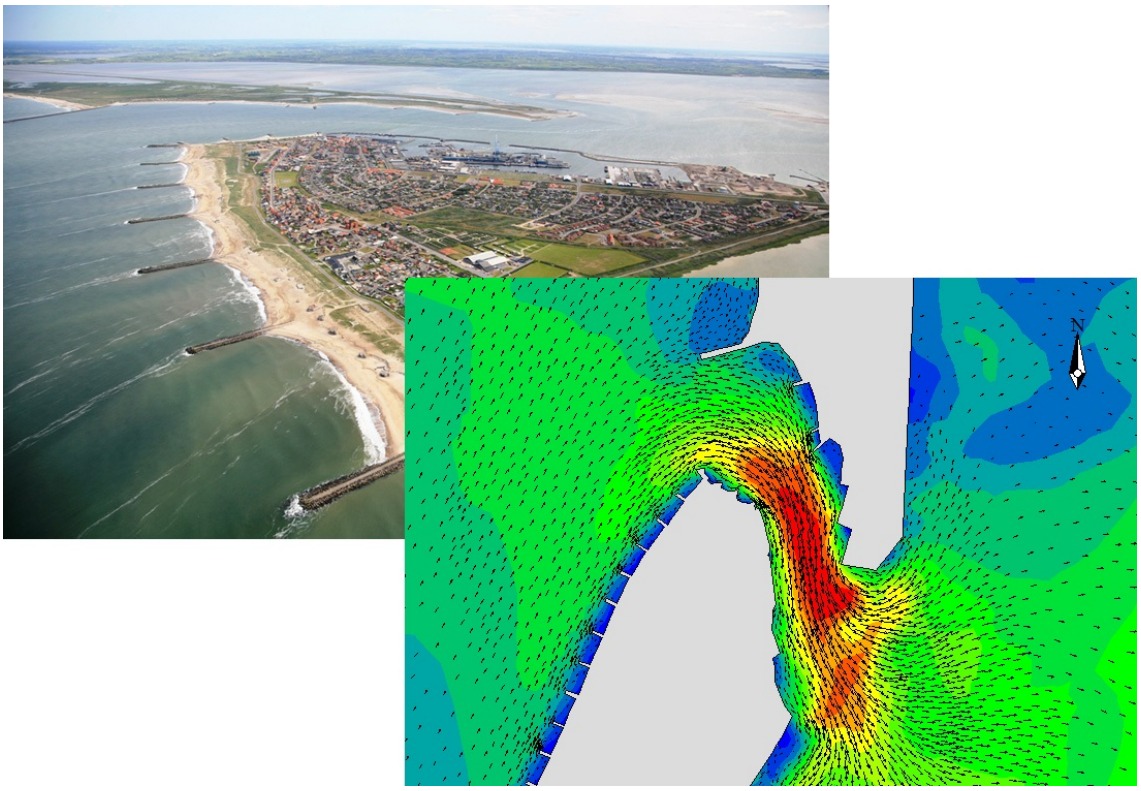

Theis Buys Petersen
M.Sc. in Structural and Civil Engineering
Master's thesis
June 8th 2017

AALBORG UNIVERSITY
STUDENT REPORT

The School of Engineering and Science
Study Board of Civil Engineering
Fibigerstræde 10, 9220 Aalborg Ø
http://www.ses.aau.dk/

Title

Sedimentation around Thyborøn Channel: Effects of Improving Storm Surge Levels in The Limfjord - Appendices

Project period

February 2017 - June 2017

Author

Theis Buys Petersen

Supervisors

Torben Larsen
Professor in Hydraulic Engineering (Aalborg University)

Jørgen Q. H. Nørgaard
Associate Professor (Aalborg University)
Senior Coastal Engineer (Ramboll Consulting Engineers)

Completed on June 8th 2017.

Synopsis:

The Danish Limfjord experiences increased storm surge levels due to an increasing cross section in Thyborøn Channel which connects the Limfjord to the North Sea. Several suggestions to a solution to the problem have been made, among them building a dam with a sluice to be closed during storms. This project assesses the sediment related consequences of implementing the proposed solutions. The assessment is made through simulations of sediment transport in the area caused by both severe and relatively mild storms chosen through analyses on meteorological and oceanographic data. The simulations are made in the software suit MIKE 21 which couples simulations of wave, flow, and sediment transport fields to model realistic processes accurately and efficiently. It is found that the construction of a dam and extension of a groyne would significantly improve sediment conditions in the area compared to only extending the groyne. Adding the dam, while expensive, is further found to improve manoeuvrability of ships in the entrance to Thyborøn Harbour and has been proved in other work to improve oxygen levels in the Limfjord.

Appendices

Thyborøn Channel and area A

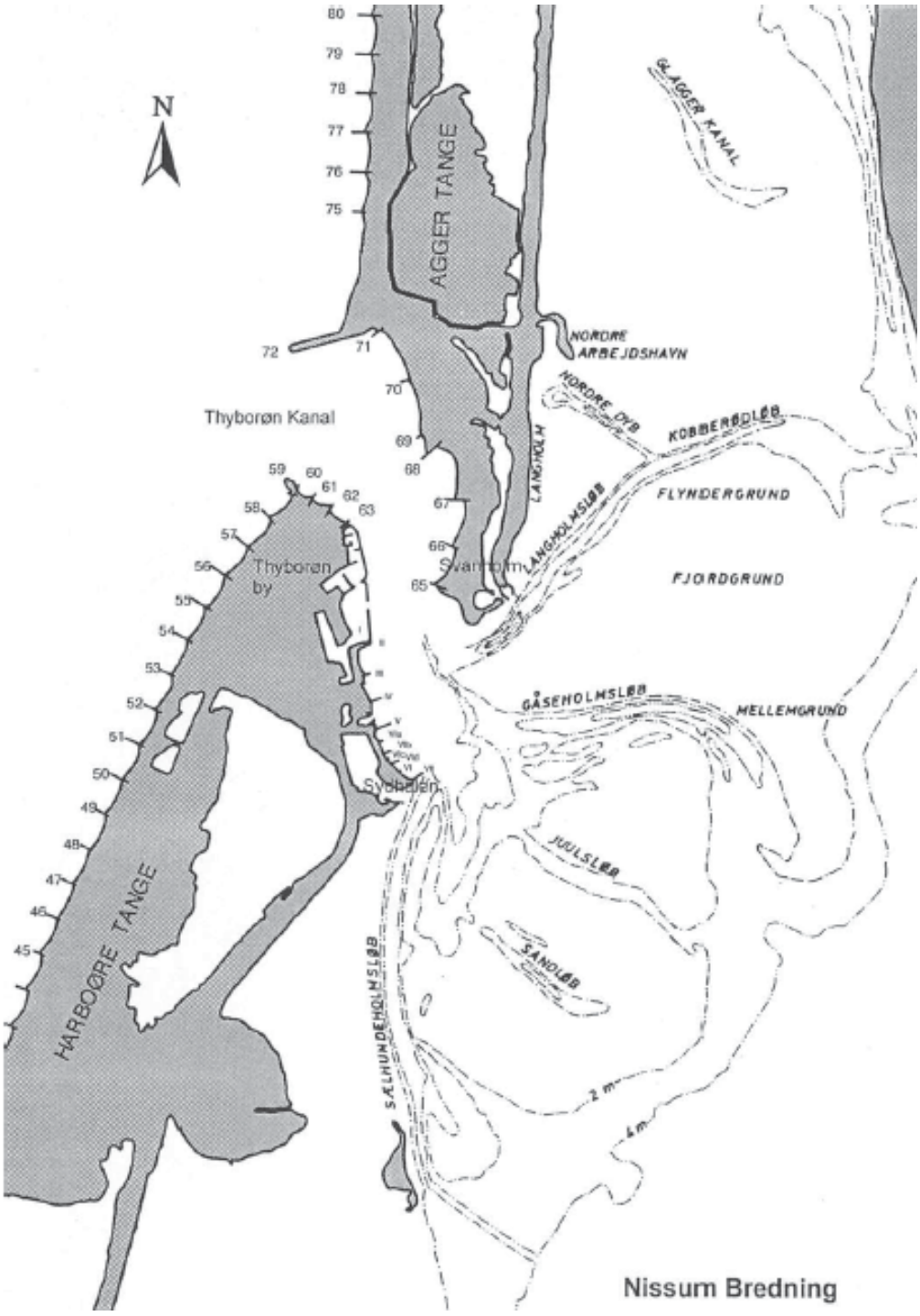

Figure A.1 Placement and numbering of groynes in and around Thyborøn Channel [KDI, 2011].

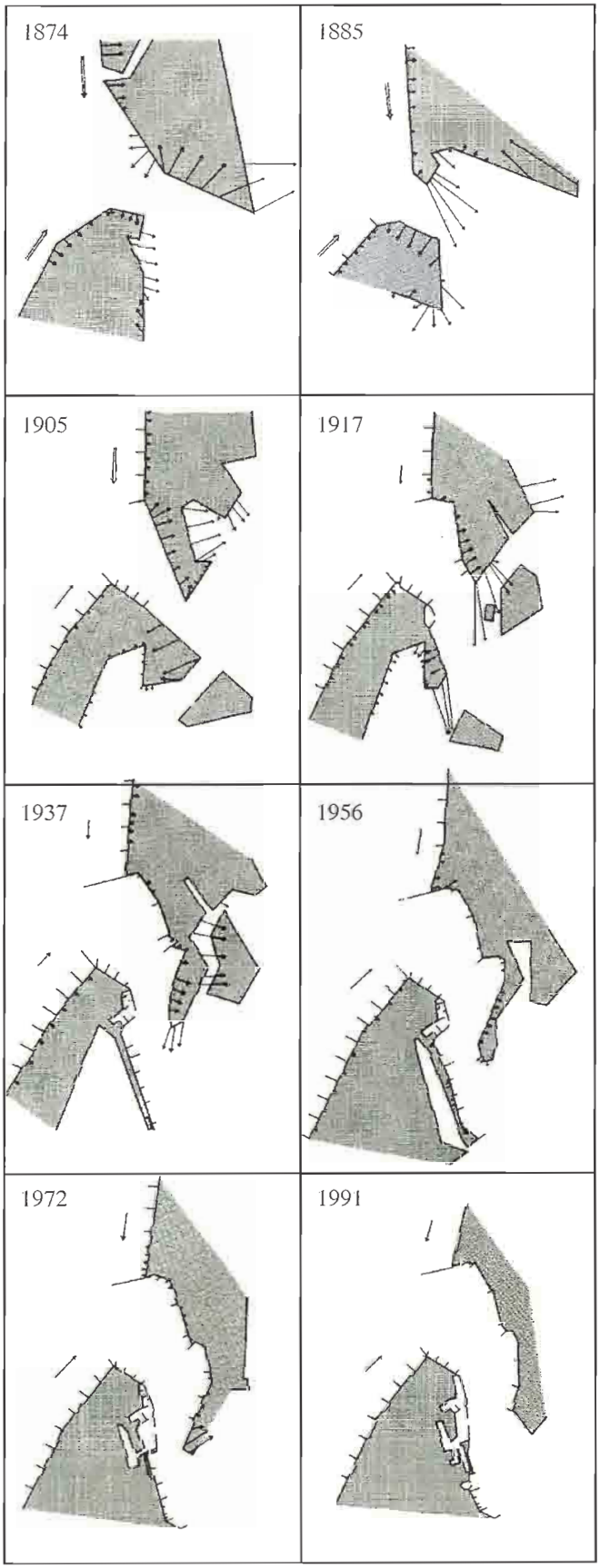

Figure A.2 Sketches of Thyborøn Channel's shape between 1874 and 1991 [Kystinspektoratet, 1995].

Figure A.3 Planed extension of Thyborøn Harbour [Rambøll, 2014].

Sediment transport on coastlines in general

B

In order to better understand the problems experienced at Thyborøn a fundamental understanding of the process behind sediment transport on coastlines is essential.

Consider a sand particle on the sea bed as shown in Figure B.1. It is affected by forces from gravity and if a current is present; lift, drag and friction. In order for the particle to move, the current speed must increase to a critical value, where the lift and drag forces overcome the friction and gravity forces [Liu, 2001].

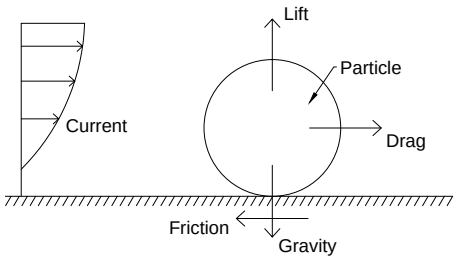

Figure B.1 Illustration of forces acting on a particle on the sea bed with a current. Inspired by Liu [2001].

In coastal areas the sediment transport is divided into two parts; the cross- and longshore transport. **Cross-shore transport** is the cross-shore transport of sediment perpendicular to the coastline while longshore transport is parallel to the coastline. To easier understand cross-shore transport, longshore is ignored for now. During calm weather periods often found in the summer, low wave heights move sand shoreward creating a uniform beach profile as illustrated in Figure B.2. During the rougher seas and larger water levels in the winter larger waves erode the beach and the undertow drags the sediment toward the sea where it settles to create bars parallel to the beach. These winter bars are created where the waves break, as there is a strong off-shore transport from the beach to the breaker zone and a weak on-shore transport from sea to the breaker zone [Kamphuis, 2010].

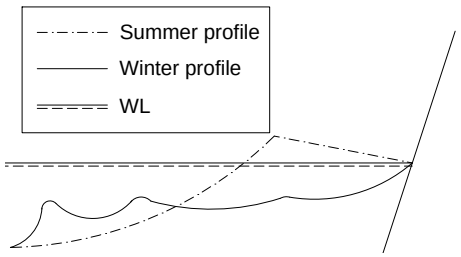

Figure B.2 Illustration of beach profiles during summer and winter.

Longshore transport is generated by the longshore current created by waves hitting the coast at an oblique angle. Two transports take place. The first, called *beach drift*, occurs when the wave pushes sediment onto the beach at an oblique angle and gravity pulls it back to sea perpendicularly. The second part occurs in the breaking zone where the turbulence created by breaking waves stirs the sediment into suspension and the longshore current generated by the momentum of the oblique waves carries it further down the beach [Kamphuis, 2010].

The current that drives all this sediment transport is generated by waves and water level differences. The waves are wind generated. Small irregularities in the atmospheric pressure generates small ripples on the water surface which increases its roughness leading to a larger energy transfer between wind and sea building up the waves [Liu and Frigaard, 2001]. The current is generated when one body of water has a lower water level than another one causing a flow similar to meteorological low and high pressure areas.

Wave parameter correlation at Fjaltring

C

Figures C.1-C.5 show the correlation between significant wave heights and peak wave periods of waves coming from S through N, respectively, at Fjaltring. Generally, good correlation is seen, especially for the larger waves from western directions.

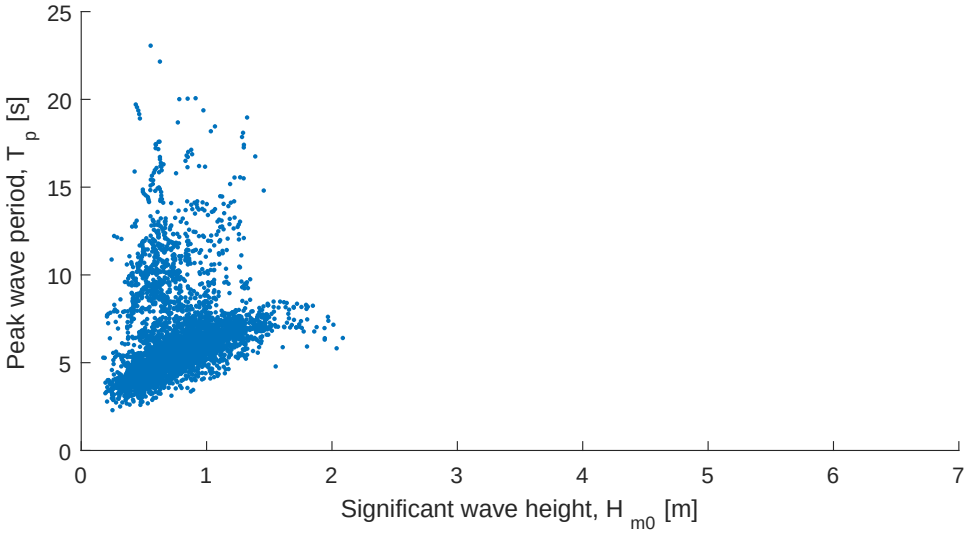

Figure C.1 Correlation between significant wave hight and peak wave period of wave from S hindcasted outside Fjaltring.

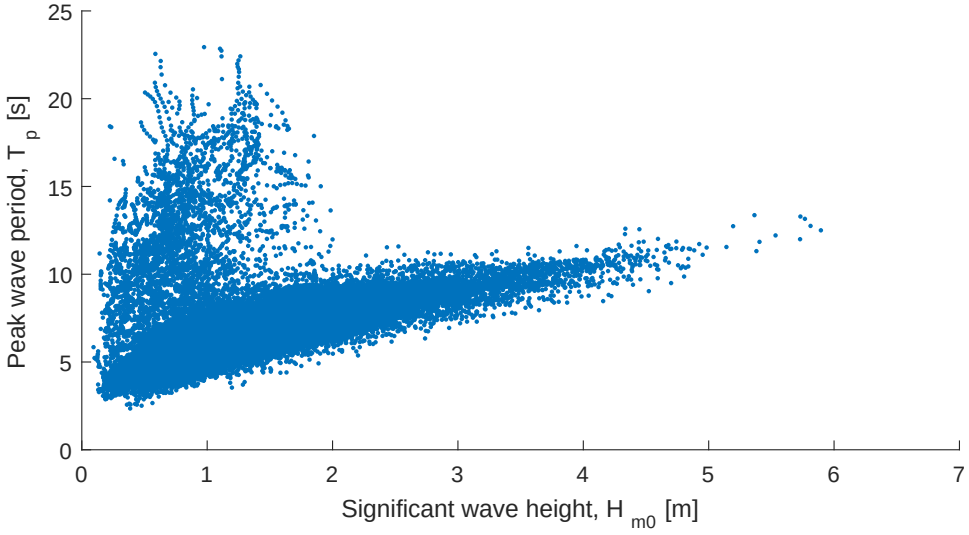

Figure C.2 Correlation between significant wave hight and peak wave period of wave from SW hindcasted outside Fjaltring.

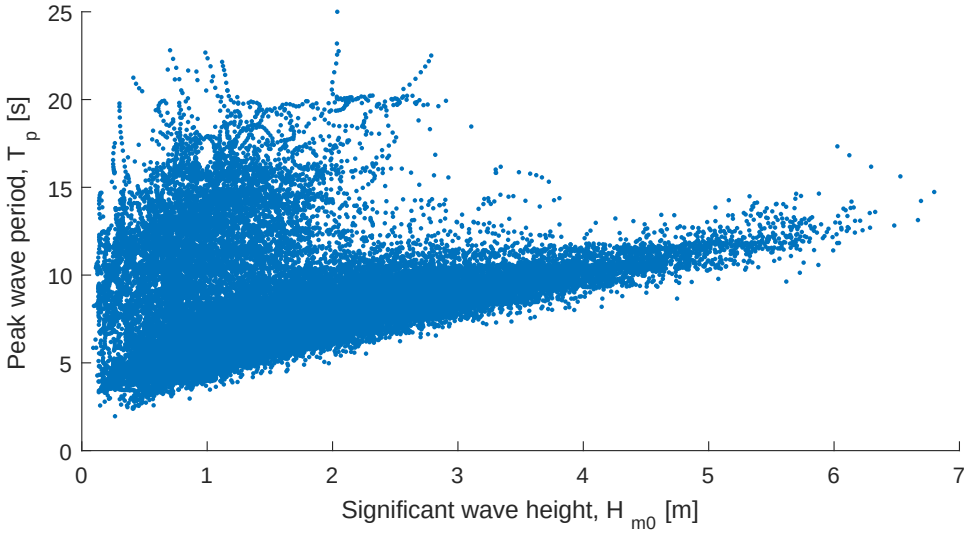

Figure C.3 Correlation between significant wave hight and peak wave period of wave from W hindcasted outside Fjaltring.

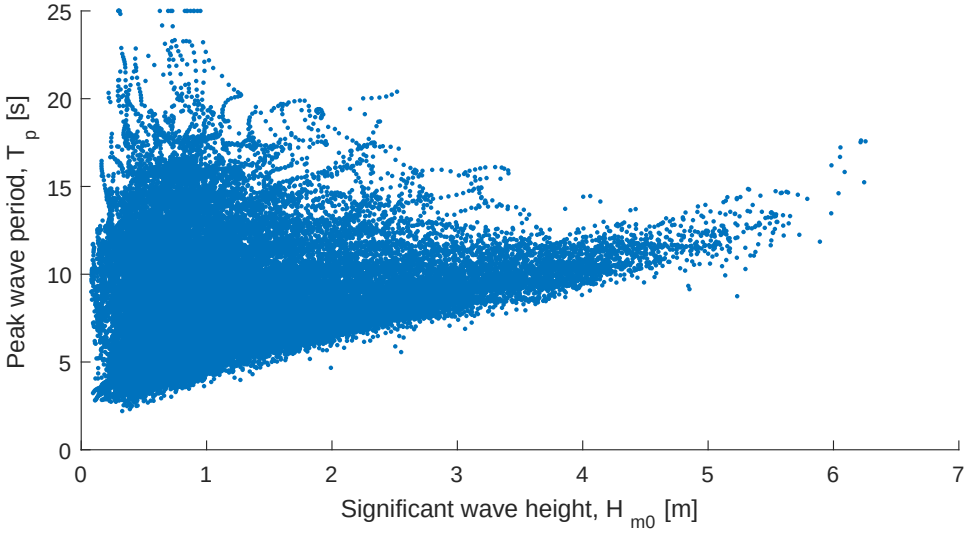

Figure C.4 Correlation between significant wave hight and peak wave period of wave from NW hindcasted outside Fjaltring.

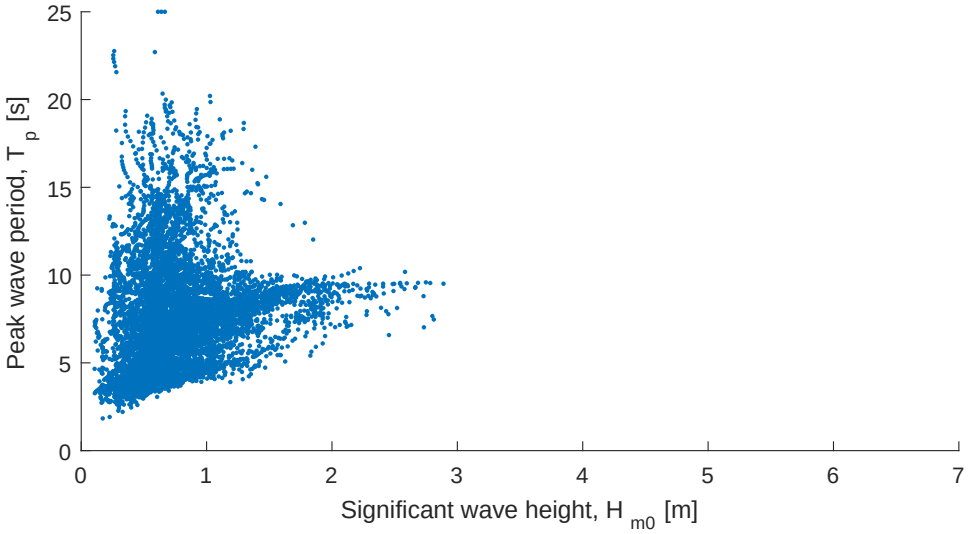

Figure C.5 Correlation between significant wave hight and peak wave period of wave from N hindcasted outside Fjaltring.

Breaking wave parameters D

This appendix explains the methods used to get the breaking parameters used in the Kamphuis formula as described by Kamphuis [2010]. The necessary data are:

- Deep water significant wave heights, H_s.
- Mean angle of wave fronts with shore, α_0.
- Slope of seabed, m.
- Peak wave periods, T_p.

First the deep water characteristics are calculated in Equation D.1.

$$\begin{aligned} L_0 &= \frac{gT^2}{2\pi} \\ C_0 &= \frac{gT}{2\pi} \\ kd_0 &= \frac{2\pi d}{L_0} \end{aligned} \tag{D.1}$$

where

L_0	Deep water wave length
C_0	Deep water wave celerity
kd_0	Deep water wave argument
d	Water depth

The wave argument which changes when approaching shore is used to calculate the wave celerity and length closer to shore.

$$\begin{aligned} C &= \sqrt{\frac{1}{kd_0 + \frac{1}{1+0.6522kd_0+0.4622kd_0^2+0.0864kd_0^4+0.0675kd_0^5}} gd} \\ L &= CT \end{aligned} \tag{D.2}$$

D.1 Refraction and shoaling

The refraction of the waves when approaching shore is taken into account by Snell's law shown in Equation D.3. The principle of refraction is illustrated in Figure D.1.

$$\frac{\sin(\alpha)}{\sin(\alpha_0)} = \frac{C}{C_0} \tag{D.3}$$

where

α	Wave angle to shore

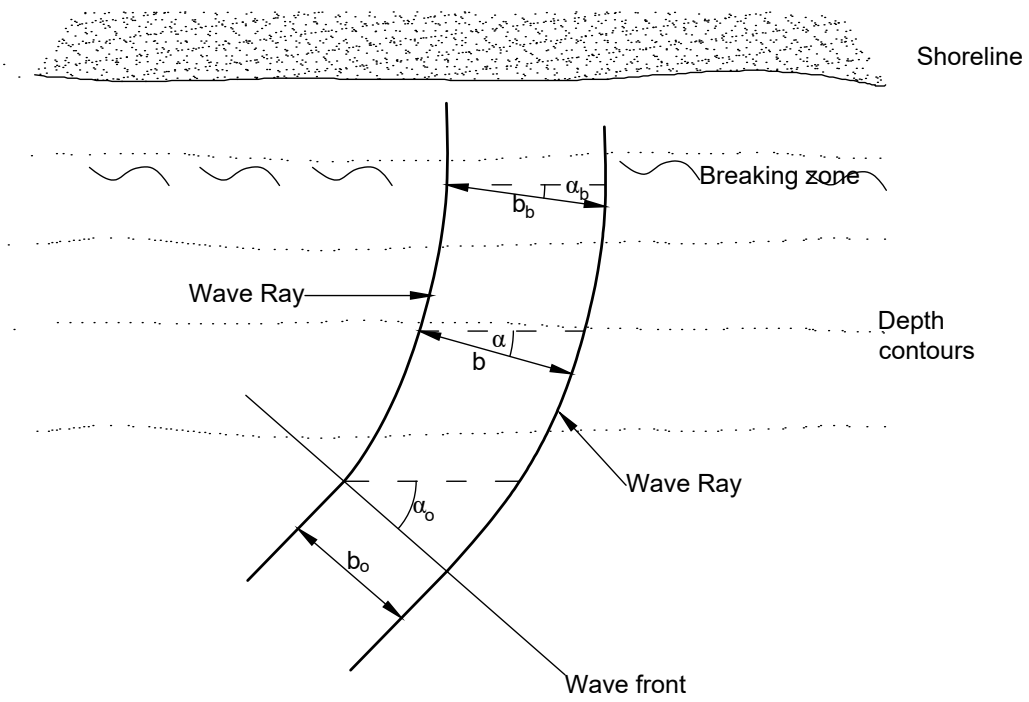

Figure D.1 Illustration of the refraction phenomenon. Inspired by Kamphuis [2010].

Shoaling is taken into account by use of Equation D.4.:

$$\begin{aligned} \frac{H}{H_0} &= \sqrt{\frac{n_0 C_0}{nC}}\sqrt{\frac{b_0}{b}} \\ n &= \frac{1}{2}\left(1+\frac{2kd}{\sinh(2kd)}\right) \end{aligned} \tag{D.4}$$

where

b	Distance between adjacent wave arrays
n	Group velocity parameter

D.2 Breaking criteria

The shoaling and refraction of the waves moving towards the shore makes them unstable leading to breaking. Two criteria, shown in Equation D.5 are used for determining when the waves break: one for steepness, and one for height compared to depth.

$$\begin{aligned} H_{b,depth} &= 0.56e^{3.5m}d_b \\ H_{b,steep} &= 0.095e^{4m}L_b\tanh(kd_{b)} \end{aligned} \tag{D.5}$$

where

$H_{b,depth}$	Breaking wave height due to depth condition
$H_{b,steep}$	Breaking wave height due to steepness condition
L_b, d_b, kd_b	Wave length, depth, and wave argument at breaking point

If the wave height calculated from Equation D.4 exceeds either of the criteria the wave breaks and the breaking parameters are determined at the breaking point.

Sediment transport rate at Fjaltring

E

To validate the Kamphuis formula for the project, it is applied to the position at Fjaltring from where the wave data is collected. Then, the results are compared to the predictions proposed by KDI [2001]. The beach profiles used are from 2010 as described in Chapter 4.4. The grain size is estimated to 0.2 mm based on the definition of fine to medium sand found in the area according to geotechnical borings [Geus, 2017]. The beach is assumed facing due west as a mean for the area.

With these assumptions, the average yearly net potential sediment transport rate is 840 000 m^3/year, southbound. When compared to the ~700 000 m^3/year of actual sediment transport rate found by KDI [2001] this number seems reasonable. The actual rate is based on a sediment budget and is therefore expected to be less than the potential rate which does not take into account limitations on sand availability and the coastal protection in the area. A sediment rose for the Fjaltring area is shown in Figure E.1. It supports the results as both the peaks and net transport are southbound which fits the prediction by KDI [2001].

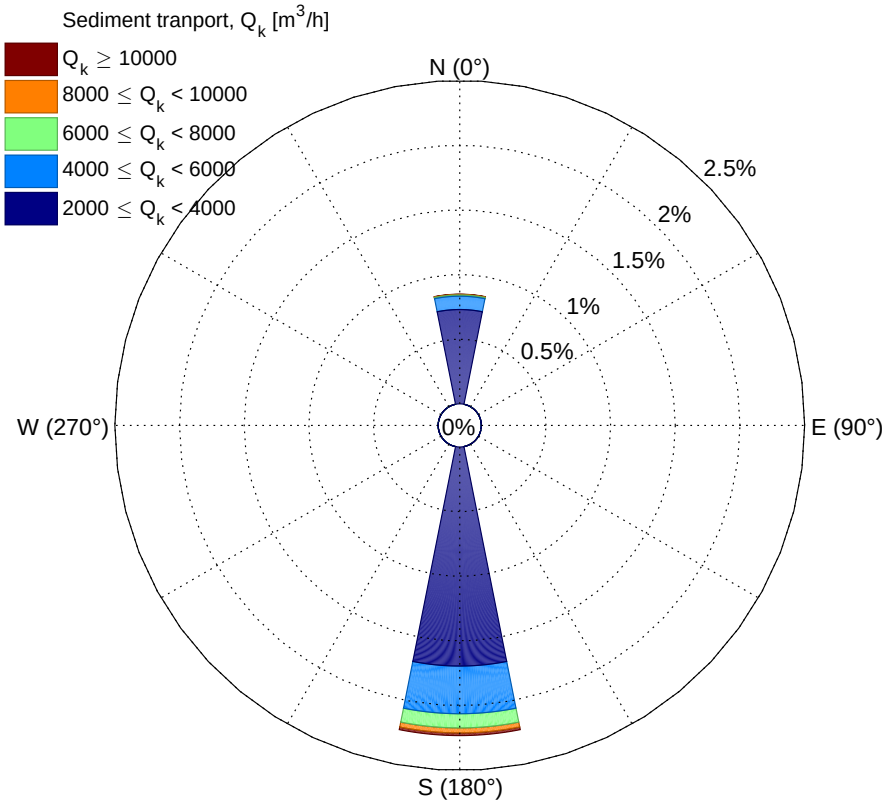

Figure E.1 Rose of potential sediment transport rate in the Fjaltring area predicted by the Kamphuis formula.

Scatter and transport matrices

F

The following figures show scatter matrices for the directions not sheltered by land. The peak periods and significant wave heights are the maximum value of the interval. As an example, the number shown for $T_p = 12\,\text{s}$ and $H_{m0} = 2.5\,\text{m}$ is the amount of waves coming from W with a peak period between 11 and 12 seconds and a significant wave height between 2 and 2.5 m, divided by the total amount of waves registered.

F.1 Scatter matrices

Table F.1 Scatter matrix of waves from N.

N	Peak period, T_p [s]																								
Significant wave height, H_{m0} [m]	1	2	3	4	5	6	7	8	9	10	11	12	13	14	15	16	17	18	19	20	21	22	23	24	25
0.5	-	-	0.01	0.16	0.15	0.06	0.04	0.03	0.03	0.04	0.03	0.02	0.01	0.00	0.00	0.00	0.00	0.00	0.00	0.00	-	-	0.00	-	-
1.0	-	-	-	0.09	0.24	0.15	0.22	0.23	0.14	0.12	0.07	0.06	0.07	0.06	0.04	0.01	0.01	0.00	0.01	0.01	-	-	0.00	-	-
1.5	-	-	-	-	0.03	0.03	0.09	0.16	0.13	0.03	0.02	0.00	0.00	0.00	0.00	0.01	0.01	0.00	0.00	-	-	-	-	-	-
2.0	-	-	-	-	-	0.00	0.01	0.01	0.02	0.01	0.00	-	-	-	-	-	-	-	-	-	-	-	-	-	-
2.5	-	-	-	-	-	-	-	0.00	0.00	-	-	-	-	-	-	-	-	-	-	-	-	-	-	-	-
3.0	-	-	-	-	-	-	-	-	0.00	-	-	-	-	-	-	-	-	-	-	-	-	-	-	-	-
3.5	-	-	-	-	-	-	-	-	-	-	-	-	-	-	-	-	-	-	-	-	-	-	-	-	-
4.0	-	-	-	-	-	-	-	-	-	-	-	-	-	-	-	-	-	-	-	-	-	-	-	-	-
4.5	-	-	-	-	-	-	-	-	-	-	-	-	-	-	-	-	-	-	-	-	-	-	-	-	-
5.0	-	-	-	-	-	-	-	-	-	-	-	-	-	-	-	-	-	-	-	-	-	-	-	-	-
5.5	-	-	-	-	-	-	-	-	-	-	-	-	-	-	-	-	-	-	-	-	-	-	-	-	-
6.0	-	-	-	-	-	-	-	-	-	-	-	-	-	-	-	-	-	-	-	-	-	-	-	-	-
6.5	-	-	-	-	-	-	-	-	-	-	-	-	-	-	-	-	-	-	-	-	-	-	-	-	-
7.0	-	-	-	-	-	-	-	-	-	-	-	-	-	-	-	-	-	-	-	-	-	-	-	-	-

Table F.2 Scatter matrix of waves from SSW.

SSW	Peak period, T_p [s]																								
Significant wave height, H_{m0} [m]	1	2	3	4	5	6	7	8	9	10	11	12	13	14	15	16	17	18	19	20	21	22	23	24	25
0.5	-	-	0.00	0.16	0.23	0.03	0.02	0.02	0.02	0.01	0.01	0.01	0.00	-	0.00	-	-	-	0.00	-	-	-	-	-	-
1.0	-	-	0.00	0.08	0.36	0.71	0.33	0.11	0.08	0.06	0.06	0.04	0.02	0.03	0.02	0.01	0.01	0.01	0.00	-	0.00	0.00	0.00	-	-
1.5	-	-	-	0.00	0.02	0.21	0.41	0.28	0.05	0.01	0.01	0.01	0.01	0.01	0.01	0.00	0.00	0.00	0.01	0.00	-	-	-	-	-
2.0	-	-	-	-	0.00	0.01	0.05	0.12	0.03	0.00	-	-	0.01	0.00	0.00	0.00	-	-	-	-	-	-	-	-	-
2.5	-	-	-	-	-	0.00	0.01	0.00	0.00	-	-	-	-	-	-	-	-	-	-	-	-	-	-	-	-
3.0	-	-	-	-	-	-	-	0.00	-	-	-	-	-	-	-	-	-	-	-	-	-	-	-	-	-
3.5	-	-	-	-	-	-	-	-	-	-	-	-	-	-	-	-	-	-	-	-	-	-	-	-	-
4.0	-	-	-	-	-	-	-	-	-	-	-	-	-	-	-	-	-	-	-	-	-	-	-	-	-
4.5	-	-	-	-	-	-	-	-	-	-	-	-	-	-	-	-	-	-	-	-	-	-	-	-	-
5.0	-	-	-	-	-	-	-	-	-	-	-	-	-	-	-	-	-	-	-	-	-	-	-	-	-
5.5	-	-	-	-	-	-	-	-	-	-	-	-	-	-	-	-	-	-	-	-	-	-	-	-	-
6.0	-	-	-	-	-	-	-	-	-	-	-	-	-	-	-	-	-	-	-	-	-	-	-	-	-
6.5	-	-	-	-	-	-	-	-	-	-	-	-	-	-	-	-	-	-	-	-	-	-	-	-	-
7.0	-	-	-	-	-	-	-	-	-	-	-	-	-	-	-	-	-	-	-	-	-	-	-	-	-

Table F.3 Scatter matrix of waves from SW.

SW	Peak period, T_p [s]																								
Significant wave height, H_{m0} [m]	1	2	3	4	5	6	7	8	9	10	11	12	13	14	15	16	17	18	19	20	21	22	23	24	25
0.5	-	-	0.01	0.18	0.33	0.16	0.05	0.03	0.05	0.03	0.03	0.02	0.01	0.02	0.01	0.00	0.00	-	-	-	-	-	-	-	-
1.0	-	-	-	0.15	0.66	1.22	0.93	0.20	0.09	0.08	0.09	0.08	0.07	0.06	0.06	0.03	0.03	0.02	0.01	0.01	0.01	-	-	-	-
1.5	-	-	-	-	0.13	0.69	1.14	0.70	0.17	0.05	0.03	0.01	0.02	0.02	0.01	0.02	0.02	0.03	0.02	0.01	0.01	-	0.00	-	-
2.0	-	-	-	-	0.00	0.09	0.50	0.76	0.43	0.10	0.01	0.01	0.00	0.00	0.00	-	0.00	0.00	0.00	0.00	-	-	-	-	-
2.5	-	-	-	-	-	0.00	0.09	0.36	0.35	0.16	0.01	-	-	-	-	-	-	-	-	-	-	-	-	-	-
3.0	-	-	-	-	-	-	0.00	0.06	0.18	0.14	0.03	-	-	-	-	-	-	-	-	-	-	-	-	-	-
3.5	-	-	-	-	-	-	-	0.01	0.05	0.05	0.01	0.00	-	-	-	-	-	-	-	-	-	-	-	-	-
4.0	-	-	-	-	-	-	-	0.00	0.00	0.02	0.01	-	-	-	-	-	-	-	-	-	-	-	-	-	-
4.5	-	-	-	-	-	-	-	-	0.00	0.01	0.00	-	-	-	-	-	-	-	-	-	-	-	-	-	-
5.0	-	-	-	-	-	-	-	-	-	-	0.00	0.00	0.00	-	-	-	-	-	-	-	-	-	-	-	-
5.5	-	-	-	-	-	-	-	-	-	-	-	0.00	-	-	-	-	-	-	-	-	-	-	-	-	-
6.0	-	-	-	-	-	-	-	-	-	-	-	0.00	-	-	-	-	-	-	-	-	-	-	-	-	-
6.5	-	-	-	-	-	-	-	-	-	-	-	-	-	-	-	-	-	-	-	-	-	-	-	-	-
7.0	-	-	-	-	-	-	-	-	-	-	-	-	-	-	-	-	-	-	-	-	-	-	-	-	-

Table F.4 Scatter matrix of waves from WSW.

WSW	Peak period, T_p [s]																								
Significant wave height, H_{m0} [m]	1	2	3	4	5	6	7	8	9	10	11	12	13	14	15	16	17	18	19	20	21	22	23	24	25
0.5	-	-	0.01	0.12	0.41	0.21	0.05	0.05	0.06	0.06	0.06	0.08	0.03	0.01	0.01	0.01	0.00	0.00	0.00	-	0.00	-	-	-	-
1.0	-	-	0.00	0.09	0.66	1.62	0.92	0.19	0.09	0.07	0.08	0.10	0.08	0.07	0.07	0.05	0.03	0.02	0.00	0.00	0.00	0.00	0.00	-	-
1.5	-	-	-	0.01	0.16	0.74	1.35	0.91	0.21	0.04	0.04	0.04	0.03	0.03	0.04	0.05	0.03	0.03	0.01	0.01	0.01	0.01	0.00	-	-
2.0	-	-	-	-	0.01	0.12	0.67	1.03	0.60	0.11	0.02	0.01	0.01	0.01	0.01	0.02	0.01	0.00	0.01	0.01	-	-	-	-	-
2.5	-	-	-	-	-	0.01	0.20	0.66	0.74	0.25	0.03	0.00	0.00	0.00	0.00	-	0.00	-	-	0.00	-	-	-	-	-
3.0	-	-	-	-	-	-	0.01	0.15	0.53	0.41	0.05	0.01	-	-	-	-	-	-	-	-	-	-	-	-	-
3.5	-	-	-	-	-	-	-	0.02	0.19	0.34	0.10	0.00	-	-	-	-	-	-	-	-	-	-	-	-	-
4.0	-	-	-	-	-	-	-	-	0.03	0.21	0.19	0.01	-	-	-	-	-	-	-	-	-	-	-	-	-
4.5	-	-	-	-	-	-	-	-	0.00	0.04	0.14	0.04	0.00	0.00	-	-	-	-	-	-	-	-	-	-	-
5.0	-	-	-	-	-	-	-	-	-	0.00	0.03	0.04	-	0.00	-	-	-	-	-	-	-	-	-	-	-
5.5	-	-	-	-	-	-	-	-	-	-	0.01	0.01	0.00	0.00	-	-	-	-	-	-	-	-	-	-	-
6.0	-	-	-	-	-	-	-	-	-	0.00	-	0.00	0.00	0.00	-	-	-	-	-	-	-	-	-	-	-
6.5	-	-	-	-	-	-	-	-	-	-	-	-	0.00	0.00	-	-	-	-	-	-	-	-	-	-	-
7.0	-	-	-	-	-	-	-	-	-	-	-	-	-	0.00	-	-	-	-	-	-	-	-	-	-	-

Table F.5 Scatter matrix of waves from W.

W	Peak period, T_p [s]																								
Significant wave height, H_{m0} [m]	1	2	3	4	5	6	7	8	9	10	11	12	13	14	15	16	17	18	19	20	21	22	23	24	25
0.5	-	0.00	0.01	0.05	0.38	0.09	0.04	0.06	0.11	0.06	0.08	0.06	0.03	0.02	0.02	0.00	0.00	0.00	0.00	-	-	0.00	-	-	-
1.0	-	-	0.00	0.12	0.65	1.07	0.56	0.18	0.10	0.10	0.16	0.16	0.15	0.11	0.06	0.05	0.02	0.02	0.01	0.01	-	0.00	0.00	-	-
1.5	-	-	-	0.00	0.14	0.69	0.99	0.75	0.19	0.08	0.07	0.07	0.09	0.10	0.16	0.08	0.05	0.03	0.01	0.01	0.00	0.00	-	-	-
2.0	-	-	-	-	0.00	0.13	0.68	0.88	0.59	0.13	0.04	0.04	0.03	0.03	0.04	0.03	0.02	0.02	0.00	0.01	-	-	-	-	-
2.5	-	-	-	-	-	0.00	0.18	0.49	0.62	0.26	0.06	0.02	0.02	0.01	0.00	0.01	0.01	0.00	0.01	0.01	0.01	-	-	-	-
3.0	-	-	-	-	-	-	0.01	0.18	0.42	0.36	0.08	0.01	0.00	0.01	0.00	0.00	0.00	-	0.00	0.01	0.00	-	-	-	-
3.5	-	-	-	-	-	-	-	0.02	0.18	0.38	0.10	0.02	0.01	-	-	-	-	-	0.00	-	-	-	-	-	-
4.0	-	-	-	-	-	-	-	0.00	0.03	0.21	0.16	0.03	0.01	-	0.00	-	-	-	-	-	-	-	-	-	-
4.5	-	-	-	-	-	-	-	-	0.00	0.06	0.15	0.05	0.00	0.00	-	-	-	-	-	-	-	-	-	-	-
5.0	-	-	-	-	-	-	-	-	0.00	0.01	0.07	0.07	0.01	0.00	-	-	-	-	-	-	-	-	-	-	-
5.5	-	-	-	-	-	-	-	-	-	0.00	0.01	0.04	0.01	0.00	0.00	-	-	-	-	-	-	-	-	-	-
6.0	-	-	-	-	-	-	-	-	-	-	0.00	0.01	0.02	0.01	0.00	-	-	-	-	-	-	-	-	-	-
6.5	-	-	-	-	-	-	-	-	-	-	-	0.00	0.01	0.00	0.00	-	-	-	-	-	-	-	-	-	-
7.0	-	-	-	-	-	-	-	-	-	-	-	-	-	-	0.00	-	-	-	-	-	-	-	-	-	-

Table F.6 Scatter matrix of waves from WNW.

WNW	Peak period, T_p [s]																								
Significant wave height, H_{m0} [m]	1	2	3	4	5	6	7	8	9	10	11	12	13	14	15	16	17	18	19	20	21	22	23	24	25
0.5	-	-	0.01	0.11	0.36	0.13	0.08	0.08	0.09	0.12	0.15	0.13	0.10	0.03	0.02	0.01	0.01	0.01	0.00	0.01	0.00	0.00	-	-	-
1.0	-	-	0.00	0.12	0.69	1.24	0.82	0.46	0.27	0.30	0.32	0.28	0.30	0.22	0.17	0.16	0.07	0.06	0.02	0.01	0.01	0.00	0.00	0.00	-
1.5	-	-	-	0.00	0.15	1.02	1.35	0.91	0.65	0.34	0.31	0.31	0.26	0.18	0.19	0.13	0.06	0.06	0.03	0.01	0.01	0.00	0.00	-	-
2.0	-	-	-	-	0.00	0.12	0.89	0.81	0.64	0.42	0.22	0.16	0.15	0.10	0.12	0.06	0.04	0.03	0.01	0.02	0.00	-	-	-	-
2.5	-	-	-	-	-	0.00	0.16	0.67	0.54	0.34	0.20	0.10	0.08	0.05	0.04	0.02	0.02	0.02	0.01	0.01	0.01	0.00	0.00	0.00	-
3.0	-	-	-	-	-	0.00	0.01	0.21	0.54	0.30	0.18	0.09	0.03	0.01	0.01	0.02	0.00	0.00	0.00	0.00	0.00	0.00	0.00	-	-
3.5	-	-	-	-	-	-	0.00	0.02	0.21	0.30	0.15	0.10	0.02	0.01	0.01	0.01	0.00	-	-	-	-	-	-	-	-
4.0	-	-	-	-	-	-	-	-	0.04	0.21	0.21	0.09	0.01	0.00	0.00	0.00	-	-	-	-	-	-	-	-	-
4.5	-	-	-	-	-	-	-	-	-	0.05	0.16	0.09	0.01	0.00	0.00	-	-	-	-	-	-	-	-	-	-
5.0	-	-	-	-	-	-	-	-	-	0.00	0.03	0.09	0.03	0.00	-	-	-	-	-	-	-	-	-	-	-
5.5	-	-	-	-	-	-	-	-	0.00	0.00	0.01	0.04	0.04	0.02	0.01	-	-	-	-	-	-	-	-	-	-
6.0	-	-	-	-	-	-	-	-	-	-	-	0.01	0.01	0.01	0.00	-	0.00	-	-	-	-	-	-	-	-
6.5	-	-	-	-	-	-	-	-	-	-	-	-	0.00	0.00	0.00	0.00	0.00	-	-	-	-	-	-	-	-
7.0	-	-	-	-	-	-	-	-	-	-	-	-	-	-	0.00	0.00	-	-	-	-	-	-	-	-	-

Table F.7 Scatter matrix of waves from NW.

NW	Peak period, T_p [s]																								
Significant wave height, H_{m0} [m]	1	2	3	4	5	6	7	8	9	10	11	12	13	14	15	16	17	18	19	20	21	22	23	24	25
0.5	-	-	0.02	0.23	0.48	0.35	0.28	0.24	0.25	0.22	0.18	0.17	0.11	0.07	0.07	0.04	0.02	0.02	0.01	0.01	0.01	0.00	0.00	-	0.00
1.0	-	-	0.00	0.13	0.67	1.41	1.26	0.73	0.58	0.38	0.44	0.33	0.21	0.15	0.22	0.12	0.08	0.04	0.02	0.01	0.01	0.00	0.01	0.00	0.00
1.5	-	-	-	0.00	0.08	0.60	1.27	0.89	0.43	0.22	0.24	0.19	0.12	0.07	0.05	0.04	0.03	0.01	0.00	0.01	-	-	-	-	-
2.0	-	-	-	-	-	0.05	0.75	0.68	0.36	0.20	0.13	0.11	0.06	0.01	0.03	0.00	0.00	0.00	-	-	-	-	-	-	-
2.5	-	-	-	-	-	0.00	0.11	0.57	0.42	0.13	0.09	0.07	0.04	0.03	0.01	0.00	0.00	0.00	-	-	-	-	-	-	-
3.0	-	-	-	-	-	0.00	0.00	0.11	0.35	0.16	0.09	0.06	0.03	0.01	0.01	0.00	-	-	-	-	-	-	-	-	-
3.5	-	-	-	-	-	-	-	0.00	0.09	0.16	0.09	0.04	0.01	0.00	0.00	-	-	-	-	-	-	-	-	-	-
4.0	-	-	-	-	-	-	-	0.00	0.02	0.10	0.07	0.05	0.01	-	-	-	-	-	-	-	-	-	-	-	-
4.5	-	-	-	-	-	-	-	-	-	0.01	0.03	0.04	0.02	-	0.00	-	-	-	-	-	-	-	-	-	-
5.0	-	-	-	-	-	-	-	-	-	-	0.01	0.01	0.01	0.00	-	-	-	-	-	-	-	-	-	-	-
5.5	-	-	-	-	-	-	-	-	-	-	0.00	0.00	0.01	0.00	0.00	-	-	-	-	-	-	-	-	-	-
6.0	-	-	-	-	-	-	-	-	-	-	-	0.00	-	-	0.00	-	-	-	-	-	-	-	-	-	-
6.5	-	-	-	-	-	-	-	-	-	-	-	-	-	-	-	-	-	-	-	-	-	-	-	-	-
7.0	-	-	-	-	-	-	-	-	-	-	-	-	-	-	-	-	-	-	-	-	-	-	-	-	-

Table F.8 Scatter matrix of waves from NNW.

NNW	Peak period, T_p [s]																								
Significant wave height, H_{m0} [m]	1	2	3	4	5	6	7	8	9	10	11	12	13	14	15	16	17	18	19	20	21	22	23	24	25
0.5	-	0.00	0.04	0.24	0.15	0.16	0.14	0.10	0.09	0.08	0.09	0.07	0.04	0.02	0.02	0.01	0.01	0.00	0.00	0.00	0.00	0.01	0.00	-	-
1.0	-	-	0.00	0.11	0.18	0.21	0.30	0.42	0.24	0.21	0.14	0.13	0.12	0.09	0.07	0.05	0.05	0.02	0.01	0.00	0.00	0.00	-	-	-
1.5	-	-	-	0.00	0.04	0.06	0.07	0.12	0.18	0.10	0.04	0.03	0.01	0.01	0.01	0.01	0.01	0.00	0.00	0.00	0.00	-	-	-	-
2.0	-	-	-	-	-	0.01	0.01	0.04	0.08	0.11	0.01	0.00	0.00	0.00	0.00	-	-	0.00	-	-	-	-	-	-	-
2.5	-	-	-	-	-	-	0.00	0.01	0.02	0.04	0.02	0.00	-	-	-	-	-	-	-	-	-	-	-	-	-
3.0	-	-	-	-	-	-	-	0.00	0.00	0.02	0.00	0.00	-	-	-	-	-	-	-	-	-	-	-	-	-
3.5	-	-	-	-	-	-	-	-	-	0.01	-	-	-	-	-	-	-	-	-	-	-	-	-	-	-
4.0	-	-	-	-	-	-	-	-	-	-	-	-	-	-	-	-	-	-	-	-	-	-	-	-	-
4.5	-	-	-	-	-	-	-	-	-	-	-	-	-	-	-	-	-	-	-	-	-	-	-	-	-
5.0	-	-	-	-	-	-	-	-	-	-	-	-	-	-	-	-	-	-	-	-	-	-	-	-	-
5.5	-	-	-	-	-	-	-	-	-	-	-	-	-	-	-	-	-	-	-	-	-	-	-	-	-
6.0	-	-	-	-	-	-	-	-	-	-	-	-	-	-	-	-	-	-	-	-	-	-	-	-	-
6.5	-	-	-	-	-	-	-	-	-	-	-	-	-	-	-	-	-	-	-	-	-	-	-	-	-
7.0	-	-	-	-	-	-	-	-	-	-	-	-	-	-	-	-	-	-	-	-	-	-	-	-	-

F.2 Weighted potential transport matrices for the Agger tongue

Table F.9 Weighted potential sediment transport matrix of waves from N at the Agger tounge. All transport values are in 10^5 m^3/hour. Positive values denote northbound transport.

N	Peak period, T_p [s]																									
Significant wave height, H_{m0} [m]	1	2	3	4	5	6	7	8	9	10	11	12	13	14	15	16	17	18	19	20	21	22	23	24	25
0.5	-	-	0.0	0.0	0.0	0.0	0.0	0.0	0.0	0.0	0.0	0.0	0.0	0.0	0.0	0.0	0.0	0.0	0.0	0.0	-	-	0.0	-	-
1.0	-	-	-	-0.1	-0.2	-0.1	-0.2	-0.2	-0.1	-0.1	-0.1	-0.1	-0.1	-0.1	-0.1	0.0	0.0	0.0	0.0	0.0	-	-	0.0	-	0.0
1.5	-	-	-	-	-0.1	-0.1	-0.2	-0.3	-0.3	-0.1	0.0	0.0	0.0	0.0	0.0	0.0	0.0	0.0	0.0	-	-	-	-	-	-
2.0	-	-	-	-	-	0.0	0.0	0.0	-0.1	0.0	0.0	-	-	-	-	-	-	-	-	-	-	-	-	-	-
2.5	-	-	-	-	-	-	-	0.0	0.0	-	-	-	-	-	-	-	-	-	-	-	-	-	-	-	-
3.0	-	-	-	-	-	-	-	-	0.0	-	-	-	-	-	-	-	-	-	-	-	-	-	-	-	-
3.5	-	-	-	-	-	-	-	-	-	-	-	-	-	-	-	-	-	-	-	-	-	-	-	-	-
4.0	-	-	-	-	-	-	-	-	-	-	-	-	-	-	-	-	-	-	-	-	-	-	-	-	-
4.5	-	-	-	-	-	-	-	-	-	-	-	-	-	-	-	-	-	-	-	-	-	-	-	-	-
5.0	-	-	-	-	-	-	-	-	-	-	-	-	-	-	-	-	-	-	-	-	-	-	-	-	-
5.5	-	-	-	-	-	-	-	-	-	-	-	-	-	-	-	-	-	-	-	-	-	-	-	-	-
6.0	-	-	-	-	-	-	-	-	-	-	-	-	-	-	-	-	-	-	-	-	-	-	-	-	-
6.5	-	-	-	-	-	-	-	-	-	-	-	-	-	-	-	-	-	-	-	-	-	-	-	-	-
7.0	-	-	-	-	-	-	-	-	-	-	-	-	-	-	-	-	-	-	-	-	-	-	-	-	-

Table F.10 Weighted potential sediment transport matrix of waves from SSW at the Agger tongue. All transport values are in 10^5 m^3/hour. Positive values denote northbound transport.

SSW	Peak period, T_p [s]																									
Significant wave height, H_{m0} [m]	1	2	3	4	5	6	7	8	9	10	11	12	13	14	15	16	17	18	19	20	21	22	23	24	25
0.5	-	-	0.0	0.0	0.1	0.0	0.0	0.0	0.0	0.0	0.0	0.0	0.0	-	0.0	-	-	-	0.0	-	-	-	-	-	-
1.0	-	-	0.0	0.2	1.0	2.6	1.3	0.5	0.4	0.3	0.3	0.3	0.1	0.3	0.2	0.1	0.1	0.1	0.0	-	0.0	0.0	0.0	-	-
1.5	-	-	-	0.0	0.2	2.1	4.5	3.3	0.6	0.1	0.1	0.1	0.3	0.1	0.2	0.1	0.1	0.1	0.2	0.0	-	-	-	-	-
2.0	-	-	-	-	0.0	0.2	1.1	2.6	0.8	0.1	-	-	0.2	0.2	0.0	0.1	-	-	-	-	-	-	-	-	-
2.5	-	-	-	-	-	0.0	0.2	0.2	0.0	-	-	-	-	-	-	-	-	-	-	-	-	-	-	-	-
3.0	-	-	-	-	-	-	-	0.0	-	-	-	-	-	-	-	-	-	-	-	-	-	-	-	-	-
3.5	-	-	-	-	-	-	-	-	-	-	-	-	-	-	-	-	-	-	-	-	-	-	-	-	-
4.0	-	-	-	-	-	-	-	-	-	-	-	-	-	-	-	-	-	-	-	-	-	-	-	-	-
4.5	-	-	-	-	-	-	-	-	-	-	-	-	-	-	-	-	-	-	-	-	-	-	-	-	-
5.0	-	-	-	-	-	-	-	-	-	-	-	-	-	-	-	-	-	-	-	-	-	-	-	-	-
5.5	-	-	-	-	-	-	-	-	-	-	-	-	-	-	-	-	-	-	-	-	-	-	-	-	-
6.0	-	-	-	-	-	-	-	-	-	-	-	-	-	-	-	-	-	-	-	-	-	-	-	-	-
6.5	-	-	-	-	-	-	-	-	-	-	-	-	-	-	-	-	-	-	-	-	-	-	-	-	-
7.0	-	-	-	-	-	-	-	-	-	-	-	-	-	-	-	-	-	-	-	-	-	-	-	-	-

Table F.11 Weighted potential sediment transport matrix of waves from SW at the Agger tongue.All transport values are in 10^5 m^3/hour. Positive values denote northbound transport.

SW	Peak period, T_p [s]																									
Significant wave height, H_{m0} [m]	1	2	3	4	5	6	7	8	9	10	11	12	13	14	15	16	17	18	19	20	21	22	23	24	25
0.5	-	-	0.0	0.1	0.1	0.1	0.0	0.0	0.0	0.0	0.0	0.0	0.0	0.0	0.0	0.0	0.0	-	-	-	-	-	-	-	-
1.0	-	-	-	0.4	2.4	5.9	5.2	1.3	0.6	0.7	0.8	0.8	0.7	0.7	0.8	0.5	0.4	0.4	0.2	0.3	0.1	-	-	-	-
1.5	-	-	-	-	1.4	9.1	17.7	12.2	3.4	1.1	0.8	0.3	0.7	0.6	0.4	0.8	1.1	1.6	1.0	0.8	0.4	-	0.2	-	-
2.0	-	-	-	-	0.1	2.4	15.3	26.1	16.4	4.4	0.6	0.3	0.3	0.2	0.1	-	0.2	0.1	0.4	0.2	-	-	-	-	-
2.5	-	-	-	-	-	0.1	4.3	20.0	22.3	11.4	1.0	-	-	-	-	-	-	-	-	-	-	-	-	-	-
3.0	-	-	-	-	-	-	0.3	5.0	16.6	15.1	3.4	-	-	-	-	-	-	-	-	-	-	-	-	-	-
3.5	-	-	-	-	-	-	-	1.0	6.0	8.0	2.1	0.1	-	-	-	-	-	-	-	-	-	-	-	-	-
4.0	-	-	-	-	-	-	-	0.1	0.8	4.3	2.9	-	-	-	-	-	-	-	-	-	-	-	-	-	-
4.5	-	-	-	-	-	-	-	-	0.1	1.6	0.7	-	-	-	-	-	-	-	-	-	-	-	-	-	-
5.0	-	-	-	-	-	-	-	-	-	-	0.7	0.3	0.3	-	-	-	-	-	-	-	-	-	-	-	-
5.5	-	-	-	-	-	-	-	-	-	-	-	0.3	-	-	-	-	-	-	-	-	-	-	-	-	-
6.0	-	-	-	-	-	-	-	-	-	-	-	0.4	-	-	-	-	-	-	-	-	-	-	-	-	-
6.5	-	-	-	-	-	-	-	-	-	-	-	-	-	-	-	-	-	-	-	-	-	-	-	-	-
7.0	-	-	-	-	-	-	-	-	-	-	-	-	-	-	-	-	-	-	-	-	-	-	-	-	-

Table F.12 Weighted potential sediment transport matrix of waves from WSW at the Agger tongue. All transport values are in 10^5 m^3/hour. Positive values denote northbound transport.

WSW	Peak period, T_p [s]																								
Significant wave height, H_{m0} [m]	1	2	3	4	5	6	7	8	9	10	11	12	13	14	15	16	17	18	19	20	21	22	23	24	25
0.5	-	-	0.0	0.0	0.1	0.1	0.0	0.0	0.0	0.0	0.1	0.1	0.0	0.0	0.0	0.0	0.0	0.0	0.0	-	0.0	-	-	-	-
1.0	-	-	0.0	0.2	2.1	6.7	4.5	1.1	0.6	0.5	0.7	0.9	0.8	0.8	0.9	0.7	0.5	0.4	0.1	0.1	0.1	0.0	0.1	-	-
1.5	-	-	-	0.0	1.4	8.5	18.3	14.1	3.7	0.8	0.8	0.9	0.8	0.9	1.5	1.8	1.1	1.4	0.4	0.9	0.3	0.5	0.2	-	-
2.0	-	-	-	-	0.1	2.7	17.9	31.0	20.5	4.2	1.0	0.7	0.7	0.9	0.8	1.6	0.6	0.2	0.8	0.6	-	-	-	-	-
2.5	-	-	-	-	-	0.3	8.7	33.0	41.7	16.2	2.2	0.3	0.2	0.1	0.1	-	0.2	-	-	0.1	-	-	-	-	-
3.0	-	-	-	-	-	-	0.9	11.3	45.1	39.7	5.1	0.7	-	-	-	-	-	-	-	-	-	-	-	-	-
3.5	-	-	-	-	-	-	-	2.3	22.9	46.0	15.0	0.6	-	-	-	-	-	-	-	-	-	-	-	-	-
4.0	-	-	-	-	-	-	-	-	4.4	36.8	37.5	2.1	-	-	-	-	-	-	-	-	-	-	-	-	-
4.5	-	-	-	-	-	-	-	-	0.7	8.2	37.3	11.8	0.6	0.2	-	-	-	-	-	-	-	-	-	-	-
5.0	-	-	-	-	-	-	-	-	-	1.3	11.2	15.9	-	0.3	-	-	-	-	-	-	-	-	-	-	-
5.5	-	-	-	-	-	-	-	-	-	-	2.8	4.4	1.3	0.4	-	-	-	-	-	-	-	-	-	-	-
6.0	-	-	-	-	-	-	-	-	-	0.3	-	1.4	2.4	1.3	-	-	-	-	-	-	-	-	-	-	-
6.5	-	-	-	-	-	-	-	-	-	-	-	-	0.5	0.5	-	-	-	-	-	-	-	-	-	-	-
7.0	-	-	-	-	-	-	-	-	-	-	-	-	-	0.6	-	-	-	-	-	-	-	-	-	-	-

Table F.13 Weighted potential sediment transport matrix of waves from W at the Agger tongue. All transport values are in 10^5 m^3/hour. Positive values denote northbound transport.

W	Peak period, T_p [s]																								
Significant wave height, H_{m0} [m]	1	2	3	4	5	6	7	8	9	10	11	12	13	14	15	16	17	18	19	20	21	22	23	24	25
0.5	-	0.0	0.0	0.0	0.0	0.0	0.0	0.0	0.0	0.0	0.0	0.0	0.0	0.0	0.0	0.0	0.0	0.0	0.0	-	-	0.0	-	-	-
1.0	-	-	0.0	0.1	0.6	1.3	0.8	0.3	0.2	0.2	0.4	0.4	0.5	0.4	0.2	0.2	0.1	0.1	0.0	0.1	-	0.0	0.0	-	-
1.5	-	-	-	0.0	0.4	2.4	4.0	3.5	1.0	0.5	0.5	0.6	0.8	0.9	1.7	1.0	0.7	0.4	0.1	0.2	0.0	0.0	-	-	-
2.0	-	-	-	-	0.0	0.9	5.4	8.0	6.1	1.6	0.5	0.6	0.6	0.6	0.9	0.7	0.5	0.5	0.1	0.5	-	-	-	-	-
2.5	-	-	-	-	-	0.1	2.4	7.3	10.7	5.1	1.3	0.4	0.5	0.2	0.1	0.2	0.3	0.1	0.5	0.9	0.6	-	-	-	-
3.0	-	-	-	-	-	-	0.2	4.0	10.9	10.5	2.7	0.6	0.2	0.4	0.1	0.1	0.1	-	0.1	0.9	0.3	-	-	-	-
3.5	-	-	-	-	-	-	-	0.8	6.6	15.4	4.7	1.0	0.4	-	-	-	-	-	0.1	-	-	-	-	-	-
4.0	-	-	-	-	-	-	-	0.1	1.4	11.2	10.1	2.0	0.5	-	0.1	-	-	-	-	-	-	-	-	-	-
4.5	-	-	-	-	-	-	-	-	0.1	4.0	11.9	4.1	0.2	0.1	-	-	-	-	-	-	-	-	-	-	-
5.0	-	-	-	-	-	-	-	-	0.1	0.7	6.5	7.6	0.8	0.2	-	-	-	-	-	-	-	-	-	-	-
5.5	-	-	-	-	-	-	-	-	-	0.1	1.3	5.4	2.0	0.6	0.1	-	-	-	-	-	-	-	-	-	-
6.0	-	-	-	-	-	-	-	-	-	-	0.5	2.0	4.0	1.6	0.8	-	-	-	-	-	-	-	-	-	-
6.5	-	-	-	-	-	-	-	-	-	-	-	0.3	1.3	0.8	0.2	-	-	-	-	-	-	-	-	-	-
7.0	-	-	-	-	-	-	-	-	-	-	-	-	-	-	0.2	-	-	-	-	-	-	-	-	-	-

Table F.14 Weighted potential sediment transport matrix of waves from WNW at the Agger tongue. All transport values are in 10^5 m^3/hour. Positive values denote northbound transport.

WNW	Peak period, T_p [s]																								
Significant wave height, H_{m0} [m]	1	2	3	4	5	6	7	8	9	10	11	12	13	14	15	16	17	18	19	20	21	22	23	24	25
0.5	-	-	0.0	0.0	-0.1	-0.1	0.0	0.0	-0.1	-0.1	-0.1	-0.1	-0.1	0.0	0.0	0.0	0.0	0.0	0.0	0.0	0.0	0.0	-	-	-
1.0	-	-	0.0	-0.2	-1.9	-4.5	-3.5	-2.3	-1.5	-1.9	-2.3	-2.3	-2.7	-2.3	-1.9	-2.1	-0.9	-1.0	-0.4	-0.3	-0.2	-0.1	-0.1	-0.1	-0.1
1.5	-	-	-	0.0	-1.2	-10.4	-16.1	-12.3	-10.1	-6.0	-6.2	-6.9	-6.6	-5.2	-5.9	-4.4	-2.4	-2.5	-1.5	-0.6	-0.3	-0.1	0.0	-	-
2.0	-	-	-	-	0.0	-2.4	-20.9	-21.6	-19.3	-14.4	-8.4	-7.2	-7.4	-5.4	-7.5	-4.3	-2.7	-2.6	-1.1	-2.0	-0.1	-	-	-	-
2.5	-	-	-	-	-	-0.1	-6.4	-29.8	-27.0	-19.6	-12.9	-7.2	-6.5	-4.7	-3.9	-2.2	-2.9	-2.9	-1.0	-1.2	-1.9	-0.1	-0.4	-0.2	-0.2
3.0	-	-	-	-	-	0.0	-0.3	-13.7	-40.2	-25.3	-17.8	-9.8	-3.1	-1.8	-1.8	-2.8	-0.4	-0.3	-0.1	-0.3	-0.5	-0.6	-0.4	-	-
3.5	-	-	-	-	-	-	-0.1	-1.6	-21.7	-35.8	-20.4	-14.5	-4.2	-2.0	-2.4	-2.6	-1.2	-	-	-	-	-	-	-	-
4.0	-	-	-	-	-	-	-	-	-5.9	-33.8	-36.9	-19.1	-1.8	-1.0	-0.4	-0.8	-	-	-	-	-	-	-	-	-
4.5	-	-	-	-	-	-	-	-	-	-9.9	-37.7	-24.6	-3.4	-0.4	-0.5	-	-	-	-	-	-	-	-	-	-
5.0	-	-	-	-	-	-	-	-	-	-0.8	-9.9	-28.6	-11.2	-1.9	-	-	-	-	-	-	-	-	-	-	-
5.5	-	-	-	-	-	-	-	-	-0.2	-0.2	-1.8	-17.3	-15.7	-8.5	-2.9	-	-	-	-	-	-	-	-	-	-
6.0	-	-	-	-	-	-	-	-	-	-	-	-3.1	-7.7	-5.5	-3.1	-	-0.5	-	-	-	-	-	-	-	-
6.5	-	-	-	-	-	-	-	-	-	-	-	-	-0.8	-1.9	-0.5	-1.2	-1.9	-3.5	-	-	-	-	-	-	-
7.0	-	-	-	-	-	-	-	-	-	-	-	-	-	-	-0.6	-0.7	-	-	-	-	-	-	-	-	-

Table F.15 Weighted potential sediment transport matrix of waves from NW at the Agger tongue. All transport values are in 10^5 m^3/hour. Positive values denote northbound transport.

NW	Peak period, T_p [s]																								
Significant wave height, H_{m0} [m]	1	2	3	4	5	6	7	8	9	10	11	12	13	14	15	16	17	18	19	20	21	22	23	24	25
0.5	-	-	0.0	-0.1	-0.2	-0.2	-0.2	-0.2	-0.2	-0.2	-0.2	-0.2	-0.1	-0.1	-0.1	-0.1	0.0	0.0	0.0	0.0	0.0	0.0	0.0	-	0.0
1.0	-	-	0.0	-0.3	-2.5	-6.8	-7.1	-4.6	-4.1	-3.0	-4.0	-3.3	-2.4	-1.9	-3.0	-1.9	-1.4	-0.8	-0.5	-0.3	-0.2	-0.1	-0.2	-0.1	-0.1
1.5	-	-	-	0.0	-0.9	-8.1	-19.8	-15.6	-8.4	-5.0	-6.1	-5.2	-3.7	-2.4	-2.0	-1.5	-1.2	-0.7	-0.1	-0.4	-	-	-	-	-
2.0	-	-	-	-	-	-1.4	-23.0	-23.6	-14.0	-8.8	-6.2	-6.0	-3.5	-0.9	-2.0	-0.1	-0.2	-0.3	-	-	-	-	-	-	-
2.5	-	-	-	-	-	0.0	-5.6	-32.7	-27.1	-9.7	-6.9	-6.6	-4.2	-3.0	-1.0	-0.1	-0.2	-0.8	-	-	-	-	-	-	-
3.0	-	-	-	-	-	0.0	-0.1	-9.1	-33.2	-17.6	-10.3	-8.6	-5.2	-1.5	-2.5	-0.1	-	-	-	-	-	-	-	-	-
3.5	-	-	-	-	-	-	-	-0.5	-11.8	-23.3	-14.9	-7.5	-1.8	-0.3	-1.2	-	-	-	-	-	-	-	-	-	-
4.0	-	-	-	-	-	-	-	-0.1	-3.0	-19.1	-16.1	-11.6	-2.6	-	-	-	-	-	-	-	-	-	-	-	-
4.5	-	-	-	-	-	-	-	-	-	-1.8	-9.6	-13.5	-8.0	-	-0.3	-	-	-	-	-	-	-	-	-	-
5.0	-	-	-	-	-	-	-	-	-	-	-2.8	-4.5	-4.7	-2.0	-	-	-	-	-	-	-	-	-	-	-
5.5	-	-	-	-	-	-	-	-	-	-	-0.3	-1.3	-3.2	-1.2	-1.8	-	-	-	-	-	-	-	-	-	-
6.0	-	-	-	-	-	-	-	-	-	-	-	-0.4	-	-	-1.1	-	-	-	-	-	-	-	-	-	-
6.5	-	-	-	-	-	-	-	-	-	-	-	-	-	-	-	-	-	-	-	-	-	-	-	-	-
7.0	-	-	-	-	-	-	-	-	-	-	-	-	-	-	-	-	-	-	-	-	-	-	-	-	-

Table F.16 Weighted potential sediment transport matrix of waves from NNW at the Agger tongue. All transport values are in 10^5 m^3/hour. Positive values denote northbound transport.

NNW	Peak period, T_p [s]																								
Significant wave height, H_{m0} [m]	1	2	3	4	5	6	7	8	9	10	11	12	13	14	15	16	17	18	19	20	21	22	23	24	25
0.5	-	0.0	0.0	-0.1	-0.1	-0.1	-0.1	-0.1	-0.1	-0.1	-0.1	-0.1	0.0	0.0	0.0	0.0	0.0	0.0	0.0	0.0	0.0	0.0	0.0	-	0.0
1.0	-	-	0.0	-0.2	-0.6	-0.9	-1.4	-2.1	-1.3	-1.3	-1.0	-0.9	-1.0	-0.8	-0.8	-0.5	-0.6	-0.3	-0.2	-0.1	0.0	0.0	-	-	-0.1
1.5	-	-	-	0.0	-0.3	-0.7	-0.9	-1.7	-2.8	-1.7	-0.8	-0.7	-0.2	-0.2	-0.3	-0.3	-0.2	-0.2	-0.1	-0.1	0.0	-	-	-	-
2.0	-	-	-	-	-	-0.2	-0.3	-1.2	-2.4	-3.6	-0.5	0.0	-0.2	0.0	-0.1	-	-	0.0	-	-	-	-	-	-	-
2.5	-	-	-	-	-	-	0.0	-0.5	-1.2	-2.4	-1.2	-0.2	-	-	-	-	-	-	-	-	-	-	-	-	-
3.0	-	-	-	-	-	-	-	-0.3	-0.3	-1.3	-0.2	-0.1	-	-	-	-	-	-	-	-	-	-	-	-	-
3.5	-	-	-	-	-	-	-	-	-	-0.6	-	-	-	-	-	-	-	-	-	-	-	-	-	-	-
4.0	-	-	-	-	-	-	-	-	-	-	-	-	-	-	-	-	-	-	-	-	-	-	-	-	-
4.5	-	-	-	-	-	-	-	-	-	-	-	-	-	-	-	-	-	-	-	-	-	-	-	-	-
5.0	-	-	-	-	-	-	-	-	-	-	-	-	-	-	-	-	-	-	-	-	-	-	-	-	-
5.5	-	-	-	-	-	-	-	-	-	-	-	-	-	-	-	-	-	-	-	-	-	-	-	-	-
6.0	-	-	-	-	-	-	-	-	-	-	-	-	-	-	-	-	-	-	-	-	-	-	-	-	-
6.5	-	-	-	-	-	-	-	-	-	-	-	-	-	-	-	-	-	-	-	-	-	-	-	-	-
7.0	-	-	-	-	-	-	-	-	-	-	-	-	-	-	-	-	-	-	-	-	-	-	-	-	-

F.3 Weighted potential transport matrices for the Harboøre tongue

Table F.17 Weighted potential sediment transport matrix of waves from N at the Thyborøn tongue. All transport values are in 10^5 m^3/hour. Positive values denote northbound transport.

N	Peak period, T_p [s]																								
Significant wave height, H_{m0} [m]	1	2	3	4	5	6	7	8	9	10	11	12	13	14	15	16	17	18	19	20	21	22	23	24	25
0.5	-	-	0.0	0.0	0.0	0.0	0.0	0.0	0.0	0.0	0.0	0.0	0.0	0.0	0.0	0.0	0.0	0.0	0.0	0.0	-	-	0.0	-	-
1.0	-	-	-	-0.2	-0.7	-0.6	-1.0	-1.1	-0.7	-0.7	-0.4	-0.4	-0.5	-0.5	-0.4	-0.1	-0.1	0.0	-0.1	-0.1	-	-	0.0	-	0.0
1.5	-	-	-	-	-0.2	-0.3	-1.1	-2.2	-1.8	-0.5	-0.3	-0.1	0.0	0.0	-0.1	-0.2	-0.2	-0.1	0.0	-	-	-	-	-	-
2.0	-	-	-	-	-	-0.1	-0.2	-0.3	-0.5	-0.2	0.0	-	-	-	-	-	-	-	-	-	-	-	-	-	-
2.5	-	-	-	-	-	-	-	-0.1	0.0	-	-	-	-	-	-	-	-	-	-	-	-	-	-	-	-
3.0	-	-	-	-	-	-	-	-	0.0	-	-	-	-	-	-	-	-	-	-	-	-	-	-	-	-
3.5	-	-	-	-	-	-	-	-	-	-	-	-	-	-	-	-	-	-	-	-	-	-	-	-	-
4.0	-	-	-	-	-	-	-	-	-	-	-	-	-	-	-	-	-	-	-	-	-	-	-	-	-
4.5	-	-	-	-	-	-	-	-	-	-	-	-	-	-	-	-	-	-	-	-	-	-	-	-	-
5.0	-	-	-	-	-	-	-	-	-	-	-	-	-	-	-	-	-	-	-	-	-	-	-	-	-
5.5	-	-	-	-	-	-	-	-	-	-	-	-	-	-	-	-	-	-	-	-	-	-	-	-	-
6.0	-	-	-	-	-	-	-	-	-	-	-	-	-	-	-	-	-	-	-	-	-	-	-	-	-
6.5	-	-	-	-	-	-	-	-	-	-	-	-	-	-	-	-	-	-	-	-	-	-	-	-	-
7.0	-	-	-	-	-	-	-	-	-	-	-	-	-	-	-	-	-	-	-	-	-	-	-	-	-

Table F.18 Weighted potential sediment transport matrix of waves from SW at the Thyborøn tongue. All transport values are in 10^5 m^3/hour. Positive values denote northbound transport.

SW	Peak period, T_p [s]																								
Significant wave height, H_{m0} [m]	1	2	3	4	5	6	7	8	9	10	11	12	13	14	15	16	17	18	19	20	21	22	23	24	25
0.5	-	-	0.0	0.0	0.1	0.1	0.0	0.0	0.0	0.0	0.0	0.0	0.0	0.0	0.0	0.0	0.0	-	-	-	-	-	-	-	-
1.0	-	-	-	0.3	2.0	4.7	4.0	0.9	0.4	0.5	0.5	0.5	0.5	0.5	0.5	0.3	0.3	0.2	0.1	0.2	0.1	-	-	-	-
1.5	-	-	-	-	1.1	7.3	13.7	9.0	2.4	0.8	0.5	0.2	0.5	0.4	0.2	0.5	0.7	1.0	0.7	0.5	0.3	-	0.1	-	-
2.0	-	-	-	-	0.1	1.9	11.8	19.1	11.5	3.0	0.4	0.2	0.2	0.1	0.1	-	0.1	0.0	0.2	0.2	-	-	-	-	-
2.5	-	-	-	-	-	0.1	3.3	14.7	15.7	7.8	0.7	-	-	-	-	-	-	-	-	-	-	-	-	-	-
3.0	-	-	-	-	-	-	0.2	3.7	11.7	10.4	2.3	-	-	-	-	-	-	-	-	-	-	-	-	-	-
3.5	-	-	-	-	-	-	-	0.7	4.2	5.5	1.4	0.1	-	-	-	-	-	-	-	-	-	-	-	-	-
4.0	-	-	-	-	-	-	-	0.1	0.6	3.0	1.9	-	-	-	-	-	-	-	-	-	-	-	-	-	-
4.5	-	-	-	-	-	-	-	-	0.1	1.1	0.5	-	-	-	-	-	-	-	-	-	-	-	-	-	-
5.0	-	-	-	-	-	-	-	-	-	-	0.5	0.2	0.2	-	-	-	-	-	-	-	-	-	-	-	-
5.5	-	-	-	-	-	-	-	-	-	-	-	0.2	-	-	-	-	-	-	-	-	-	-	-	-	-
6.0	-	-	-	-	-	-	-	-	-	-	-	0.3	-	-	-	-	-	-	-	-	-	-	-	-	-
6.5	-	-	-	-	-	-	-	-	-	-	-	-	-	-	-	-	-	-	-	-	-	-	-	-	-
7.0	-	-	-	-	-	-	-	-	-	-	-	-	-	-	-	-	-	-	-	-	-	-	-	-	-

Table F.19 Weighted potential sediment transport matrix of waves from WSW at the Thyborøn tongue. All transport values are in 10^5 m^3/hour. Positive values denote northbound transport.

WSW	Peak period, T_p [s]																								
Significant wave height, H_{m0} [m]	1	2	3	4	5	6	7	8	9	10	11	12	13	14	15	16	17	18	19	20	21	22	23	24	25
0.5	-	-	0.0	0.0	0.2	0.1	0.0	0.0	0.0	0.1	0.1	0.1	0.0	0.0	0.0	0.0	0.0	0.0	0.0	-	0.0	-	-	-	-
1.0	-	-	0.0	0.2	2.4	7.8	5.2	1.2	0.7	0.6	0.7	1.0	0.9	0.9	0.9	0.7	0.5	0.4	0.1	0.1	0.1	0.0	0.1	-	-
1.5	-	-	-	0.0	1.6	9.9	21.1	16.0	4.1	0.9	0.9	1.0	0.8	0.9	1.6	2.0	1.2	1.5	0.4	0.9	0.4	0.5	0.2	-	-
2.0	-	-	-	-	0.1	3.1	20.6	35.3	23.0	4.6	1.1	0.8	0.8	0.9	0.8	1.7	0.6	0.3	0.9	0.6	-	-	-	-	-
2.5	-	-	-	-	-	0.4	10.0	37.5	46.8	17.9	2.4	0.4	0.2	0.1	0.1	-	0.2	-	-	0.1	-	-	-	-	-
3.0	-	-	-	-	-	-	1.0	12.9	50.6	44.0	5.6	0.8	-	-	-	-	-	-	-	-	-	-	-	-	-
3.5	-	-	-	-	-	-	-	2.6	25.7	51.1	16.5	0.6	-	-	-	-	-	-	-	-	-	-	-	-	-
4.0	-	-	-	-	-	-	-	-	5.0	40.8	41.2	2.3	-	-	-	-	-	-	-	-	-	-	-	-	-
4.5	-	-	-	-	-	-	-	-	0.7	9.1	41.1	12.9	0.7	0.3	-	-	-	-	-	-	-	-	-	-	-
5.0	-	-	-	-	-	-	-	-	-	1.4	12.3	17.4	-	0.3	-	-	-	-	-	-	-	-	-	-	-
5.5	-	-	-	-	-	-	-	-	-	-	3.1	4.8	1.4	0.4	-	-	-	-	-	-	-	-	-	-	-
6.0	-	-	-	-	-	-	-	-	-	0.3	-	1.5	2.6	1.4	-	-	-	-	-	-	-	-	-	-	-
6.5	-	-	-	-	-	-	-	-	-	-	-	-	0.5	0.6	-	-	-	-	-	-	-	-	-	-	-
7.0	-	-	-	-	-	-	-	-	-	-	-	-	-	0.7	-	-	-	-	-	-	-	-	-	-	-

Table F.20 Weighted potential sediment transport matrix of waves from W at the Thyborøn tongue. All transport values are in 10^5 m^3/hour. Positive values denote northbound transport.

W	Peak period, T_p [s]																								
Significant wave height, H_{m0} [m]	1	2	3	4	5	6	7	8	9	10	11	12	13	14	15	16	17	18	19	20	21	22	23	24	25
0.5	-	0.0	0.0	0.0	0.1	0.0	0.0	0.0	0.1	0.0	0.1	0.1	0.0	0.0	0.0	0.0	0.0	0.0	0.0	-	-	0.0	-	-	-
1.0	-	-	0.0	0.3	2.0	4.2	2.6	1.0	0.6	0.7	1.2	1.4	1.5	1.2	0.7	0.7	0.4	0.3	0.1	0.2	-	0.0	0.0	-	-
1.5	-	-	-	0.0	1.2	7.6	12.8	11.1	3.1	1.4	1.6	1.8	2.6	2.9	5.3	3.2	2.1	1.2	0.4	0.5	0.1	0.0	-	-	-
2.0	-	-	-	-	0.1	2.8	17.2	25.3	19.3	4.9	1.6	2.0	1.8	1.7	2.8	2.3	1.5	1.5	0.4	1.4	-	-	-	-	-
2.5	-	-	-	-	-	0.2	7.5	23.2	33.8	16.1	4.2	1.2	1.5	0.8	0.3	0.6	0.9	0.4	1.5	2.7	1.8	-	-	-	-
3.0	-	-	-	-	-	-	0.7	12.6	34.4	33.1	8.5	1.8	0.6	1.2	0.3	0.2	0.3	-	0.2	2.6	1.0	-	-	-	-
3.5	-	-	-	-	-	-	-	2.5	20.9	48.5	14.6	3.0	1.3	-	-	-	-	-	0.2	-	-	-	-	-	-
4.0	-	-	-	-	-	-	-	0.3	4.3	35.3	31.5	6.1	1.6	-	0.2	-	-	-	-	-	-	-	-	-	-
4.5	-	-	-	-	-	-	-	-	0.4	12.6	37.4	13.0	0.6	0.2	-	-	-	-	-	-	-	-	-	-	-
5.0	-	-	-	-	-	-	-	-	0.3	2.1	20.2	23.7	2.6	0.6	-	-	-	-	-	-	-	-	-	-	-
5.5	-	-	-	-	-	-	-	-	-	0.2	4.2	17.0	6.3	1.8	0.4	-	-	-	-	-	-	-	-	-	-
6.0	-	-	-	-	-	-	-	-	-	-	1.5	6.4	12.4	5.1	2.4	-	-	-	-	-	-	-	-	-	-
6.5	-	-	-	-	-	-	-	-	-	-	-	0.8	4.0	2.5	0.6	-	-	-	-	-	-	-	-	-	-
7.0	-	-	-	-	-	-	-	-	-	-	-	-	-	-	0.6	-	-	-	-	-	-	-	-	-	-

Table F.21 Weighted potential sediment transport matrix of waves from WNW at the Thyborøn tongue. All transport values are in 10^5 m^3/hour. Positive values denote northbound transport.

WNW	Peak period, T_p [s]																								
Significant wave height, H_{m0} [m]	1	2	3	4	5	6	7	8	9	10	11	12	13	14	15	16	17	18	19	20	21	22	23	24	25
0.5	-	-	0.0	0.0	0.0	0.0	0.0	0.0	0.0	0.0	0.0	0.0	0.0	0.0	0.0	0.0	0.0	0.0	0.0	0.0	0.0	0.0	-	-	-
1.0	-	-	0.0	0.0	0.2	0.5	0.4	0.3	0.2	0.2	0.3	0.3	0.3	0.3	0.2	0.2	0.1	0.1	0.0	0.0	0.0	0.0	0.0	0.0	0.0
1.5	-	-	-	0.0	0.1	1.2	1.9	1.4	1.2	0.7	0.7	0.8	0.8	0.6	0.7	0.5	0.3	0.3	0.2	0.1	0.0	0.0	0.0	-	-
2.0	-	-	-	-	0.0	0.3	2.4	2.5	2.3	1.7	1.0	0.8	0.9	0.6	0.9	0.5	0.3	0.3	0.1	0.2	0.0	-	-	-	-
2.5	-	-	-	-	-	0.0	0.7	3.5	3.2	2.3	1.5	0.9	0.8	0.6	0.5	0.3	0.3	0.3	0.1	0.1	0.2	0.0	0.1	0.0	0.0
3.0	-	-	-	-	-	0.0	0.0	1.6	4.7	3.0	2.1	1.2	0.4	0.2	0.2	0.3	0.0	0.0	0.0	0.0	0.1	0.1	0.0	-	-
3.5	-	-	-	-	-	-	0.0	0.2	2.5	4.2	2.4	1.7	0.5	0.2	0.3	0.3	0.1	-	-	-	-	-	-	-	-
4.0	-	-	-	-	-	-	-	-	0.7	4.0	4.3	2.3	0.2	0.1	0.0	0.1	-	-	-	-	-	-	-	-	-
4.5	-	-	-	-	-	-	-	-	-	1.2	4.4	2.9	0.4	0.1	0.1	-	-	-	-	-	-	-	-	-	-
5.0	-	-	-	-	-	-	-	-	-	0.1	1.2	3.4	1.3	0.2	-	-	-	-	-	-	-	-	-	-	-
5.5	-	-	-	-	-	-	-	-	0.0	0.0	0.2	2.0	1.9	1.0	0.3	-	-	-	-	-	-	-	-	-	-
6.0	-	-	-	-	-	-	-	-	-	-	-	0.4	0.9	0.6	0.4	-	0.1	-	-	-	-	-	-	-	-
6.5	-	-	-	-	-	-	-	-	-	-	-	-	0.1	0.2	0.1	0.1	0.2	0.4	-	-	-	-	-	-	-
7.0	-	-	-	-	-	-	-	-	-	-	-	-	-	-	0.1	0.1	-	-	-	-	-	-	-	-	-

Table F.22 Weighted potential sediment transport matrix of waves from NW at the Thyborøn tongue. All transport values are in 10^5 m^3/hour. Positive values denote northbound transport.

NW	Peak period, T_p [s]																								
Significant wave height, H_{m0} [m]	1	2	3	4	5	6	7	8	9	10	11	12	13	14	15	16	17	18	19	20	21	22	23	24	25
0.5	-	-	0.0	-0.1	-0.2	-0.1	-0.1	-0.1	-0.2	-0.2	-0.2	-0.2	-0.1	-0.1	-0.1	-0.1	0.0	0.0	0.0	0.0	0.0	0.0	0.0	-	0.0
1.0	-	-	0.0	-0.3	-2.0	-5.5	-5.8	-3.8	-3.4	-2.5	-3.3	-2.8	-2.0	-1.6	-2.6	-1.7	-1.2	-0.7	-0.4	-0.2	-0.1	-0.1	-0.2	-0.1	-0.1
1.5	-	-	-	0.0	-0.7	-6.5	-16.1	-12.8	-7.0	-4.2	-5.1	-4.5	-3.1	-2.1	-1.7	-1.3	-1.1	-0.6	-0.1	-0.3	-	-	-	-	-
2.0	-	-	-	-	-	-1.1	-18.6	-19.4	-11.7	-7.4	-5.2	-5.1	-3.0	-0.8	-1.8	-0.1	-0.2	-0.3	-	-	-	-	-	-	-
2.5	-	-	-	-	-	0.0	-4.5	-26.9	-22.5	-8.1	-5.9	-5.6	-3.6	-2.6	-0.8	-0.1	-0.2	-0.7	-	-	-	-	-	-	-
3.0	-	-	-	-	-	0.0	-0.1	-7.5	-27.6	-14.7	-8.7	-7.4	-4.5	-1.3	-2.1	-0.1	-	-	-	-	-	-	-	-	-
3.5	-	-	-	-	-	-	-	-0.4	-9.8	-19.5	-12.6	-6.4	-1.5	-0.3	-1.0	-	-	-	-	-	-	-	-	-	-
4.0	-	-	-	-	-	-	-	-0.1	-2.5	-16.1	-13.6	-9.9	-2.2	-	-	-	-	-	-	-	-	-	-	-	-
4.5	-	-	-	-	-	-	-	-	-	-1.5	-8.1	-11.5	-6.9	-	-0.3	-	-	-	-	-	-	-	-	-	-
5.0	-	-	-	-	-	-	-	-	-	-	-2.4	-3.8	-4.0	-1.7	-	-	-	-	-	-	-	-	-	-	-
5.5	-	-	-	-	-	-	-	-	-	-	-0.2	-1.1	-2.8	-1.0	-1.5	-	-	-	-	-	-	-	-	-	-
6.0	-	-	-	-	-	-	-	-	-	-	-	-0.3	-	-	-0.9	-	-	-	-	-	-	-	-	-	-
6.5	-	-	-	-	-	-	-	-	-	-	-	-	-	-	-	-	-	-	-	-	-	-	-	-	-
7.0	-	-	-	-	-	-	-	-	-	-	-	-	-	-	-	-	-	-	-	-	-	-	-	-	-

Table F.23 Weighted potential sediment transport matrix of waves from NNW at the Thyborøn tongue. All transport values are in 10^5 m^3/hour. Positive values denote northbound transport.

NNW	Peak period, T_p [s]																								
Significant wave height, H_{m0} [m]	1	2	3	4	5	6	7	8	9	10	11	12	13	14	15	16	17	18	19	20	21	22	23	24	25
0.5	-	0.0	0.0	-0.1	-0.1	-0.1	-0.1	-0.1	-0.1	-0.1	-0.1	-0.1	-0.1	0.0	0.0	0.0	0.0	0.0	0.0	0.0	0.0	0.0	0.0	-	0.0
1.0	-	-	0.0	-0.3	-0.7	-1.0	-1.7	-2.6	-1.7	-1.7	-1.3	-1.3	-1.4	-1.1	-1.0	-0.8	-0.9	-0.4	-0.2	-0.1	0.0	0.0	-	-	-0.1
1.5	-	-	-	0.0	-0.4	-0.8	-1.0	-2.2	-3.6	-2.3	-1.1	-0.9	-0.3	-0.3	-0.4	-0.4	-0.3	-0.2	-0.1	-0.1	0.0	-	-	-	-
2.0	-	-	-	-	-	-0.2	-0.3	-1.5	-3.1	-4.7	-0.6	0.0	-0.2	0.0	-0.1	-	-	-0.1	-	-	-	-	-	-	-
2.5	-	-	-	-	-	-	0.0	-0.6	-1.6	-3.2	-1.6	-0.2	-	-	-	-	-	-	-	-	-	-	-	-	-
3.0	-	-	-	-	-	-	-	-0.3	-0.4	-1.7	-0.3	-0.1	-	-	-	-	-	-	-	-	-	-	-	-	-
3.5	-	-	-	-	-	-	-	-	-	-0.8	-	-	-	-	-	-	-	-	-	-	-	-	-	-	-
4.0	-	-	-	-	-	-	-	-	-	-	-	-	-	-	-	-	-	-	-	-	-	-	-	-	-
4.5	-	-	-	-	-	-	-	-	-	-	-	-	-	-	-	-	-	-	-	-	-	-	-	-	-
5.0	-	-	-	-	-	-	-	-	-	-	-	-	-	-	-	-	-	-	-	-	-	-	-	-	-
5.5	-	-	-	-	-	-	-	-	-	-	-	-	-	-	-	-	-	-	-	-	-	-	-	-	-
6.0	-	-	-	-	-	-	-	-	-	-	-	-	-	-	-	-	-	-	-	-	-	-	-	-	-
6.5	-	-	-	-	-	-	-	-	-	-	-	-	-	-	-	-	-	-	-	-	-	-	-	-	-
7.0	-	-	-	-	-	-	-	-	-	-	-	-	-	-	-	-	-	-	-	-	-	-	-	-	-

Meshes used in Limfjord model calibration

G

Different meshes are created to investigate the important aspects of the final mesh for the Limfjord model. Figures G.1-G.4 show the different meshes applied in the calibration. The eastern part of the Limfjord is also meshed, however, to improve visibility of the rest, it is not shown in the figures.

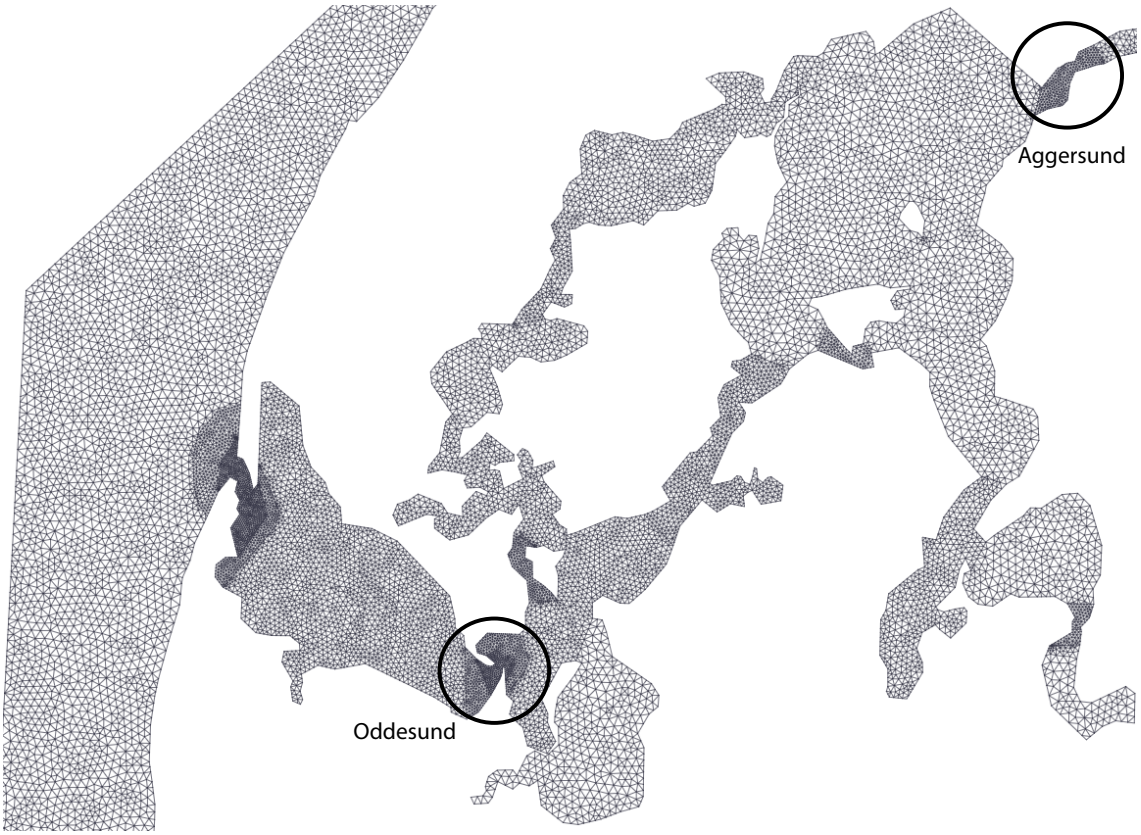

Figure G.1 5th iteration of the mesh.

Regarding the fifth iteration shown in Figure G.1 it was found that modelling such a large part of the west coast was unnecessary. Therefore the sixth one is drastically reduced.

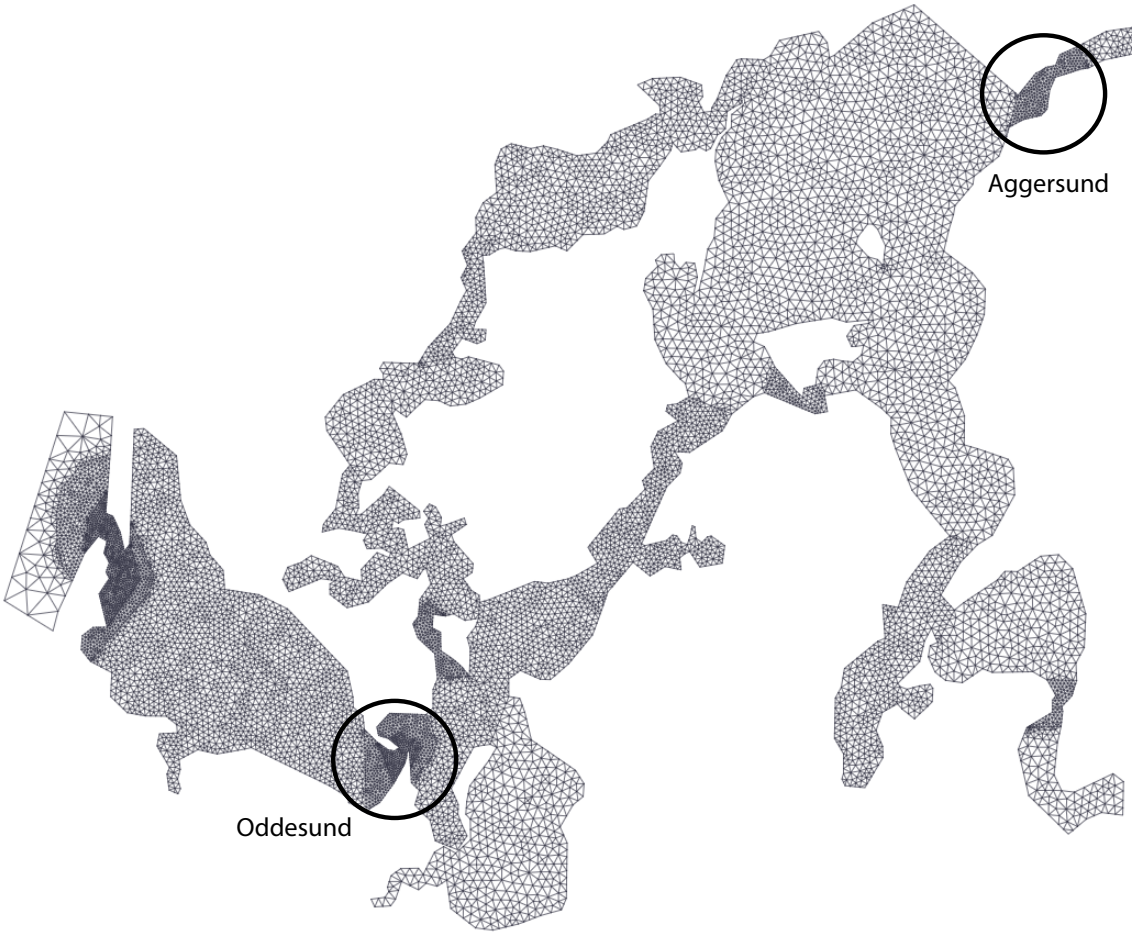

Figure G.2 6^{th} iteration of the mesh.

The seventh and eights mesh iterations shown in Figures G.3 and G.4 investigates the influence of refining the mesh.

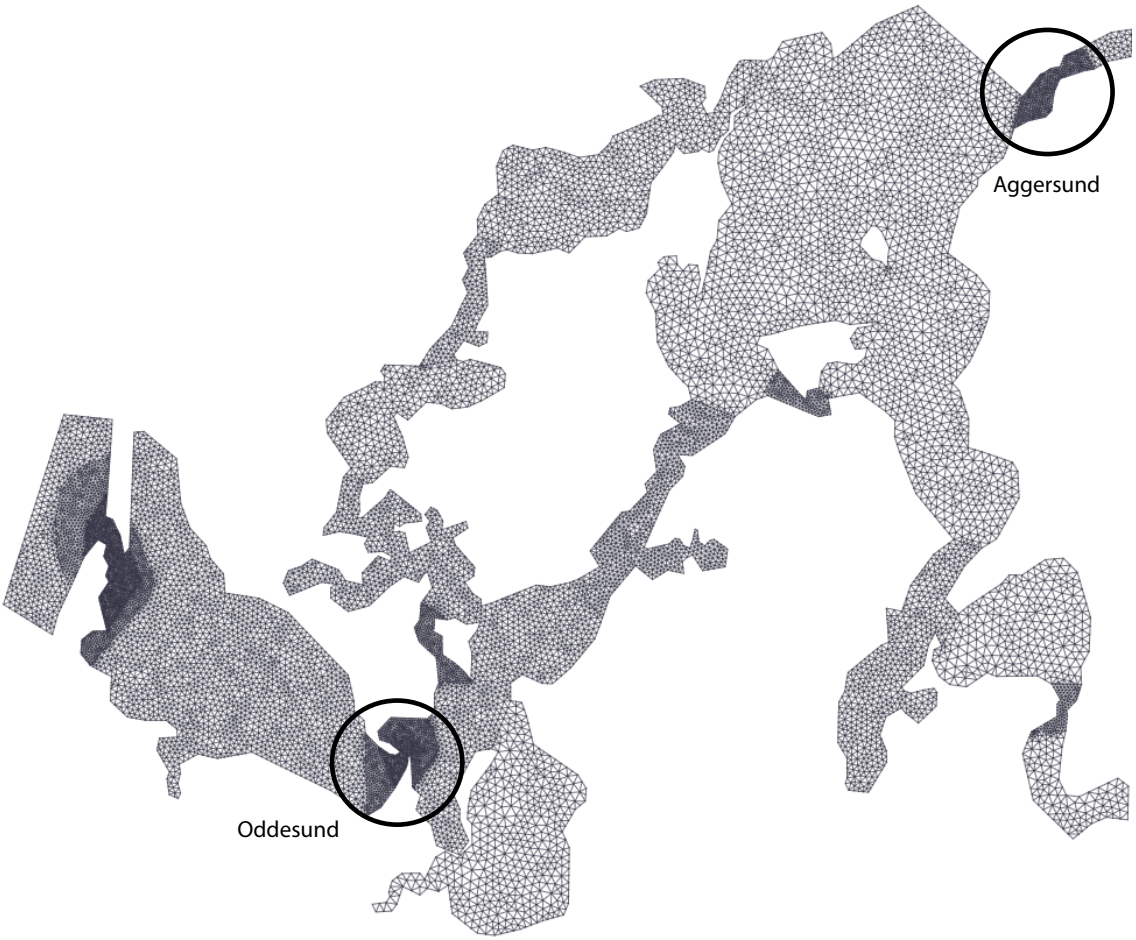

Figure G.3 7th iteration of the mesh.

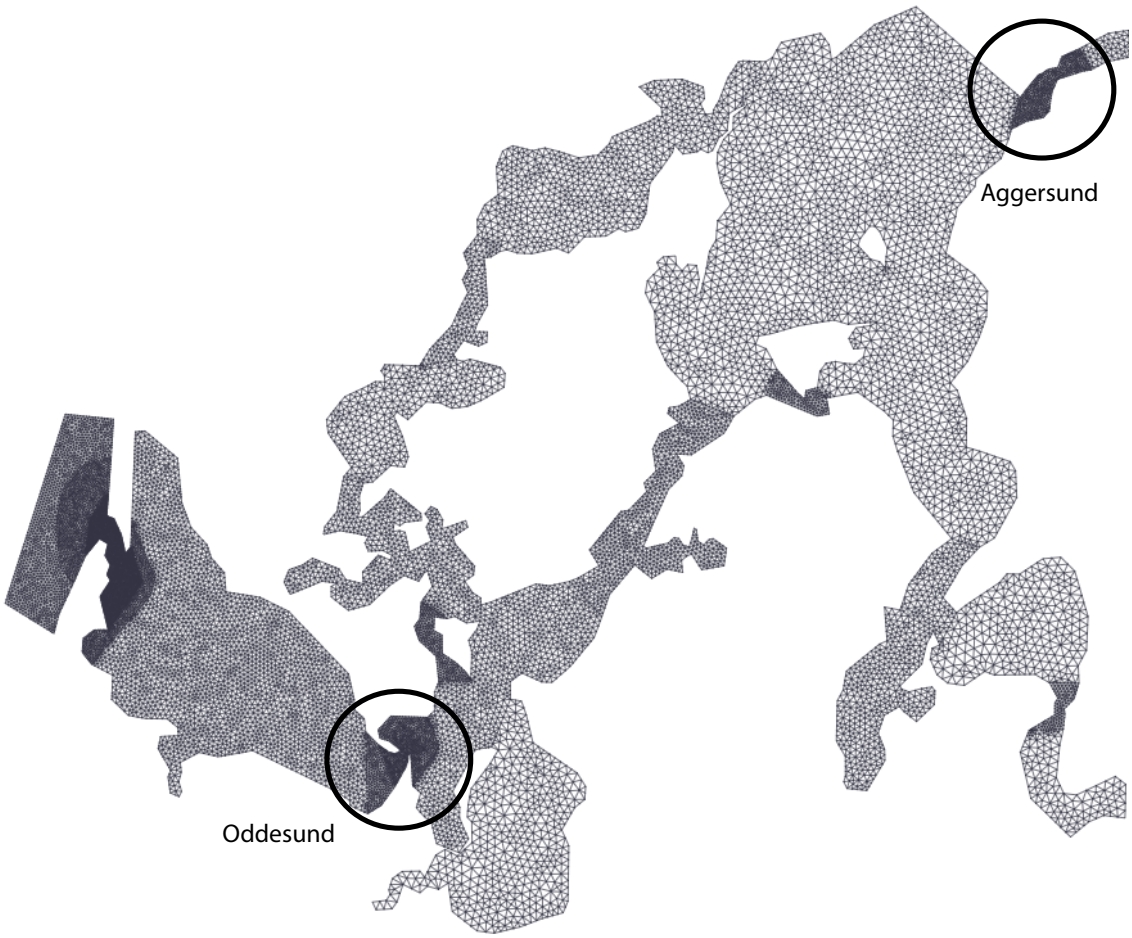

Figure G.4 8th iteration of the mesh.

It is found that the seventh iteration is the best alternative as the difference in velocities in Thyborøn Channel are small between this and the 8th mesh. The mesh is refined in areas where velocities are expected to accelerate, Oddesund and Thyborøn Channel for instance.

Tide isolation from surface elevations

H

As the wind directions in the data are deemed questionable, an isolation of the tides from the signal in order to eliminate wind from the model is made. The following shows an example using the surface elevation at Thyborøn.

Figure H.1 shows the signal converted to frequency domain using a fast furrier transform algorithm. The parts corresponding to the 10 strongest tidal constituents in Table H.1 are marked in red.

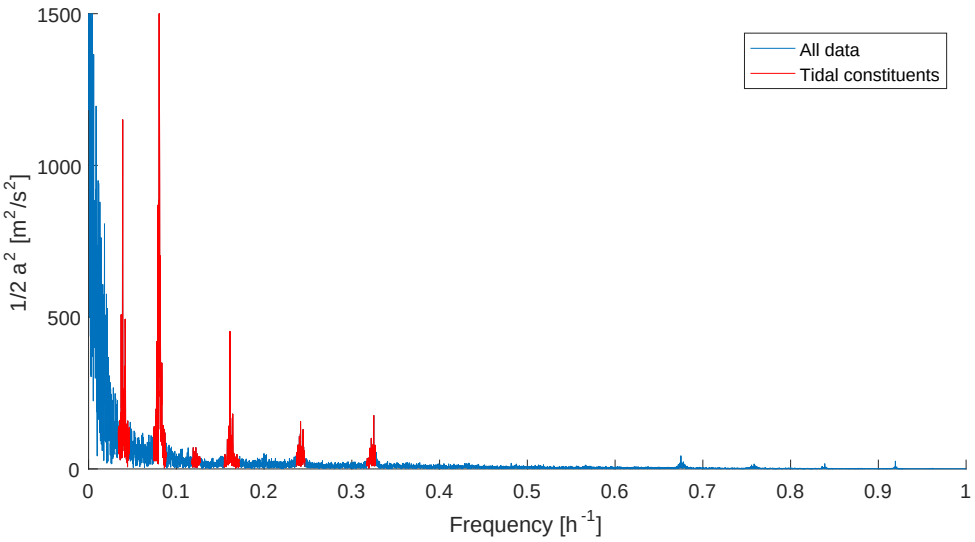

Figure H.1 Surface elevation variation at Thyborøn converted to frequency domain to isolate tidal constituents.

Table H.1 Tidal constituents used when isolating the tides from the surface elevation variation signal.

Constituent	M2	S2	N2	K1	M4	O1	M6	MK3	S4	MN4
Period [h]	12.42	12.00	12.66	23.93	6.21	25.82	4.14	8.18	6.00	6.27

The tidal part is isolated and converted back to time domain as shown in Figure H.2. The tidal trend is clearly seen and the amplitude of about 0.4 m fits the one recorded by DMI [2017].

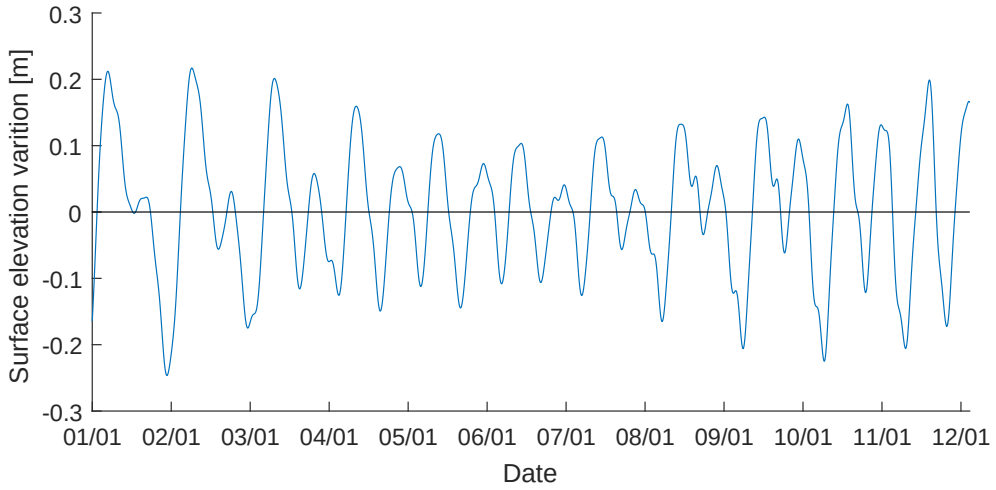

Figure H.2 Isolated tides from surface elevation variation at Thyborøn.

H.1 Limfjord model results simulating only tides

The models run using only tides are shown in Table H.2.

Table H.2 Selection of models used for assessing tides in the Limfjord.

Model	Mesh	Roughness height, k_s [m]
V27Tide	V6	0.9 & 6.8
V30Tide	V6	0.9
V32Tide	V7	0.9

Figures H.3 and H.4 show the difference between the tides isolated from the calibration basis and the ones simulated by isolating tides from the boundary conditions at Hals and Thyborøn. It is apparent that the tides do not match perfectly. The amplitudes, however, seem to be modelled fairly well, especially at Skive. Reasons for the mismatch could be that the models or the isolation of tides from the different signals are inaccurate. Considering that the models including wind predict the water level fairly well, it is likely the isolation of tides that is off. As amplitudes are expected to influence wave height while phase influence which periods are high and low tides, the difference in phase is accepted and model 32 is further validated as the best compromise between accuracy and computational time.

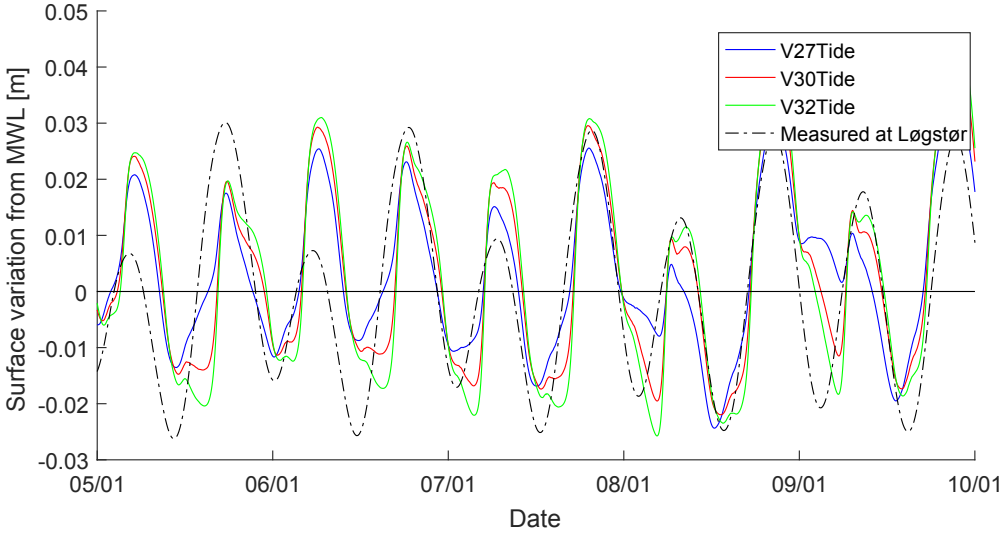

Figure H.3 Comparison of simulated tides and tides isolated from measured surface elevation data at Løgstør.

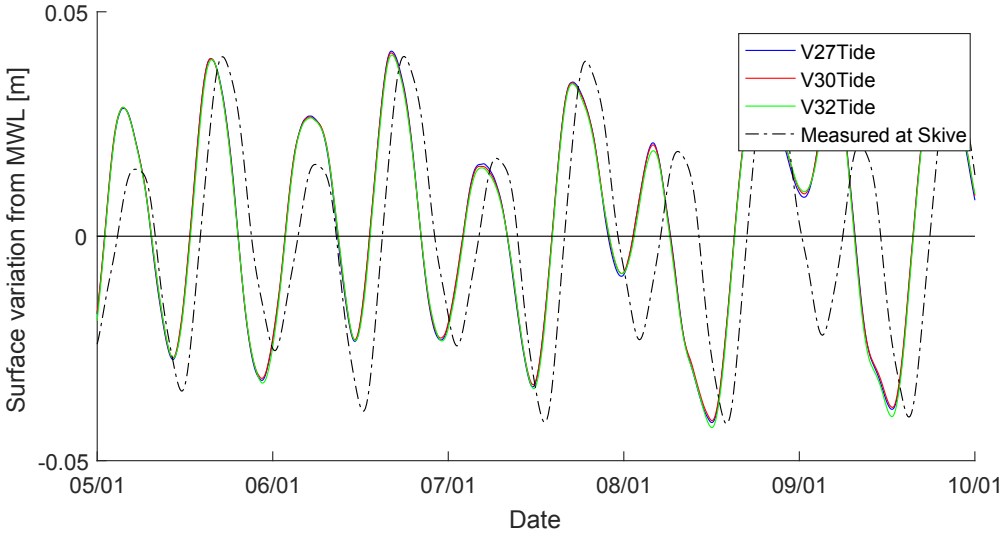

Figure H.4 Comparison of simulated tides and tides isolated from measured surface elevation data at Skive.

Convergence analysis on the Thyborøn model

I

In this appendix, convergence of the JanRef model is investigated by examining results of simulations run with varying mesh density. Coarse, medium, and fine mesh densities with 35630, 52680, and 63156 elements, respectively, are modelled. Figures I.1-I.3 show the accumulated bed level change caused by the January storm on the reference bathymetry.

As seen from the figures, some change between coarse and medium mesh density is predicted while very little change is seen between the medium and fine mesh densities, suggesting that the solution in the simulation using the medium mesh density is converged. Hence the medium mesh density is used for the sediment simulations in the project.

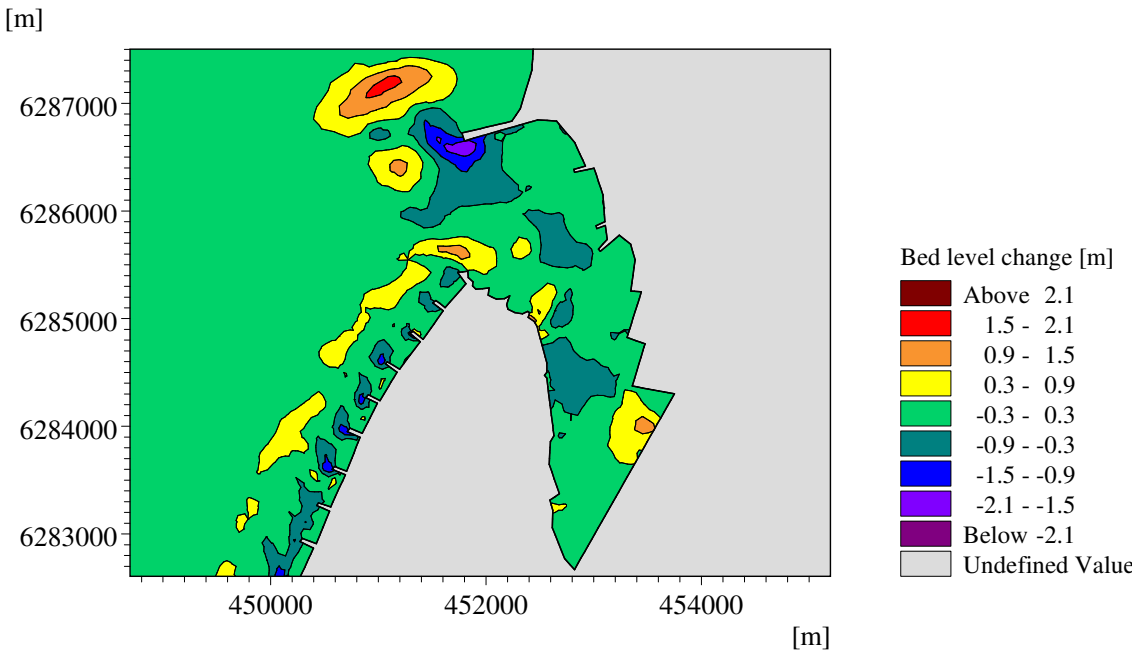

Figure I.1 Accumulated bed level change caused in the coarse mesh simulation.

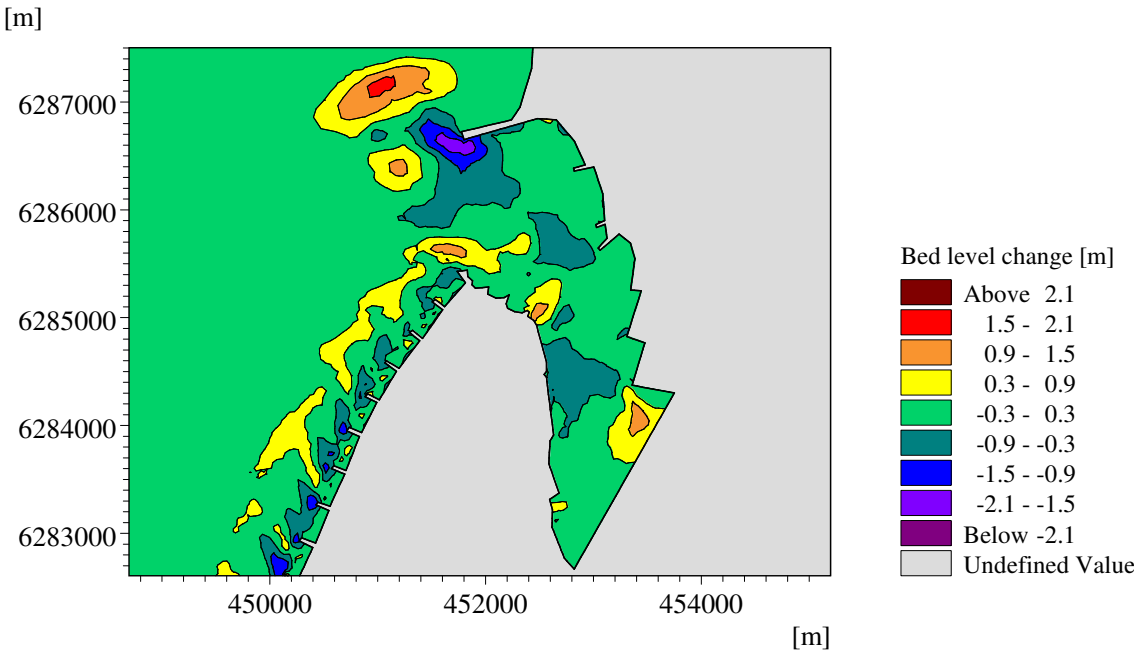

Figure I.2 Accumulated bed level change caused in the reference mesh simulation.

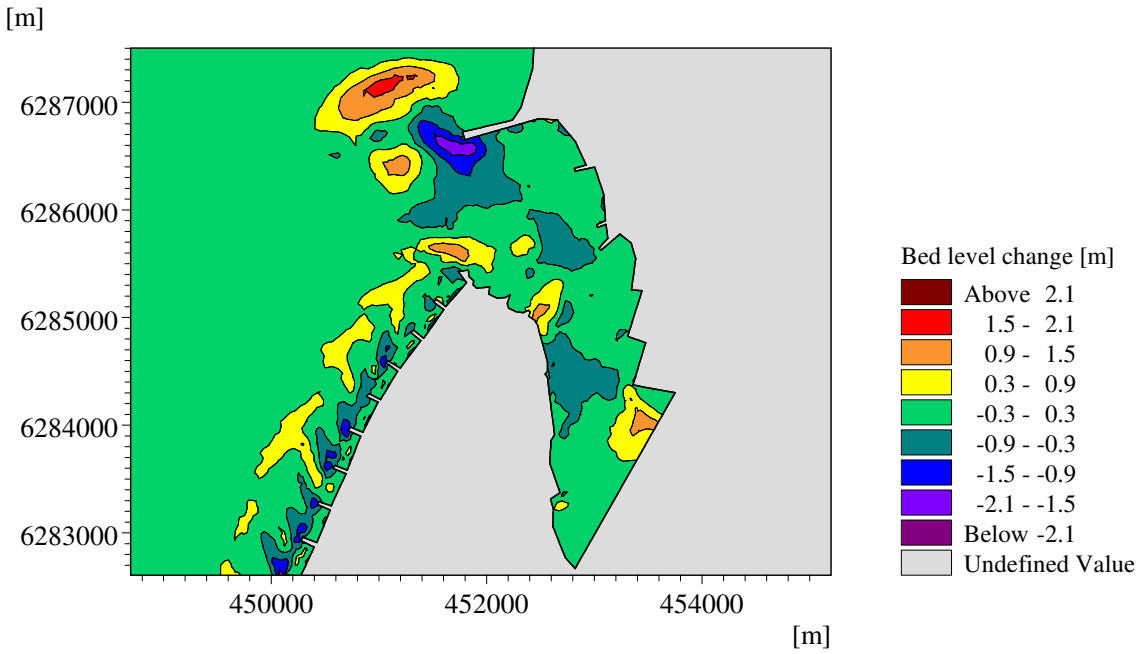

Figure I.3 Accumulated bed level change caused in the fine mesh simulation.

Simulated flow patterns at Thyborøn J

In this appendix, flow patterns for the different models during peak in- and outflows of the different storms are shown. For the JanDam and DecDam models only one flow is shown as there is no flow through the channel.

J.1 January storm flow patterns

The inflow during the January storm peaks on the 8th at 3 pm, and the outflow on the 10th at 1 am.

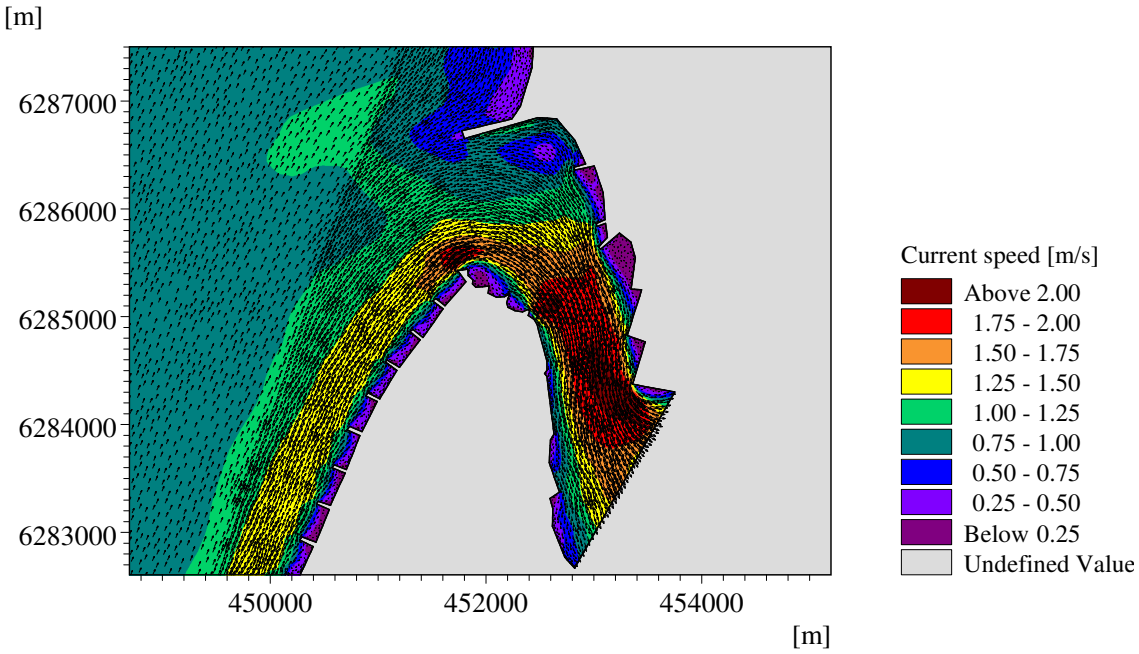

Figure J.1 Flow pattern for the reference model during the peak of the inflow during the January storm.

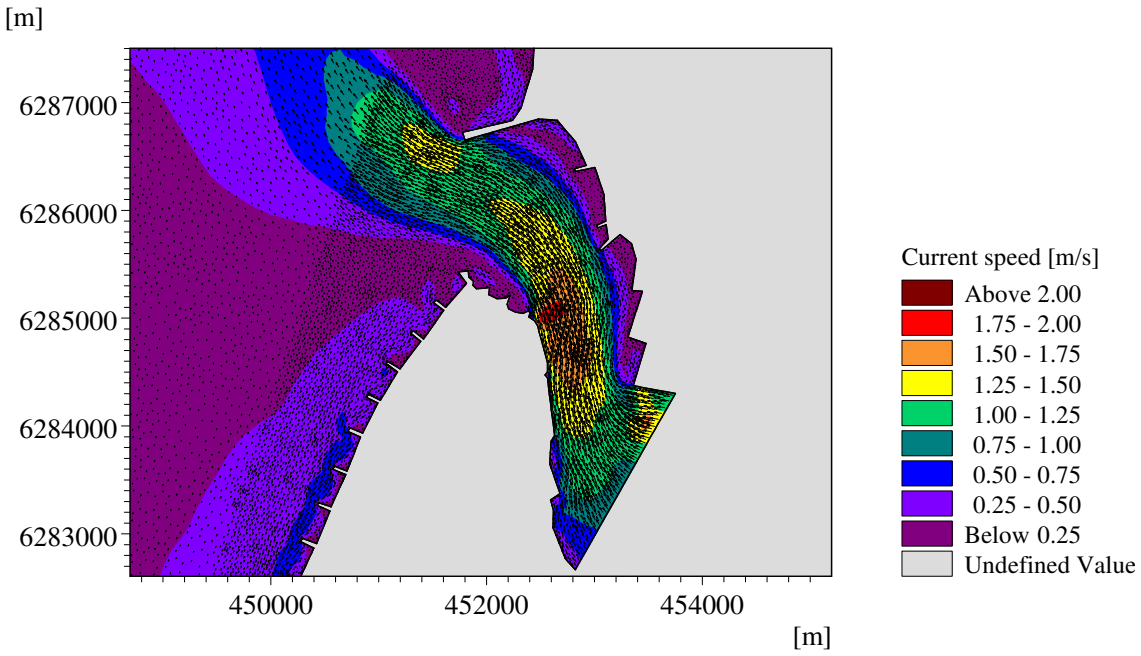

Figure J.2 Flow pattern for the reference model at the peak of the outflow speed during the January storm.

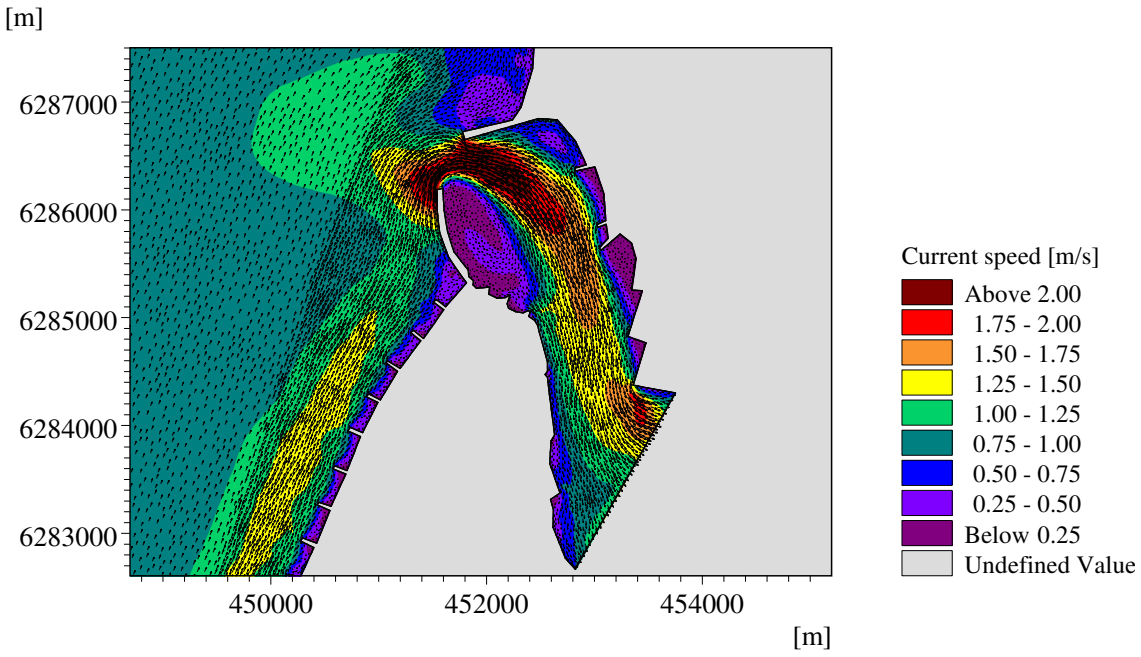

Figure J.3 Flow pattern for the groyne extension model at the peak of the inflow speed during the January storm.

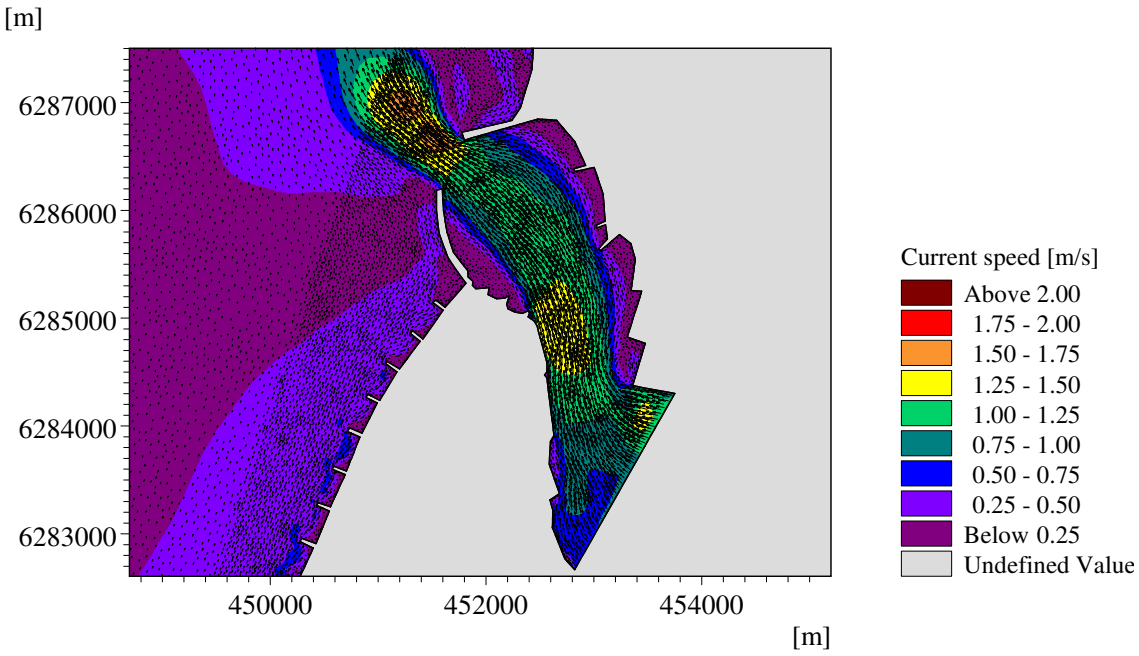

Figure J.4 Flow pattern for the groyne extension model at the peak of the outflow speed during the January storm.

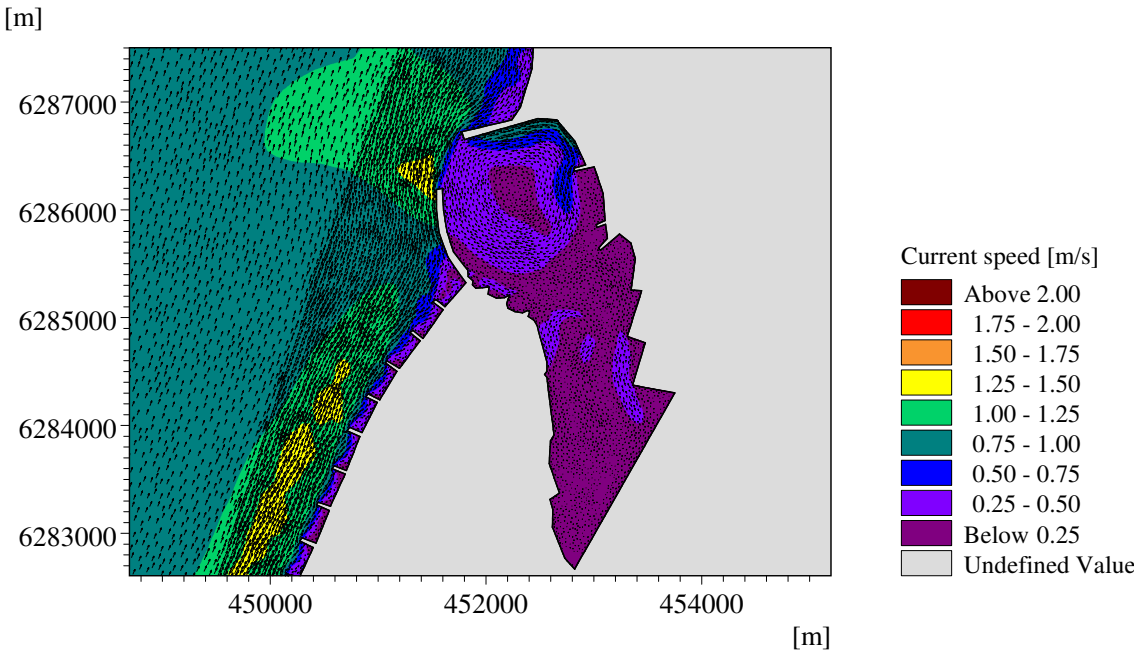

Figure J.5 Flow pattern for the dam model at the peak of the flow speed during the January storm.

J.2 December storm flow fields

The inflow during the December storm peaks on the 13th at 2 am, and the outflow on the 15th at 5 am.

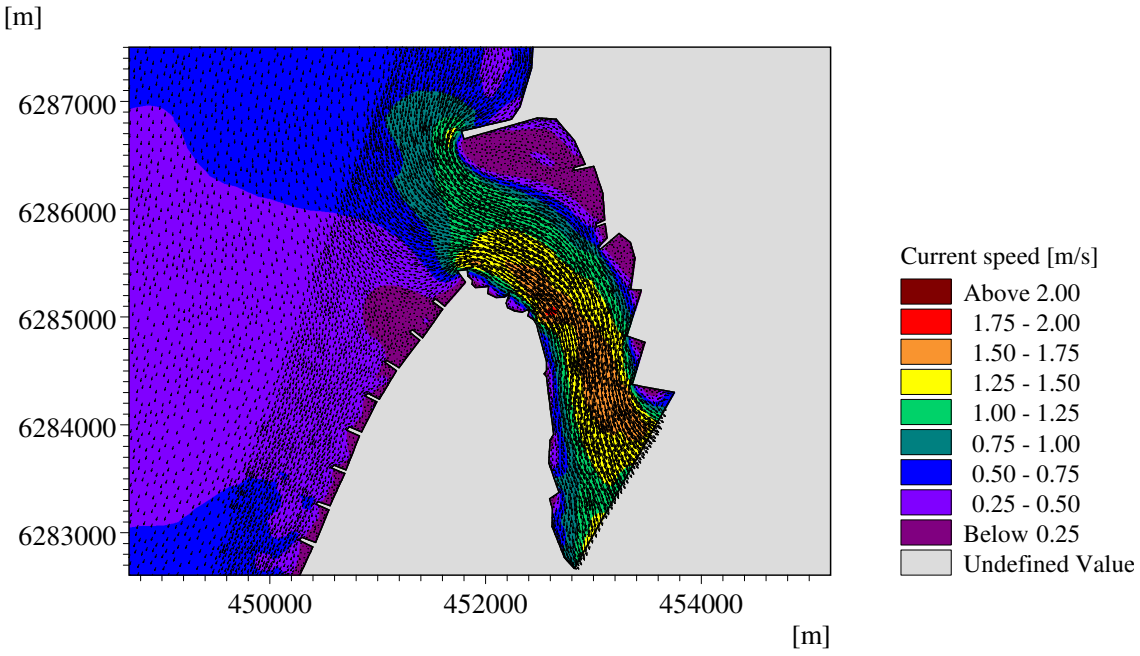

Figure J.6 Flow pattern for the reference model at the peak of the inflow speed during the December storm.

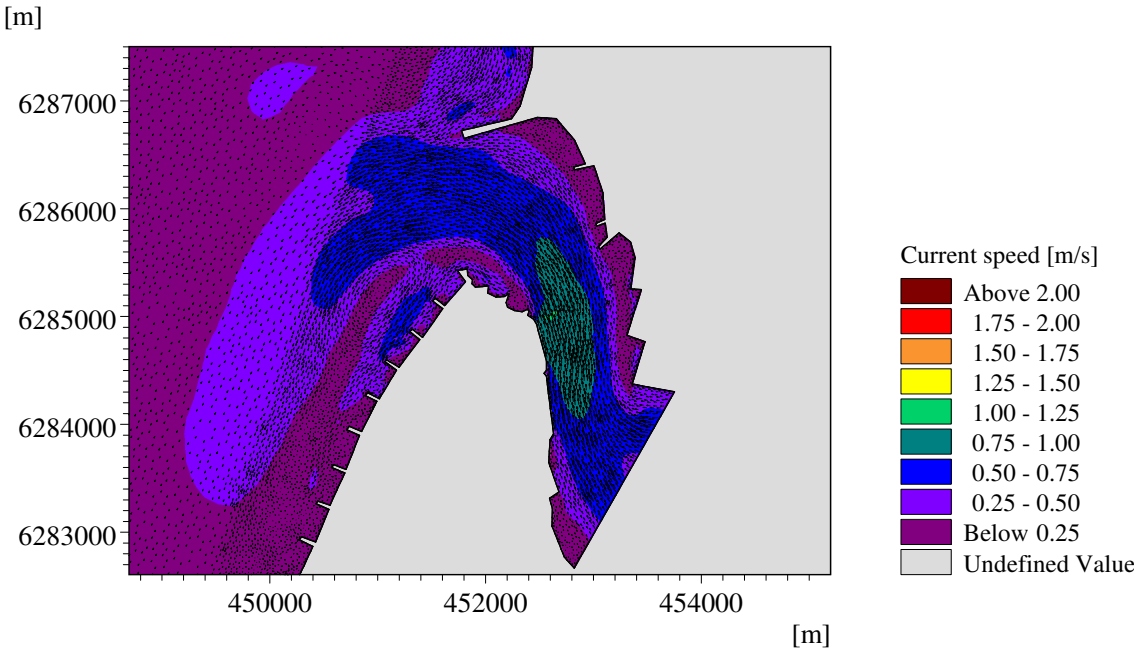

Figure J.7 Flow pattern for the reference model at the peak of the outflow speed during the December storm.

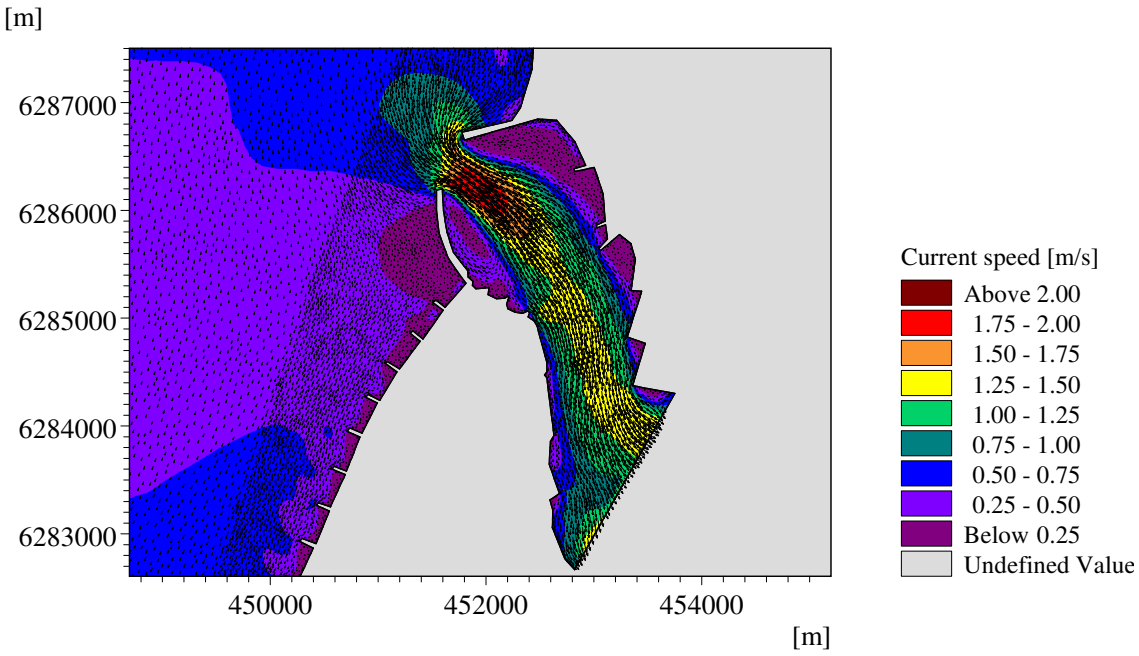

Figure J.8 Flow pattern for the groyne extension model at the peak of the inflow speed during the December storm.

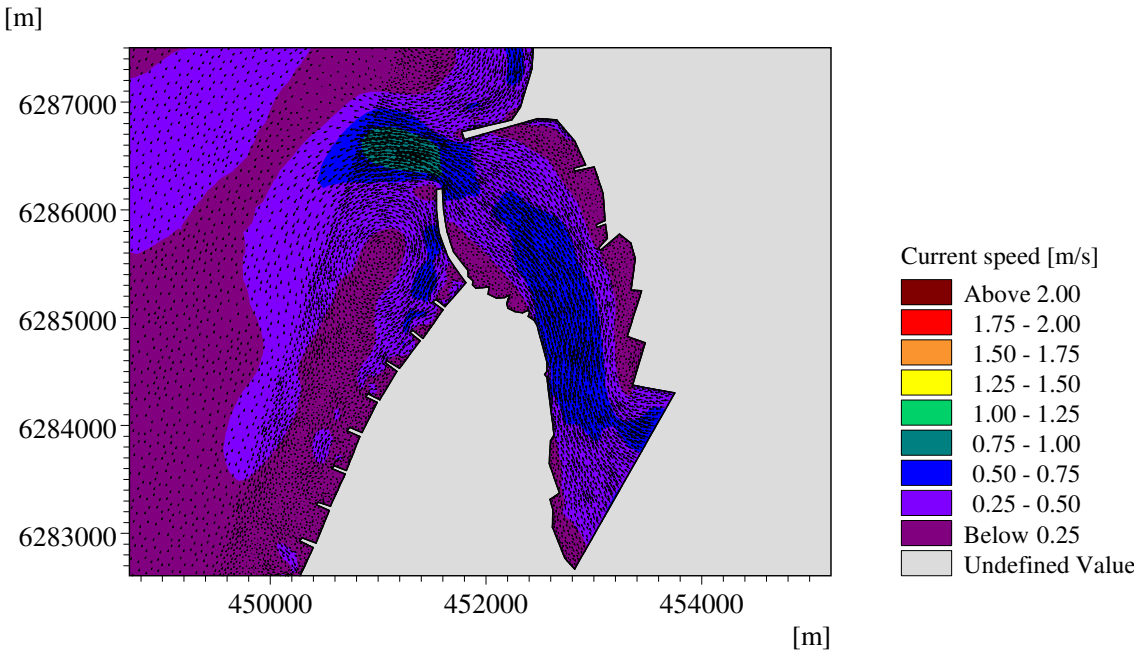

Figure J.9 Flow pattern for the groyne extension model at the peak of the outflow speed during the December storm.

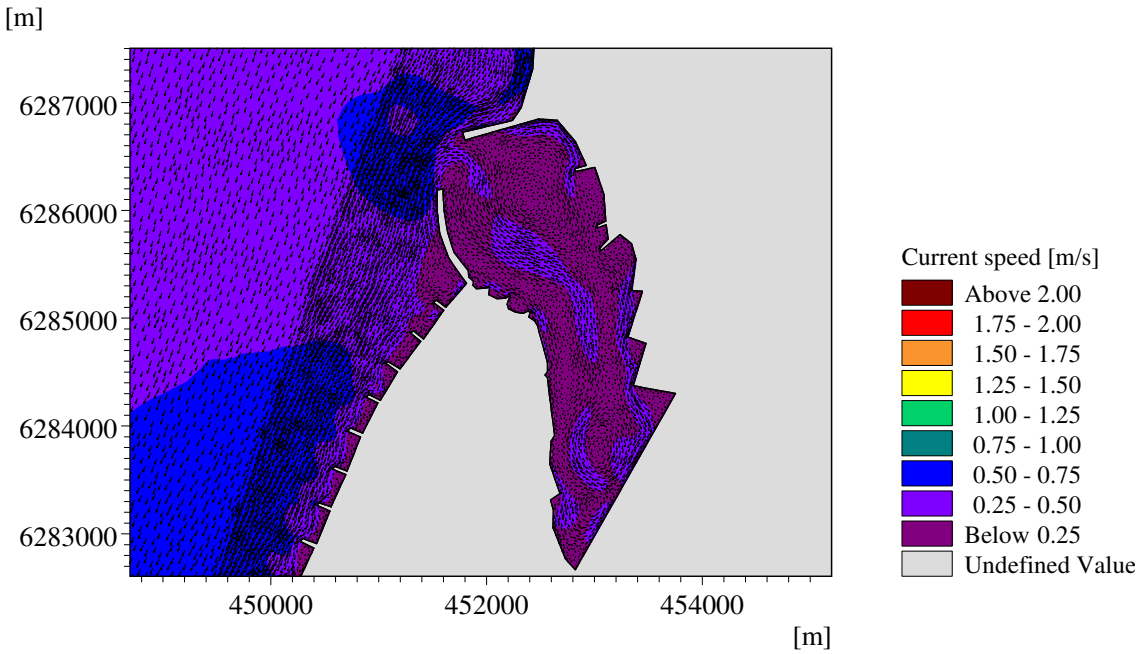

Figure J.10 Flow pattern for the dam model at the peak of the flow speed during the December storm.